UNIVERSITY OF CALIFORNIA
RIVERSIDE

Optimal Operation of Energy Storage in Power Transmission and Distribution

A Dissertation submitted in partial satisfaction
of the requirements for the degree of

Doctor of Philosophy

in

Electrical Engineering

by

Seyed Hossein Akhavan Hejazi

March 2016

Dissertation Committee:

Dr. Hamed Mohsenian-rad, Chairperson
Dr. Matthew J. Barth
Dr. Kurt Schwabe

The Dissertation of Seyed Hossein Akhavan Hejazi is approved:

Committee Chairperson

University of California, Riverside

Acknowledgments

I thank my supervisor Dr. Hamed Mohsenian-rad, without whose help, I could not complete this work. This work was supported in part by NSF grant ECCS, and UCR New Faculty Initial Compliment grant. The content of this thesis has also appeared in the following publications:

- H. Akhavan-Hejazi, H. Mohsenian-Rad, "Energy Storage Planning in Active Distribution Grids: A Chance-Constrained Optimization with Non-Parametric Probability Functions," Under Review (second round) at IEEE Trans. on Smart Grid, 2015.
- H. Akhavan-Hejazi, H. Mohsenian-Rad, "Optimal Operation of Independent Storage Systems in Energy and Reserve Markets With High Wind Penetration," IEEE Trans. on Smart Grid, vol. 5, no. 2, pp. 1088-1097, March 2014.
- H. Akhavan-Hejazi, A. Araghi, B. Vahidi, S. Hosseinian, M. Abedi, and H. Mohsenian-Rad, "Independent Distributed Generation Planning to Profit Both Utility and DG Investors", IEEE Trans. on Power Systems, vol. 28, no. 2, pp. 1170-1178, July, 2013.
- H. Akhavan-Hejazi, H. Mohsenian-Rad, "Optimal Operation of Independent Storage Systems in Energy and Reserve Markets with High Wind Penetration", in Energy Storage for Smart Grids: Planning and Operation for Renewable and Variable Energy Resources, Edited by Pengwei Du and Ning Lu, Elsevier, 2014.
- H. Akhavan-Hejazi, B. Asghari, R. Sharma, "A joint bidding and operation strategy for battery storage in multi-temporal energy markets," in Proc. of the IEEE PES Innovative Smart Grid Technologies Conference, Washington, DC, Feb. 2015.
- H. Akhavan-Hejazi, H. Mohsenian-Rad, A. Nejat, "Developing a test data set for electric vehicle applications in smart grid research," in Proc of the IEEE Vehicular Technology Conference, Vancouver, BC, 2014.
- H. Akhavan-Hejazi, H. Mohsenian-Rad, "A Stochastic Programming Framework for Optimal Storage Bidding in Energy and Reserve Markets" in Proc. of the IEEE PES Innovative Smart Grid Technologies Conference, Washington, DC, Feb. 2013.
- H. Akhavan-Hejazi, Z. Bahar, H. Mohsenian-Rad, "Challenges and Opportunities in Large-Scale Deployment of Automated Energy Consumption Scheduling in Smart

Grid", in Proc. of the IEEE Conf. on Smart Grid Communications, Tainan, Taiwan, Oct. 2012.

To my parents.

ABSTRACT OF THE DISSERTATION

Optimal Operation of Energy Storage in Power Transmission and Distribution

by

Seyed Hossein Akhavan Hejazi

Doctor of Philosophy, Graduate Program in Electrical Engineering
University of California, Riverside, March 2016
Dr. Hamed Mohsenian-rad, Chairperson

In this thesis, we investigate optimal operation of energy storage units in power transmission and distribution grids. At transmission level, we investigate the problem where an *investor-owned independently-operated* energy storage system seeks to offer energy and ancillary services in the day-ahead and real-time markets. We specifically consider the case where a significant portion of the power generated in the grid is from renewable energy resources and there exists significant uncertainty in system operation. In this regard, we formulate a stochastic programming framework to choose optimal energy and reserve bids for the storage units that takes into account the fluctuating nature of the market prices due to the randomness in the renewable power generation availability. At distribution level, we develop a comprehensive data set to model various stochastic factors on power distribution networks, with focus on networks that have high penetration of electric vehicle charging load and distributed renewable generation. Furthermore, we develop a data-driven stochastic model for energy storage operation at distribution level, where the distribution of nodal voltage and line power flow are modelled as stochastic functions of the energy storage unit's charge and discharge schedules. In particular, we develop new closed-form stochastic models for such key operational parameters in the system. Our approach is analytical and allows formulating tractable optimization problems. Yet, it does not involve any restricting assumption on the distribution of random parameters, hence, it results in accurate modeling of uncertainties. By considering the specific characteristics of random variables, such as their statistical dependencies and often irregularly-shaped probability distributions, we propose a non-parametric chance-constrained optimization approach to operate and plan energy stor-

age units in power distribution girds. In the proposed stochastic optimization, we consider uncertainty from various elements, such as solar photovoltaic , electric vehicle chargers, and residential baseloads, in the form of discrete probability functions. In the last part of this thesis we address some other resources and concepts for enhancing the operation of power distribution and transmission systems. In particular, we proposed a new framework to determine the best sites, sizes, and optimal payment incentives under special contracts for committed-type DG projects to offset distribution network investment costs. In this framework, the aim is to allocate DGs such that the profit gained by the distribution company is maximized while each DG unit's individual profit is also taken into account to assure that private DG investment remains economical.

Keywords: Independent energy storage systems, energy and reserve markets, wind power integration, stochastic optimization, demand response, power system simulation, distribution grid, non-parametric probability distributions, chance-constrained optimization.

Contents

List of Figures

List of Tables

Chapter 1

Introduction

1.1 Motivation and Objectives

The electric power system is rapidly changing as more grid-connected technologies such as renewable and distributed generation [1], and electric vehicles [2] are being deployed. The fluctuations in both generation and demand have made the power system more unpredictable, both at *transmission* and *distribution* levels, making it more challenging to assure reliability, stability, and security. Note that, transmission grid refers to the system which delivers electricity from bulk generators to consumer locations while distribution grid refers to the system that carries electricity from the transmission system to end consumers.

One promising solution to uncertainty in power systems is to install energy storage devices at both power transmission and distribution grids. Energy storage, whether at the transmission level or at the distribution level, is playing an increasingly important role in helping to balance supply and demand in power systems and to ensure system reliability and stability. As distributed energy resources become more prominent, with attributes such as scalability, location, and application, the role of energy storage systems becomes more critical in creating a modern and smart electric system. For example, in California, the California Public Utilities Commission has mandated that the three largest investor-owned utility companies install a total of 1,325 megawatts new energy storage units by 2020. Over 50% of such new energy storage installations are expected to be at the transmission level. About 35% will be at the distribution level and the remaining will be at the consumer level in form of behind-the-meter energy storage resources [3]. The focus of this thesis is on deployment and operation of energy storage units both at the transmission and distribution

grids.

Considering the challenges at power transmission grids, a recent study in [4] has shown that significant wind power curtailment may become inevitable if more renewable power generation resources are installed without improving the existing infrastructure or using energy storage. Other studies, e.g., in [5–7] have similarly suggested that energy storage can potentially help in integrating renewable energy resources. Although this basic idea has been widely speculated in the smart grid community, it is still not clear *how we can encourage major investment for building large-scale independently-owned storage units and how we should utilize the many different opportunities existing for these units.* Addressing these open problems is one of the main focus areas in this thesis.

At distribution grids, storage operation is also a promising option to manage the network in the presence of new elements that challenge the traditional structure of distribution feeders [8]. However, the storage objectives and context are different from those in transmission grids [9]. Energy storage is likely to be installed by users or a utility company. The distributed energy storage systems may have the ability to provide multiple services to the distribution grid. These services include:

- electric supply capacity and energy time shift,
- distribution system support and investment differals,
- energy cost management for electric utility customers,
- distributed renewable energy integration,
- enhancing the security of the grid and its stability,
- and providing ancillary services.

Now, the question is: *how can we stablish and optimally manage a system of distributed storage units in power distribution grid and perform various reliable and compatible services for both the system and the users?* Answering this question is also another goal of this research.

Finally, in the third part of this thesis we address some other resources and concepts for enhancing the operation of power distribution and transmission systems. In this regard, we proposed a new algorithm to determine the best sites, sizes, and optimal payment

incentives under special contracts for committed-type DG projects to offset distribution network investment costs. In this framework, the aim is to allocate DGs such that the profit gained by the distribution company is maximized while each DG unit's individual profit is also taken into account to assure that private DG investments remain economical. We also address the case of automated demand side management where a large portion of loads in the grid are active participants under a real-time pricing framework.

1.2 Summary of Contributions and Publications

The research performed in this thesis can be outlined under three thrusts. First, we address the optimal operation of large size energy storage on transmission grids. In this thrust, we are interested in investigating the best operation strategy for independent energy storage systems and developing optimization frameworks for investor-owned energy storage systems to offer various services in two-settlement electricity markets.

Second, we attend to the problem of medium size distributed energy storage systems operating at the distribution grid. In this regard, we develop models for stochastic representation of the distribution grid features, such as the load and generation of various contemporary smart grid elements, as well as the key operational parameters of the system including bus voltages and line flows. We use a non-parametric chance-constrained optimization method to identify the best operation schedule of energy storage systems and the best size and location of such systems at the distribution grid.

Finally, in the third part of the thesis, we further examine the operation and deployment of distributed energy resources, but for energy resources other than energy storage. First, we study the optimal planning of the distribution grids to include the contribution of distributed generation under incentivated contracts. Next, we address the wide spread deployment of automated demand side management devices in the distribution networks, and the issue that may arise under a real-time pricing structure known as *load synchronization*. We investigate how load management of automated devices in response to locational marginal prices may impact the operation of the transmission power system.

The following publications are resulted from this thesis:

- H. Akhavan-Hejazi, H. Mohsenian-Rad, "Energy Storage Planning in Active Distribution Grids: A Chance-Constrained Optimization with Non-Parametric Probability

Functions," Under Review (second round) at IEEE Trans. on Smart Grid, 2015.

- H. Akhavan-Hejazi, H. Mohsenian-Rad, "Optimal Operation of Independent Storage Systems in Energy and Reserve Markets With High Wind Penetration," IEEE Trans. on Smart Grid, vol. 5, no. 2, pp. 1088-1097, March 2014.

- H. Akhavan-Hejazi, A. Araghi, B. Vahidi, S. Hosseinian, M. Abedi, and H. Mohsenian-Rad, "Independent Distributed Generation Planning to Profit Both Utility and DG Investors", IEEE Trans. on Power Systems, vol. 28, no. 2, pp. 1170-1178, July, 2013.

- H. Akhavan-Hejazi, H. Mohsenian-Rad, "Optimal Operation of Independent Storage Systems in Energy and Reserve Markets with High Wind Penetration", in Energy Storage for Smart Grids: Planning and Operation for Renewable and Variable Energy Resources, Edited by Pengwei Du and Ning Lu, Elsevier, 2014.

- H. Akhavan-Hejazi, B. Asghari, R. Sharma, "A joint bidding and operation strategy for battery storage in multi-temporal energy markets," in Proc. of the IEEE PES Innovative Smart Grid Technologies Conference, Washington, DC, Feb. 2015.

- H. Akhavan-Hejazi, H. Mohsenian-Rad, A. Nejat, "Developing a test data set for electric vehicle applications in smart grid research," in Proc of the IEEE Vehicular Technology Conference, Vancouver, BC, 2014.

- H. Akhavan-Hejazi, H. Mohsenian-Rad, "A Stochastic Programming Framework for Optimal Storage Bidding in Energy and Reserve Markets" in Proc. of the IEEE PES Innovative Smart Grid Technologies Conference, Washington, DC, Feb. 2013.

- H. Akhavan-Hejazi, Z. Bahar, H. Mohsenian-Rad, "Challenges and Opportunities in Large-Scale Deployment of Automated Energy Consumption Scheduling in Smart Grid", in Proc. of the IEEE Conf. on Smart Grid Communications, Tainan, Taiwan, Oct. 2012.

Next, we summarize the main results in each research thrust.

1.2.1 Energy Storage Operation on Transmission Grid

The first part of the thesis includes two research projects that are closely interrelated. They are centered around optimal operation and bidding of energy storage in

electricity markets. The key question is: *How can an energy storage unit that is owned and operated by an independent investor bid in electricity market to maximize its profit, when there exists considerable uncertainties?* Answering this question is the focus of the first part of this thesis.

In this regard, in Chapter 2, we develop a stochastic optimization framework for energy storage system optimal operation and bidding at the day-ahead market to provide energy and reserve services. We assume a reserve market structure similar to a simplified version of the *day ahead scheduling reserve market* in the PJM (Pennsylvania, New Jersey, Maryland) inter-connection [10], where the exact utilization of the reserve bids is not decided by the storage unit; instead, it is decided by the market. As a result, finding the optimal charge and discharge schedules is particularly challenging when the storage unit participates in the *reserve* market. Another challenge is to formulate the bidding optimization problem as a convex program to make it tractable and appropriate for practical scenarios.

In Chapter 3, we look into the problem of coordinated bidding and operation of energy storage system at day-ahead and real-time markets to provide energy services. Again, accounting for the uncertainties of the real-time market prices is a key feature in this work. We investigate the inter-dependencies of energy storage system operation at day-ahead and real-time markets and how the bids in one market affects the revenues in the other. We also account for the risk associated with withholding of energy storage capacity to participate in the real-time market. We propose an optimization framework to obtain the best bidding strategies in both day-ahead and real-time markets, and coordinate battery schedules accordingly. A receding time horizon optimization is derived that updates input information in the operating-day continuously as new forecasts, etc. becomes available and updates energy storage system decisions accordingly. In presented framework, the Value-at-Risk of revenues due to errors in forecasts is calculated and controlled throughout both stages of optimization in day-ahead and real-time markets. Again, obtaining convex formulation and models for the problem so that it can be solved effectively in real-time is an essential part of this study.

One journal paper, two conference papers, and one book chapter resulted from the first part of this thesis.

1.2.2 Energy Storage Operation on Distribution Grid

At distribution level, the main purpose of using storage devices is to expand the service capacity of the network without jeopardizing the reliability and security of the system. The design objective can be to maximize the profit in a flexible and scalable manner, while the impact of new technologies such as distributed renewable energy sources and plug-in electric vehicles is taken into account. In order to achieve a flexible and scalable design, it is usually preferred by the utilities that ownership and operation of energy storage systems (ESSs) be independent, distributed and modular [9].

Therefore, in the second part of the thesis, we look into the problem of energy storage system operation and planning at the distribution grid. Accounting for the uncertainty introduced to the distribution grid, as a result of fluctuating load and generation of contemporary elements such as photovoltaic distributed generators (PV-DGs) and electric vehicle (EV) chargers, and designing the best energy storage operation and planning accordingly is the focus of this part.

An important problem in this regard, which is addressed in Chapter 4, is to obtain the statistical characteristics of various elements of the system such as the electric vehicle charging load, solar PV-DG generation, and baseload of residential users from the historical data. Obtaining statistical characteristics of the charging load of electric vehicles is particularly challenging. The main issue comes from the lack of data on real measurement of the electric vehicle charge loads. Therefore, in Chapter 4, we analyze the driving traces for 536 GPS-equipped non-PHEV taxi vehicles in [11] and combine them with the features and technical characteristics of different PHEV brands in order to obtain a new test data set to support our investigation of stochastic features of a smart distribution grid. Additionally, we obtain the statistical features of the solar PV-DGs by synthesizing the load of a solar panel using a real-time digital simulator from the historical recorded measurements of the solar irradiation and temperature obtained from [12]. We also obtain the statistical features of residential baseloads, by combining the metered hourly loads of 600 residential consumers from PECON Street database [13].

In Chapter 5, we address the question that *given the statistical features of various elements in a distribution grid, how can we obtain the probability distribution of the various operational parameters such as bus voltages and line flows so that with proper energy storage operation we mitigate the probability of system violations?* We are interested in obtaining the

distribution of operational parameters analytically without restricting a specific parametric distribution on the input random variables. In fact, those distributions are obtained directly from a history of local measurement data. We obtain an analytical representation of the key operational parameters which enables us to have a deeper understanding of statistical behaviours of these parameters making the designs and upgrade of the system more efficient. For example, this model makes it possible to have clear solutions, when it comes to the probability of having over-/ under- voltage in any bus, or an over flow in any line. Our analytical model is used as well to formulate a chance-constrained optimization for energy storage system optimal daily operation plan as well as the optimal site and size of the energy storage system. Our novel non-parametric chance-constrained optimization model enables a more effective energy storage operation and deployment planning. We accurately obtain the probability of violation for various system operational parameters and compensate accordingly with the optimal operation of energy storage system, so that we achieve the safe operation of the power distribution grid at a minimum cost.

One journal paper and one conference paper resulted from the second part of this thesis.

1.2.3 Distributed Generation and Demand Response

In the third and last part of this thesis, we address some other novel paradigms in smart grid operation and planning. Specifically, demand side management and dispatchable distributed generation are optimized to relive pressure from the power grids. The results are presented in Chapters 6 and 7. These studies were carried out in the early stages of this research. Although not related to energy storage system, the goals and the context of these projects are in-line with energy storage operation.

In Chapter 6, we investigate the optimal expansion planning of the distribution grid to support the increasing load, and relieve pressure from the substation by the aid of dispatchable distributed generation. We aim to find the best mixture of power procurement from both DGs and the energy market so as to minimize the energy cost and the upgrade cost of the distribution grid, while maintaining energy production profitable for the DG investors. The design and assumptions in the proposed approach are well aligned with the current structure of California utilities. We obtain the best rates for energy at off-peak and peak periods, as well as the optimal sizes and locations of the DGs in the contract based

power procurement.

Finally, in Chapter 7, we address the demand side management in the distribution grids. We investigate the large deployment of automated demand response designs in the distribution grids and their impacts on the power system operation. Specifically, we address an important challenge in large-scale deployment of automated demand response under real-time pricing structure, known as *load synchronization*. The problem arises when in response to real-time prices a large portion of automated load scheduling devices shift their consumption from peak price time intervals to low price periods. This leads to a shift in the load of a portion of consumers that may cause new peak periods. The fluctuations in the electricity prices that may occur as a result, can makes the system unstable. To tackle this problem, we propose to use a moving average smoothing mechanism for LMPs. Our simulation results show that the proposed approach works well and can assure system stability. Furthermore, we show that the proposed large-scale deployment of ECS devices approximates optimal performance in terms of reducing PAR in the aggregate load demand, minimizing the total power generation cost in the system, and reducing each user's individual electricity bill payments.

One journal paper and one conference paper resulted from the third part of this thesis.

1.2.4 Thesis Organization

This thesis is organized as follows:

The Part I of this thesis is focused on Optimal Energy Storage Operation at the Transmission Grid. In this regard, the Chapter 2 is dedicated to operation of independent large-scale battery storage systems in energy and reserve markets with high wind penetration. Chapter 3 presents a joint bidding and operation strategy for battery storage in multi-temporal energy markets. The Part I of this thesis is focused on Energy Storage Operation at the Distribution Grid. Accordingly, Chapter 4 is focused on data synthesis to model power distribution networks. Chapter 5 presents a novel approach on energy storage planning in active distribution grids. A chance-Constrained optimization is proposed in this chapter with non-parametric probability functions. The Part III of this thesis is focused on distributed generation and demand response planing at the distribution grid. Chapter 6 is dedicated to distributed generation planning in order to profit both utility and DG investors.

And finally in Chapter 7 we address some challenges and opportunities in large-scale deployment of automated energy consumption scheduling systems in smart grids. Chapter 8 concludes this thesis and identifies some future work directions for the research performed in this thesis.

Part I

Optimal Energy Storage Operation at the Transmission Grid

Chapter 2

Operation of Independent Large-Scale Battery Storage Systems in Energy and Reserve Markets with High Wind Penetration

In this chapter, we consider a scenario where a group of *investor-owned independently-operated* storage units seek to offer energy and reserve in the day-ahead market and energy in the hour-ahead market. We are particularly interested in the case where a significant portion of the power generated in the grid is from wind and other intermittent renewable energy resources. In this regard, we formulate a stochastic programming framework to choose optimal energy and reserve bids for the storage units that takes into account the fluctuating nature of the market prices due to the randomness in the renewable power generation availability. We show that the formulated stochastic program can be converted to a convex optimization problem to be solved efficiently. Our simulation results also show that our design can assure profitability of the private investment on storage units. We also investigate the impact of various design parameters, such as the size and location of the storage unit on increasing the profit.

2.1 Introduction

Due to their *intermittency* and *inter-temporal variations*, the integration of renewable energy sources is very challenging [14]. A recent study in [4] has shown that significant wind power curtailment may become inevitable if more renewable power generation resources are installed without improving the existing infrastructure or using energy storage. Other studies, e.g., in [5–7] have similarly suggested that energy storage can potentially help integrate renewable, in particular wind, energy resources. Although this basic idea has been widely speculated in the smart grid community, it is still not clear how we can encourage major investment for building large-scale independently-owned storage units and how we should utilize the many different opportunities existing for these units. Addressing these open problems is the focus of this chapter.

The existing literature on integrating energy storage into smart grid is diverse. One thread of research, e.g. in [15–17], seeks to achieve various social objectives such as increasing the power system reliability, reducing carbon emissions, and minimizing the total power generation cost. They do *not* see the storage units as independent entities and rather assume that the operation of energy storage systems is governed by a centralized controller. As a result, they do not address the profitability of investment in the storage sector and the possibility for storage units to participate in the wholesale market. Another thread of research, e.g., in [18–21], seeks to optimally operate a storage unit when it is combined and co-located with a wind farm. They essentially assume that it is the owner of the wind farm that must pay for the storage units. Clearly, this assumption may not always hold and it can certainly limit the opportunities to attract investment to build new energy storage systems. Finally, there are some papers, such as [21–25], that aim to select optimal strategies for certain storage technologies, e.g., pumped hydro storage units, to bid in the electricity market. However, they typically do not account for the uncertainties in the market prices which can be a major decision factor if the amount of renewable power generation is significant. Moreover, they do not consider the opportunities for the energy storage systems to participate in both energy markets and reserve markets. Finally, the operation of large storage units such as pumped hydro are different from that of *limited energy* storage units which are of interest in this work. While pumped hydro units are mostly limited to the discharge rate or the capacity of turbines, batteries are limited by the available sate of charge.

Therefore, the following question is yet to be answered: *How can an energy storage unit that is owned and operated by a private investor bid in both energy and reserve markets to maximize its profit, when there exists significant wind power penetration in the power grid?* The storage unit may or may not be collocated with renewable or traditional generators. In fact, the location and size of the unit is decided by investors based on factors such as land availability and spot price profile. In order to optimally operate the storage unit of interest, we propose a stochastic optimization approach to bid for energy and reserve in the day-ahead market and energy in the hour-ahead markets. Here, we assume a reserve market structure similar to a simplified version of the *day ahead scheduling reserve market* in the PJM (Pennsylvania, New Jersey, Maryland) inter-connection [10], where the exact utilization of the reserve bids is not decided by the storage unit; instead, it is decided by the market. As a result, finding the optimal charge and discharge schedules is particularly challenging when the storage unit participates in the *reserve* market. Another challenge is to formulate the bidding optimization problem as a convex program to make it tractable and appropriate for practical scenarios. Our contributions in this chapter can be summarized as follows.

- We propose a new stochastic optimization bidding mechanism for *independent* storage units in the day-ahead and hour-ahead *energy and reserve* markets. Our design operates the charge and discharge cycles for the batteries to assure meeting the future reserve commitments under different scenarios, regardless of the uncertainties that are present in the decision making process.

- An important feature in our proposed market participation model is that the power grid does *not* treat independent storage units any different from other energy and reserve resources. Therefore, our design can be used to encourage large-scale integration of energy storage resources without the need for restructuring the market.

- We show through computer simulations that our proposed optimal energy and reserve bidding mechanism is highly beneficial to independent storage units as it assures the profit gain of their investment. We also investigate the impact of various design parameters, such as the size and location of the storage unit on increasing the profit.

The rest of this chapter is organized as follows. The system model and the optimal bidding problem formulation are explained in Section 2.2. Two different tractable design

approaches to solve the formulated problems are presented in Section 2.3. Simulation results are presented in Section 2.4. The concluding remarks and future work are discussed in Section 2.5.

2.2 Problem Formulation

Consider a power grid with several traditional and renewable power generators as well as multiple independent energy storage systems. We assume that not only the generators but also the storage units can bid and participate in the deregulated electricity market. As pointed out in Section 2.1, our key assumption is that the storage units are not treated any differently from other generators that participate in the energy or reserve markets. Since the energy storage units in the system are owned and operated by private entities, they naturally seek to maximize their own profit. The stochastic wind generation, however, may create some extra benefits for storage units, considering that energy and reserve market prices may fluctuate significantly, giving them more opportunities to gain profit, in the presence of high wind power penetration. The assumption of high wind power penetration adds to the load forecast error component of the operating (day-ahead scheduling) reserve[1], since the wind generation is typically considered as part of the *net load*. With more fluctuations in the net load, the operating reserves are more likely to be called up frequently. We also assume that the storage unit operates as a price taker, i.e., it operates as a self-scheduling (must-run) unit and does not bid for price. Therefore, the storage unit will be compensated based on market clearing prices. Of course, at the time of bidding in the day ahead market, the storage unit does not know the actual prices, rather it only has an estimate of them. We also assume that the storage unit's operation does not have impact on market prices due to its typically lower size (in megawatts) compared to traditional generators.

The main decision variables of the storage unit in our system model are the energy and reserve quantities for different hours in the day-ahead market. However, the storage decisions and operation in the dayahead market and hour ahead (real time) market are highly tied together. The storage unit's bid in the day-ahead market has direct impact on

[1]Based on the market setup at PJM RTO, the reserves are procured on a day-ahead basis in order to ensure that differences in forecasted loads and forced generator outages do not negatively impact system reliability. At PJM, day-ahead scheduling reserve comprises load forecast error component and forced outage rate component [10].

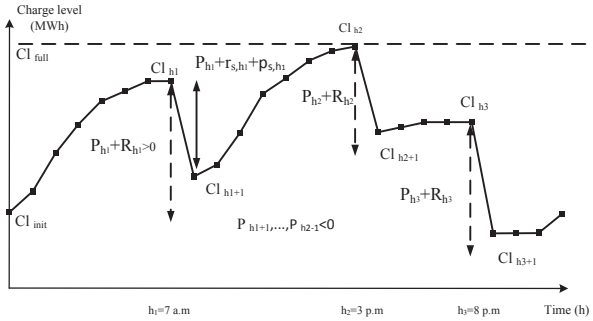

Figure 2.1: An example for the charge and discharge cycles for an independent storage unit when it participates in both energy and reserve markets.

the storage unit's future profit in the hour-ahead market, since the commitments in the day-ahead market will put some constraints in the charging and discharging profiles of the storage unit. An example for the charging and discharging cycles in the day-ahead energy and reserve markets is shown in Fig. 2.1, where the storage unit has committed to offer energy and reserve at three hours: $h_1 = 7{:}00$ AM, $h_2 = 3{:}00$ PM, and $h_3 = 8{:}00$ PM. In each case, the state-of-charge of batteries must reach a level $Cl_h \geq P_h + R_h$ for all $h \in \{h_1, h_2, h_3\}$.

When a storage unit bids for reserve at a particular hour of the day-ahead market, all, part of, or none of its committed reserve could be used. This will create *uncertainty in the charging level* of the storage unit; and depending on which value presumed for the utilization of reserve, the storage might have more or less charge available in real time. Therefore, even for the day-ahead market bidding, the storage unit should have some information on hour ahead operation model.

When an independent storage unit submits a bid to the day-ahead market (DAM), it seeks to maximize its profit in the day-ahead market *plus* the expected value of its profit in the next 24 hour-ahead markets (HAM). Therefore, prior to submitting the bids into day-ahead market, the storage unit should solve an operation optimization problem in both day-ahead and hour-ahead markets for all the services that it aims to provide. The services that we aim to consider here include: day ahead power, day ahead reserve, and hour ahead power[2]. Also the storage needs some estimation of the prices at hours $h = 1-24$ in both day

[2]The storage may also provide regulation service or synchronized reserve service in the hour-ahead (real-time) market. However, those scenarios are not considered in the formulation of this chapter.

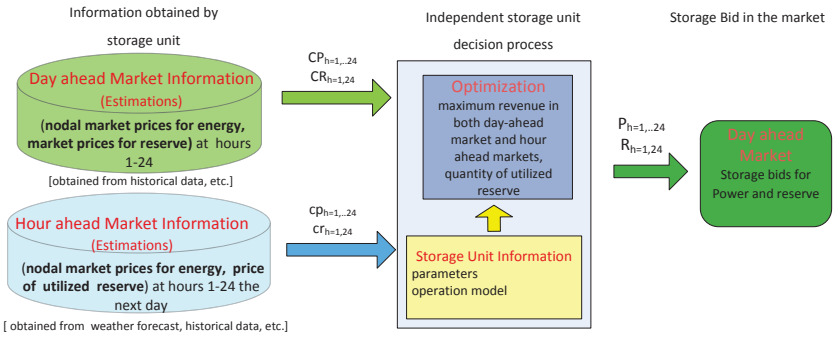

Figure 2.2: Overview of the input information and decision process for an independent storage unit that participates in the energy and reserve markets.

ahead and hour ahead markets. The prices of the hour ahead markets on the next day will have more uncertainty due to availability variation and uncertainty in wind generation. The decision process of storage and the input information required is illustrated in Fig. (2.2). This can be mathematically formulated as the following optimization problem[3]:

$$
\begin{aligned}
\underset{\mathbf{P},\mathbf{R},\mathbf{p}}{\textbf{Maximize}} \quad & \sum_{h=1}^{24}(P_h \cdot CP_h + R_h \cdot CR_h) \quad + \mathbb{E}\left\{HAM\big(\mathbf{p},\mathbf{P},\mathbf{R};\tilde{\mathbf{cp}},\tilde{\mathbf{cr}},\tilde{\mathbf{r}}\big)\right\} \\
\underset{\forall h=1,\cdots,24}{\textbf{Subject to}} \quad & \sum_{t=1}^{h}(P_t + \tilde{r}_t + p_t) \geq Cl_{init} - Cl_{full} \\
& \sum_{t=1}^{h}(P_t + \tilde{r}_t + p_t) \leq \ Cl_{init} - Cl_{min} \\
& R_h \geq 0.
\end{aligned}
\tag{2.1}
$$

Note that, $\mathbf{P}$ can take both positive and negative values while $\mathbf{R}$ is always positive. Negative values for $\mathbf{P}$ indicate purchasing power, i.e., charging. The expected value of the profit in the hour-ahead market, i.e., the second term in the objective function in (2.1), depends on not only the choices of $\mathbf{P}$ and $\mathbf{R}$, but also the storage unit's decision on the amount of power to be sold in the hour-ahead market p_h, the price of power in the hour-ahead market $\tilde{\mathbf{cp}}$, the price of reserve in the hour-ahead market $\tilde{\mathbf{cr}}$, the actual reserve utilization in the

[3]The formulation in (1) includes the basic, most dominant features of a storage unit. Other features such as storage efficiency, maximum charging current, and depreciation may also be included in the optimization problem.

hour-ahead market $\tilde{\mathbf{r}}$, and the fluctuations in wind generated. The third constraint assures that the reserve bid is non-negative. Note that, at the time of solving (1), $\tilde{cp}_h$, $\tilde{cr}_h$, and $\tilde{r}_h$, are *unknown stochastic parameters*.

Using the definition of mathematical expectation, we can rewrite the second term in (1) as a weighted summation of the aggregate hour-ahead profit terms, denoted by *HAM*, at *many* but *finite* scenarios, where the weight for each scenario is the probability for that scenario. That is, we can write

$$\mathbb{E}\left\{HAM\big(\tilde{\mathbf{p}}, \mathbf{P}, \mathbf{R}; \tilde{\mathbf{cp}}, \tilde{\mathbf{cr}}, \tilde{\mathbf{r}}\big)\right\} = \sum_{k=1}^{K} \gamma_k \, HAM_k, \tag{2.2}$$

where HAM_k denotes the aggregate hour-ahead profit when scenario k occurs. We have $\sum_{k=1}^{K} \gamma_k = 1$. It is worth clarifying that one of the main causes for profit uncertainty is the fluctuations in available wind power. Therefore, in our system model, each scenario is derived as a realization of available wind power at different wind generation locations, given the wind speed probability distribution functions, which is assumed to be available, e.g., by using the wind forecasting techniques in [26–28]. For each scenario k, the corresponding aggregate hour-ahead profit can be calculated as follows:

$$\begin{aligned}
\underset{\mathbf{p_k}}{\mathbf{Max}} \quad & HAM_k\big(\mathbf{p}, \mathbf{P}, \mathbf{R}; \mathbf{cp_k}, \mathbf{cr_k}, \mathbf{r_k}\big) = \\
\underset{\mathbf{p_k}}{\mathbf{Max}} \quad & \sum_{h=1}^{24} (p_{k,h} \cdot cp_{k,h} + r_{k,h} \cdot cr_{k,h}) \\
\underset{\forall h=1,\cdots,24}{\mathbf{S.t.}} \quad & \sum_{t=1}^{h} p_{k,t} \leq Cl_{init} - Cl_{min} - \sum_{t=1}^{h} (P_t + r_{k,t}) \\
& \sum_{t=1}^{h} p_{k,t} \geq Cl_{init} - Cl_{full} - \sum_{t=1}^{h} (P_t + r_{k,t}),
\end{aligned} \tag{2.3}$$

where $\mathbf{p_k}$ is the adjustment to the power draw or power injection of the storage unit in the hour-ahead market for $h = 1, \ldots, 24$, under scenario k. Here, $\mathbf{cp_k}$, $\mathbf{cr_k}$, and $\mathbf{r_k}$ are the actual realizations of the stochastic parameters $\tilde{\mathbf{cp}}$, $\tilde{\mathbf{cr}}$ and $\tilde{\mathbf{r}}$ when scenario k occurs. We note that they are all set by the grid operator. The constraint in (2.3) indicates that the total generation bid up to hour h of the hour-ahead market has to be limited to the total charge available to the storage unit at hour h. Such total charge is calculated as the initial charge minus the sum of all the power drawn from the storage including the bid for power,

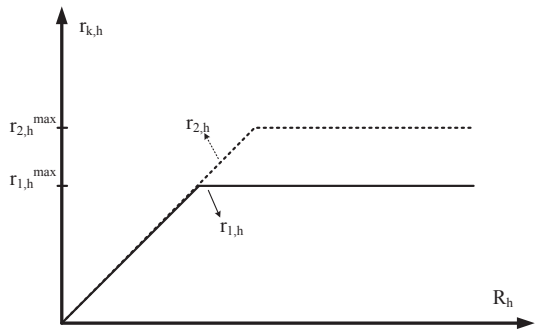

Figure 2.3: The exact utilization of the storage unit in the reserve market at hour h depends on two factors: First, the storage unit's committed reserve amount R_h. Second, the grid's need $r_{k,h}^{\max}$ under stochastic scenario k. Two examples for the value of $r_{k,h}$ as a function of R_h and $r_{k,h}^{\max}$ are shown in this figure.

i.e., P_h, and the reserve utilization in the hour-ahead market, i.e., $r_{k,h}$, for all previous hours $t = 1, \ldots, h-1$.

Note that, the actual reserve utilization $r_{k,h}$ may *not* always be as high as the committed reserve, as the grid may *not* need to utilize the entire reserve power offered by the storage unit. As a result, in the hour-ahead market, the storage unit needs to make *corrective decisions* to make the best use of any extra charge which is available due to different reserve utilizations caused by different wind availability and load scenarios. This makes dealing with parameter $r_{k,h}$ particularly complicated, as shown in Fig.2.3. Let $r_{h,k}^{\max}$ denote the maximum reserve power that the grid operator will need from the storage unit of interest at hour h if scenario k occurs. It is required that:

$$r_{k,h} \leq r_{k,h}^{\max} \qquad h = 1, \ldots, 24. \tag{2.4}$$

On the other hand, parameter $r_{k,h}$ also depends on the storage unit's reserve commitment for each hour h based on its bid in the day-ahead market. Therefore, it is further required that

$$r_{k,h} \leq R_h \qquad h = 1, \ldots, 24. \tag{2.5}$$

From (2.4) and (2.5), at each hour h and scenario k, we have:

$$r_{k,h} = \min\{r_{k,h}^{max}, R_h\}. \tag{2.6}$$

Replacing (2.6) in the hour-ahead problem (2.3), it becomes:

$$\begin{aligned}
\underset{\mathbf{p_k}}{\mathbf{Max}} \quad & \sum_{h=1}^{24}(p_{k,h}\cdot cp_{k,h}+\min\{r_{k,h}^{max},R_h\}\cdot cr_{k,h}) \\
\underset{\forall h}{\mathbf{S.t.}} \quad & \sum_{t=1}^{h}p_{k,t}+P_t+\min\{r_{k,t}^{max},R_t\}\leq Cl_{init}-Cl_{min} \\
& \sum_{t=1}^{h}p_{k,t}+P_t+\min\{r_{k,t}^{max},R_t\}\geq Cl_{init}-Cl_{full}
\end{aligned} \tag{2.7}$$

Next, we use the following equality [29]:

$$\sup_{x}\big(f(x)+\sup_{y}(g(x,y))\big)=\sup_{x,y}\big(f(x)+g(x,y)\big), \tag{2.8}$$

and combine problems (2.1) and (2.3) into a single problem:

$$\begin{aligned}
\underset{\mathbf{P},\mathbf{R},\mathbf{p}}{\mathbf{Max}} \quad & \sum_{h=1}^{24}(P_h\cdot CP_h+R_h\cdot CR_h)+\sum_{k=1}^{K}\gamma_k\sum_{h=1}^{24}(p_{k,h}\cdot cp_{k,h}+\min\{r_{k,h}^{max},R_h\}\cdot cr_{k,h}) \\
\underset{\forall h,k}{\mathbf{S.t.}} \quad & \sum_{t=1}^{h}p_{k,t}+P_t+\min\{r_{k,t}^{max},R_t\}\leq Cl_{init}-Cl_{min} \\
& \sum_{t=1}^{h}p_{k,t}+P_t+\min\{r_{k,t}^{max},R_t\}\geq Cl_{init}-Cl_{full} \\
& R_h\geq 0.
\end{aligned} \tag{2.9}$$

However, optimization problem (2.9) is non-convex and hence difficult to solve. Note that, the non-convexity is due to the way that the min function has appeared in the first constraint.

2.3 Solution Methods

In this section, we consider some practical assumptions in order to make problem (2.9) more tractable. In this regard, we take two approaches for choosing $p_{k,h}$ before solving the rest of the optimization problem. In both cases, we assume that the participation of the storage unit in the hour-ahead market is mainly to sell the *unused* charge from reserve bids. Therefore, for both approaches we always have $p_{k,h}\geq 0$.

2.3.1 The First Approach

In this approach, the intuition is that the storage unit *immediately* sells any excessive power available at each hour in case the entire committed reversed power is *not* utilized.

That is, at each hour h and for each scenario k, we choose

$$p_{k,h} = R_h - r_{k,h}. \tag{2.10}$$

The second term in the objective in problem (2.9) becomes:

$$\begin{aligned} &\sum_{k=1}^{K} \gamma_k \sum_{h=1}^{24} (R_h - r_{k,h}) \cdot cp_{k,h} + r_{k,h} \cdot cr_{k,h} \\ &= \sum_{k=1}^{K} \gamma_k \sum_{h=1}^{24} R_h \cdot cp_{k,h} \quad + (cr_{k,h} - cp_{k,h}) \cdot min\{r_{k,h}^{max}, R_h\}. \end{aligned} \tag{2.11}$$

Next, we note that based on (2.10), the total power sold in the hour-ahead market at hour h is:

$$\sum_{t=1}^{h} p_{k,t} = \sum_{t=1}^{h} (R_t - min\{R_t, r_{k,t}^{max}\}). \tag{2.12}$$

Therefore, the first constraint in problem (2.9) becomes:

$$\begin{aligned} &\sum_{t=1}^{h} p_{k,t} + P_t + min\{R_t, r_t^{max}\} \\ &= \sum_{t=1}^{h} R_t + P_t \leq Cl_{init} - Cl_{min}. \end{aligned} \tag{2.13}$$

The second constraint can also be revised as

$$\begin{aligned} &\sum_{t=1}^{h} p_{k,t} + P_t + min\{R_t, r_t^{max}\} \\ &= \sum_{t=1}^{h} R_t + P_t \geq Cl_{init} - Cl_{full}. \end{aligned} \tag{2.14}$$

From (2.9), (2.11), (2.13), and (2.14), we can rewrite problem (2.9) based on (2.10) and with respect to the rest of the variables as:

$$
\begin{aligned}
\underset{\mathbf{P},\mathbf{R}}{\mathbf{Max}} \quad & \sum_{h=1}^{24}(P_h \cdot CP_h + R_h \cdot CR_h) \\
& + \sum_{k=1}^{K}\gamma_k \sum_{h=1}^{24}\Big(R_h \cdot cp_{k,h} + (cr_{k,h} - cp_{k,h}) \cdot min\{r_{k,h}^{max}, R_h\}\Big) \\
\underset{\forall h=1,\ldots,24}{\mathbf{S.t.}} \quad & \sum_{t=1}^{h}(P_t + R_t) \geq Cl_{init} - Cl_{full} \\
& \sum_{t=1}^{h}(P_t + R_t) \leq \ Cl_{init} - Cl_{min} \\
& R_h \geq 0.
\end{aligned}
\tag{2.15}
$$

Since min is a convex function and the rest of the objective function and constraints are all linear, problem (2.15) is a convex program, as long as $cr_{k,h} - cp_{k,h} \geq 0$, for all $k = 1, \ldots, K$ and for all $h = 1, \ldots, 24$. Interestingly, this condition holds in most practical markets, where reserve utilization price is relatively higher than the energy clearing price. Therefore, we maintain this assumption for the rest of this chapter. If this condition holds, then optimization problem (2.11) can further be written as a linear program. To show how, next, we introduce an auxiliary variable $v_{k,h}$ and rewrite problem (2.15) as

$$
\begin{aligned}
\underset{\mathbf{P},\mathbf{R},\mathbf{v}}{\mathbf{Max}} \quad & \sum_{h=1}^{24}(P_h \cdot CP_h + R_h \cdot CR_h) + \\
& \sum_{k=1}^{K}\gamma_k \sum_{h=1}^{24}\Big(R_h \cdot cp_{k,h} + v_{k,h} \cdot (cr_{k,h} - cp_{k,h})\Big) \\
\underset{\forall h=1,\ldots,24}{\mathbf{S.t.}} \quad & v_{k,h} \leq r_{k,h}^{max} && \forall k = 1, \ldots, K \\
& v_{k,h} \leq R_h && \forall k = 1 \ldots, K \\
& v_{k,h} \geq 0 && \forall k = 1 \ldots, K \\
& \sum_{t=1}^{h}(P_t + R_t) \geq Cl_{init} - Cl_{full} \\
& \sum_{t=1}^{h}(P_t + R_t) \leq \ Cl_{init} - Cl_{min} \\
& R_h \geq 0.
\end{aligned}
\tag{2.16}
$$

where $\mathbf{v}$ is a $24\,K \times 1$ vector of all auxiliary variables. It is easy to show that at optimality, for all $k = 1, \ldots, K$ and any $h = 1, \ldots, 24$, we have $v_{k,h} = \min\{r_{k,h}^{max}, R_h\}$. Therefore, while problems (2.15) and (2.16) are *not* exactly the same, yet they are *equivalent*, i.e., they both lead to the same optimal solutions [29, Chapter 4]. As a result, solving one problem readily gives the solution for the other problem. Linear program (2.16) can be solved efficiently using the interior point method [29].

2.3.2 The Second Approach

In this approach, instead of immediately selling the excessive power $R_h - r_{k,h}$ at hour h, we may wait and sell accumulated unused reserve powers in an hour-ahead market with *high price* of electricity. We define an hour h^* as a "peak hour" if there does not exist any $h > h^*$ such that $cp_{k,h} > cp_{k,h^*}$. Based on the second approach, for each $k = 1, \ldots, K$ and $h = 2, ..., 24$, we select $p_{k,h}$ as follows:

- If h is not a peak hour then $p_{k,h} = 0$.
- If h is the jth peak hour, $j = 1, ..., \mathcal{P}$, then,

$$p_{k,h_j^*} = \sum_{h=h_{j-1}^*+1}^{h_j^*} (R_h - r_{k,h}). \tag{2.17}$$

At each peak hour, the amount of electricity sold is equal to the total unused reserve since the previous peak-hour. Next, we replace $p_{k,h}$ in (2.9) with selling strategy explained above. The second term in the objective function in problem (2.9) becomes

$$\sum_{k=1}^{K} \gamma_k \sum_{j=0}^{\mathcal{P}} \Bigg(\sum_{h=h_j^*+1}^{h_{j+1}^*} R_h \cdot cp_{k,h_{j+1}^*} + \min\{r_{k,h}^{max}, R_h\} \cdot (cr_{k,h} - cp_{k,h_{j+1}^*}) \Bigg), \tag{2.18}$$

where

$$0 = h_0^* < h_1^* < h_j^* < h_{\mathcal{P}}^* = 24. \tag{2.19}$$

Next, we note that from (2.17), we have

$$p_{k,h} \geq 0, \quad \forall k = 1, \ldots, K, \ h = 1, \ldots, 24, \tag{2.20}$$

and

$$\sum_{t=1}^{h} p_{k,h} + \min\{r_{k,t}^{min}, R_t\} \leq \sum_{t=1}^{h} R_t, \quad \forall k = 1. \tag{2.21}$$

Therefore, a *sufficient condition* for the first constraint in (2.9) to hold is to satisfy the following more restrictive constraint:

$$\sum_{t=1}^{h}(P_t + R_t) \leq Cl_{init} - Cl_{min} \qquad \forall h. \tag{2.22}$$

Next, consider the second constraint in (2.9). Given the complexity of this constraint, we need to separately analyze two different cases. On one hand, for each peak hour h_j^*, we have

$$\sum_{t=1}^{h_j^*} p_{k,t} = \sum_{h^* \in \{h_1^*,...,h_j^*\}} p_{k,h^*} = \sum_{t=1}^{h_j^*}(R_t - r_{k,t}). \tag{2.23}$$

By replacing (2.23) in the second constraint in (2.9) it becomes

$$\sum_{t=1}^{h_j^*} p_{k,t} + P_t + r_{k,t} = \sum_{t=1}^{h_j^*}(P_t + R_t) \geq Cl_{init} - Cl_{full}. \tag{2.24}$$

On the other hand, at each non-peak hour $h = h_j^* + 1, ..., h_{j+1}^* - 1$, since no power is sold in the hour-ahead market, we only need that the sum of the day-ahead power bids and the actual reserve utilization do not exceed the maximum charge level permitted for the batteries. The second constraint in (2.9) for each non-peak hour $h \in \{h_j^* + 1, ..., h_{j+1}^* - 1\}$ becomes

$$\begin{aligned} &\sum_{t=1}^{h} p_{k,t} + \sum_{t=1}^{h} P_t + \sum_{t=1}^{h} r_{k,t} \\ &= \sum_{t=1}^{h_j^*}(P_t + R_t) + \sum_{t=h_j^*+1}^{h}(P_t + r_{k,t}) \\ &\geq Cl_{init} - Cl_{full} \end{aligned} \tag{2.25}$$

From (2.9), (2.18), (2.22), (2.24), and (2.25) and after using the auxiliary variable vector $\mathbf{v}$, we propose to solve the following optimization problem as our second approach:

$$
\begin{aligned}
\underset{\mathbf{P},\mathbf{R},\mathbf{v}}{\mathbf{Max}} \quad & \sum_{h=1}^{24}(P_h \cdot CP_h + R_h \cdot CR_h)+ \\
& \sum_{k=1}^{K}\gamma_k \sum_{j=1}^{\mathcal{P}}\Bigg(\sum_{h=h_j^*+1}^{h_{j+1}^*} R_h \cdot cp_{k,h_{j+1}^*} + v_{k,h}\cdot(cr_{k,h} - cp_{k,h_{j+1}^*})\Bigg) \\
\underset{\forall k=1,\ldots,K}{\mathbf{S.t.}} \quad & \sum_{t=1}^{h} P_t + R_t \leq Cl_{init} - Cl_{min} \qquad \forall h = 1,\ldots,24 \\
& \sum_{t=1}^{h_j^*} P_t + R_t \geq Cl_{init} - Cl_{full} \qquad \forall h_j^* \in \{h_1^*,\ldots,h_{\mathcal{P}}^*\} \\
& \sum_{t=1}^{h} P_t + \sum_{t=1}^{h_j^*} R_t + \sum_{t=h_j^*+1}^{h} v_{k,t} \geq Cl_{init} - Cl_{full} \qquad \forall h_j^* < h < h_{j+1}^*, \;\; h_j^* \in \{h_1^*,\ldots,h_{\mathcal{P}}^*\} \\
& v_{k,h} \leq r_{k,h}^{max} \\
& v_{k,h} \leq R_h \\
& v_{k,h} \geq 0 \\
& R_h \geq 0.
\end{aligned}
\tag{2.26}
$$

Unlike problem (2.9), problem (2.26) is a convex program. Therefore, problem (2.26) is significantly more tractable as it can be solved using standard convex optimization techniques, e.g., see [29]. However, in general, solving problem (2.26) gives a sub-optimal (not necessarily optimal) solution for the original optimization problem (2.9) because of the following two reasons. First, the first constraint in (2.26) is more restrictive than the first constraint in (2.9). This can limit the feasible set. Second, there is no guarantee for problem (2.26) that at its optimality we have $v_{k,h} = \min\{r_{k,h}^{max}, R_h\}$. Therefore, it is possible that the optimal solution of problem (2.26) does not satisfy the second constraint in problem (2.9). In such rare cases, in order to maintain a feasible solution, the storage unit needs to sell any excessive stored energy into the hour-ahead energy market, even if the next hour is not a peak price hour. This corrective action can cause some minor sub-optimality. Nevertheless, we will see in our simulation results that the optimality gap of our second approach is very minor.

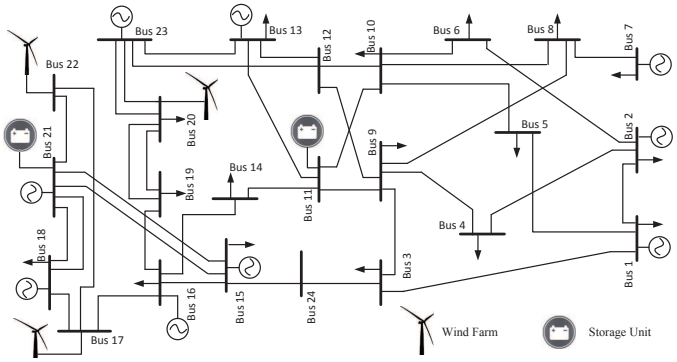

Figure 2.4: The IEEE 24 bus test system with independent storage units at buses 11 and 21. There are also three wind farms at buses 17, 20, and 22.

2.3.3 Selecting Stochastic Price Parameters

Before we end this section, we note that in order to solve problems (2.16) and (2.26), we must know the values of $r_{k,h}^{max}$, $cp_{k,h}$, and $cr_{k,h}$ as well as CP_h and CR_h. These parameters are obtained in an off-line calculation by solving a standard *stochastic unit commitment* (SUC), as explained in the Appendix. Once the SUC problem is solved, since the storage units are price-taker, we can calculate $cp_{k,h}$ from the Lagrange multipliers of the hour-ahead market constraints in the SUC problem. To calculate $cr_{k,h}$, we assume that it is proportional to $cp_{k,h}$. Next, we obtain CP_h using the definition of locational marginal price (LMP) and by comparing the SUC's optimal objective values *with* and *without* having an additional unit of load at each bus [30]. After that, we set CR_h equal to the reserve market clearing price, which is calculated based on the opportunity costs for generation units [31]. Here, we assume that the independent system operator (ISO), uniformly utilizes all available units which are deployed for reserve service. Therefore, parameter $r_{k,h}^{max}$ is obtained by dividing the total reserve utilization in each scenario by the total number of units that offer reserve. Note that, all these parameters could be obtained based on historical data on previous market operations, i.e., by following the standard procedure in solving SUCs for *different scenarios*. The obtained solutions are then placed in look-up tables to be used every time that problem (2.16) is solved by the independent storage unit.

2.4 Numerical Results

2.4.1 Simulation Setting and Experimental Data

In this section, we consider the modified IEEE 24-bus test system [32], as shown in Fig. 2.4. At any hour, the maximum total load in the system is 2850 MW. There are three wind farms with 150, 70, and 30 wind turbines at buses 22, 17, and 11, respectively. Each wind turbine is assumed to have a maximum generation capacity of 1.5 MW. Therefore, the wind penetration is about 13 percent. The wind speed across these three wind sites is assumed to be the same, due to relative proximity. The wind speed data was obtained from the Alternative Energy Institute Wind Test Center [33] for the duration of September-November 2012. The wind speed probability distribution curves, such as the one shown in Fig. 2.5, was derived separately for every hour of the day. Given the wind speed probability distribution curves, we generate 200 daily wind power generation scenarios for the purpose of our analysis. In order to make our simulations more realistic, 180 scenarios are used as *training scenarios* to run the standard SUC to obtain the price values used for the storage stochastic bidding optimization which can be thought of as *historical data*. The remaining 20 scenarios are used as *unseen test scenarios* to evaluate the actual operation of the storage unit, after it bids in the day-ahead market during its run time.

Two independent investor-owned 4.5 MWhs storage units are assumed at buses 21 and 11. The initial charge level for both units is 1.5 MW. The price values for the day-ahead and the hour-ahead markets are obtained from the standard SUC analysis that we explained in Section 2.2. The price curves for the day-ahead energy market, and the *average* prices in the hour-ahead energy markets across all scenarios, at bus 21, are shown in Fig. 2.6. Depending on the scenarios, the hour-ahead prices may go up to \$215/MWh. The price curves for the day-ahead market and for different scenarios of the hour-ahead market are used to set the storage bid for purchasing or selling of energy and reserve services in the day-ahead market.

2.4.2 Stochastic versus Deterministic Design

To understand the differences across different design methods, we start by showing the state-of-charge for each method in Fig. 2.4.2. The deterministic optimization method

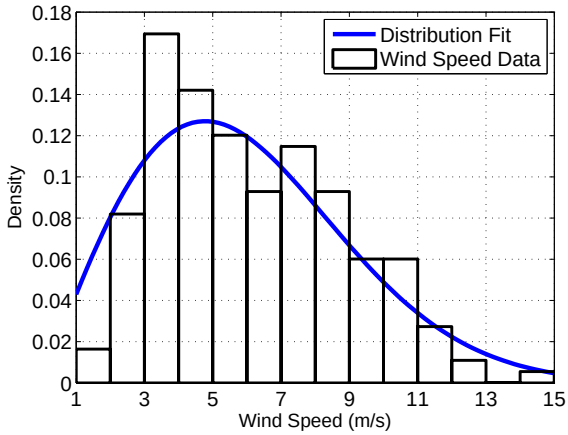

Figure 2.5: An example hourly wind speed distribution from empirical data.

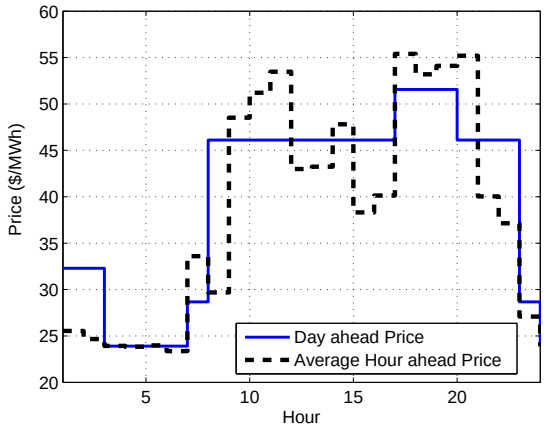

Figure 2.6: Day-ahead and average hour-ahead market prices at bus 21.

is intended to serve as a base for comparison, where we use the expected values of the hour-ahead market prices instead considering each random scenario separately. The two stochastic optimization approaches are those that we proposed in Sections 2.3.1 and 2.3.2, respectively. Note that, while the state-of-charge does *not* change across different scenarios when Approach 1 is used, it does change when Approach 2 is used as shown by different dashed lines for different scenarios in Fig. 2.4.2(c).

Table 2.1: Actual Hour-ahead Operation of the Storage Unit for 10 Unseen Test Scenarios

Scenario Number	**1**	**2**	**3**	**4**	**5**	**6**	**7**	**8**	**9**	**10**
Power Sold at Peak Hours (MW)	7.08	6.52	7.13	4.09	7.08	7.06	6.72	6.92	4.23	7.12
Power Sold at off-Peak Hours (MW)	0.93	0.46	0.88	0	0.89	0.95	0.70	0.63	0	0.61
Optimality Loss (%)	4.37	3.53	4.69	0	4.54	4.45	4.78	3.73	0	3.67

2.4.3 Optimality

Recall from Section 2.3.2 that our second approach may sometimes be sub-optimal due to the slight differences between the constraints in optimization problems (2.9) and (2.26). Therefore, in this section, we examine the optimality of the second approach. The results for 10 different unseen test scenarios are shown in Table 3.1. Here, the optimality loss was calculated based on the difference in the amount of revenue if the unused reserve power is sold only during the peak hours in the hour ahead market. We can see that for two scenarios, 4 and 9, the exact optimal solution was achieved as there was no need to sell power in any off-peak hour. For the rest of the scenarios, although the solution was sub-optimal, the optimality loss was very minor. On average, the optimality loss across all 10 scenarios is only 3.367%.

2.4.4 Day-ahead versus Hour-ahead Operation

In this section, we take a closer look at the operation of the storage unit in the day-ahead and the hour-ahead markets based on an example solution that we obtained by using our second approach. The day-ahead energy and reserve bids in this example are shown in Fig. 2.8(a). Here, any negative bar indicates charging of the batteries in an hour h, where $P_h < 0$ and $R_h = 0$. In contrast, any positive bar indicates discharging of the batteries in

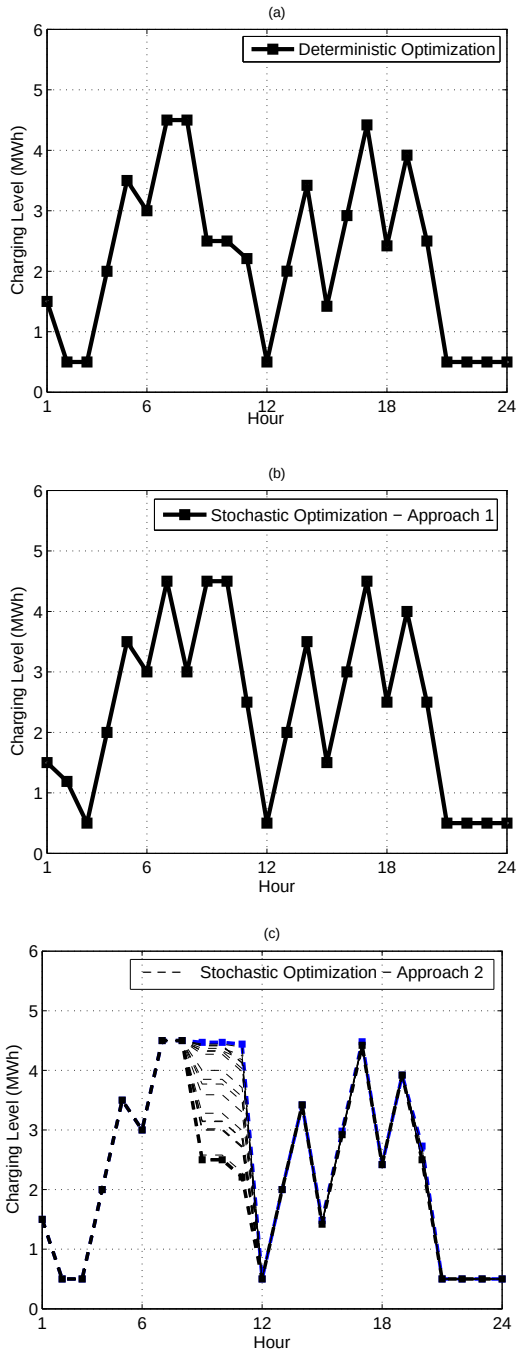

Figure 2.7: Comparing the state-of-charge when a deterministic optimization as well as our two proposed stochastic optimization designs are implemented. (a) The state-of-charge level when a deterministic optimization design is used. (b) The state-of-charge level when a stochastic optimization design based on our first approach is used. (c) The state-of-charge level when a stochastic optimization design based on our second approach is being used.

an hour h, where $P_h \geq 0$ and $R_h \geq 0$. Recall that the exact utilization of the reserve power and the amount of power sold in the hour-ahead market are determined later during the operation time. Therefore, different operation scenarios can lead to different outcomes when it comes to the participation of the storage unit in the hour-ahead market. Three examples based on three different scenarios are shown in Figs 2.8(b) and (c). We can see that, at each hour, the amount of reserve that is sold in the hour-ahead market is always limited by the amount of reserve that the storage unit is committed to in the day-ahead market, i.e., $r_{r,h} \leq R_h$ for any scenario k. Moreover, the unused reserve power that is sold in the hour-ahead market, i.e., $p_{h,k}$, is almost always sold during the peak-hours to maximize the storage unit's profit.

2.4.5 Impact of Increasing the Storage Capacity

The daily revenue obtained using various design approaches are shown in Fig. 2.9, where the storage capacity grows from 4.5 MW to $4.5 \times 10 = 45$ MW. We can see that both stochastic optimization approaches outperform deterministic optimization while the second stochastic optimization approach outperforms the first stochastic optimization approach. The performance gains maintain across all storage capacity scenarios. When the storage size is as high as 50 MW, the merit of using our proposed approaches become particularly evident.

2.4.6 Optimal Storage Capacity Planning

The results in Fig. 2.9 can also be used for *optimal capacity planning* of investor-owned storage units by examining both revenue and cost. This issue is better illustrated in Fig.2.10, where we have plotted the net daily profit, i.e., the revenue minus the cost, versus the size of the storage units. The battery investment cost was obtained per cycle of charge and discharge for units with WB-LYP1000AHA lithium ion 1000 Ah battery modules with 3.2V discharge voltage [34]. The life time of the batteries was assumed to be 12000 cycles and the listed price was \$1660 per module which we assumed to decrease to \$1000 as more batteries are installed. We can see that there is a trade-off between revenue and cost and the optimal profit can be reached for certain sizes of the storage system.

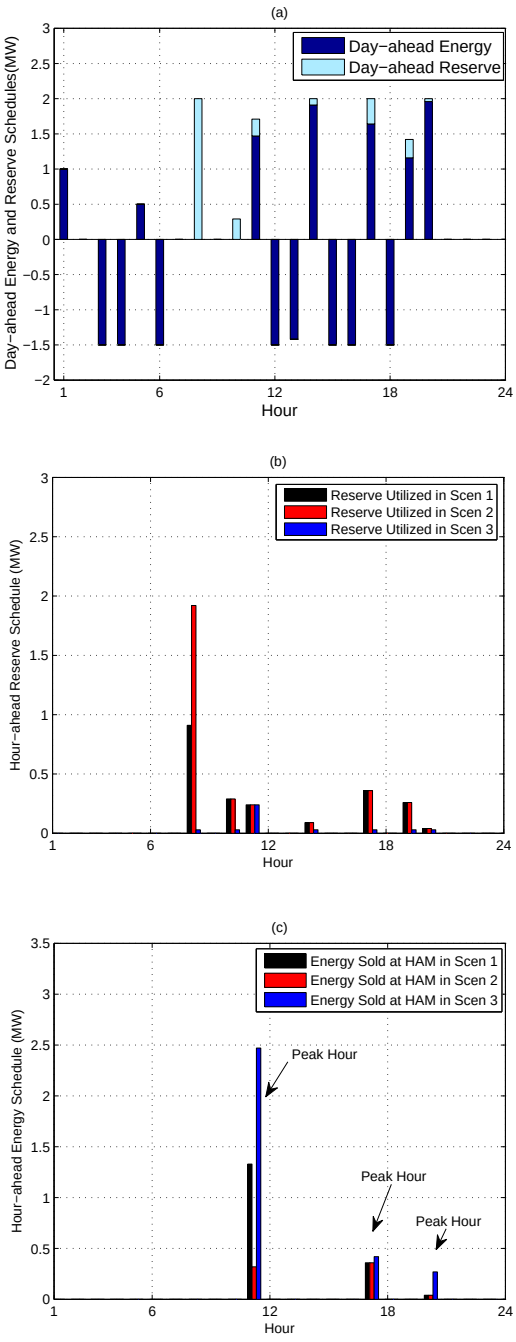

Figure 2.8: A detailed example for the operation of the storage unit based on our second approach: (a) Day-ahead energy and reserve schedules. Reserve bids are submitted only when the storage unit can be discharged. (b) Hour-ahead reserve schedule for three different unseen test scenarios. At each hour, the amount of reserve that is sold in the hour-ahead market is always upper bounded by the amount of reserve that the storage unit is committed to in the day-ahead market. (c) Hour-ahead energy schedule for the same three unseen test scenarios. The unused reserve power is typically sold during peak hours.

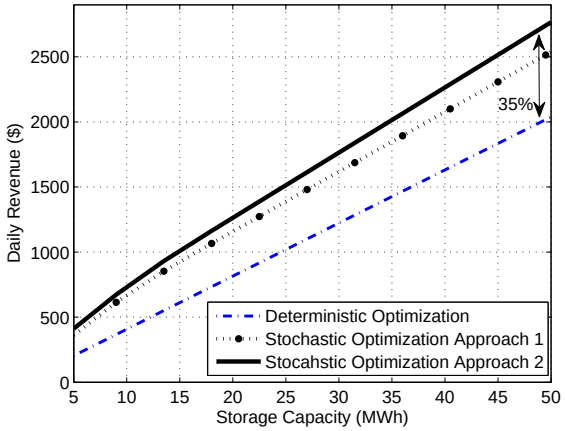

Figure 2.9: The daily revenue of an independent storage unit versus its storage capacities for various choices of deterministic and stochastic design schemes.

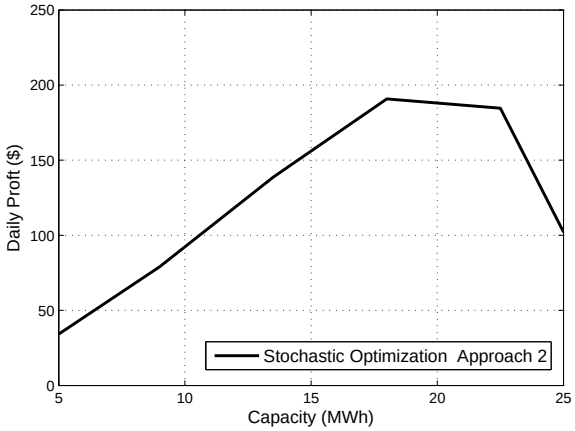

Figure 2.10: The trade-off in selecting the storage capacity to maximize profit.

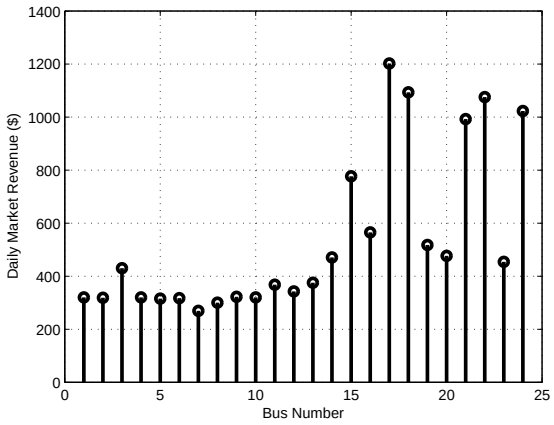

Figure 2.11: The daily profit of an independent storage unit at different buses. In all cases, the first stochastic optimization approach is being used.

2.4.7 Impact of Location

Next, we investigate the impact of location for the storage unit with respect to the revenue achieved. In this regard, we run the simulations for 24 different scenarios, each for a case where the storage unit is assumed to be located at one of the 24 different buses in the system. The results are shown in Fig. 2.11. We can see that different buses provide different opportunities for the storage units, making it more desirable to build the storage unit at certain locations. The differences are mainly due to changes in the LMP's at different buses which is caused by different line congestion scenarios. In our study, in order to see the effect of line congestions, the capacity of some of the 500 MW transmission lines of the standard test system was reduced to 200 MW. Note that, the results in Fig. 2.11 are based on the first stochastic optimization approach, i.e., by solving optimization problem (2.16). That is, we separately obtained the optimal bids and charge/discharge schedules for the case of placing the storage unit at each of the buses. As an example, the charging level when the storage unit is located at buses 21 and 11 are separately plotted in Fig. 2.12.

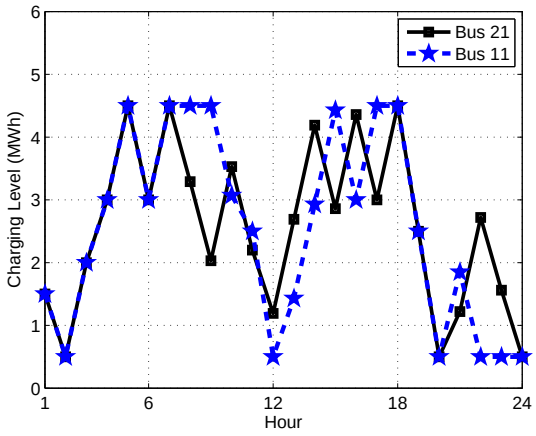

Figure 2.12: The charging level when operating two independent storage units at buses 11 and 21 using the second stochastic optimization approach is used.

2.5 Conclusions

Integration of large-scale storage systems in the power system is a key component of the future smart grids. In this chapter, a novel approach is proposed to optimally operate such storage systems that are owned by independent private investors. In particular, we proposed an optimal bidding mechanism for storage units to offer both energy and reserve in the day-ahead and the hour-ahead markets when significant fluctuation exists in the market prices due to high penetration of wind and intermittent renewable energy resources. Our design was based on formulating a stochastic programming framework to select different bidding variables. We showed that the formulated optimization problem can be transformed into convex optimization problems that are tractable and appropriate for implementation. We showed that accounting for the unpredictable feature of market prices due to wind power fluctuations can improve the decisions made by large storage units, hence increasing their profit. We also investigated the impact of various design parameters, such as the size and location of the storage unit on increasing profit.

Chapter 2, Appendix I: Stochastoc Unit Commitment

First, we explain the new set of notations that we need in order to formulate and solve the standard stochastic unit commitment problem. $C(.)$ denotes the cost of a particular

service. $Com_{i,h}$ denotes commitment of ith unit in hour h. $P_{i,h}$ denotes generation of ith unit in hour h. $R_{i,h}$ denotes reserve commitment of ith unit in hour h. P_i^+ denotes maximum capacity of ith unit. P_i^- denotes minimum capacity of ith unit. $Ramp_i^+$ denotes maximum ramp up of ith unit. $Ramp_i^-$ denotes maximum ramp down of ith unit. G_f denotes subset of fast generators. $p_{i,k,h}$ denotes generation of ith fast unit in the hour ahead market for hour h and scenario k. $r_{i,k,h}$ denotes reserve usage of ith unit in the hour ahead market for hour h and scenario k. $NL_{k,h}$ denotes the total *net load* in hour h of scenario k which is the actual demand minus the wind power generation. Given these notations and parameters, we can now formulate the standard SUC as follows, in which the realization scenarios are considered in order to minimize the the expected value of the unit commitment cost in the system:

$$
\begin{aligned}
\underset{Com,P,R,p_k,r_k}{\textbf{min}} \quad & \sum_h \sum_i C_{Com_i}.Com_{i,h} + C_{P_i}.P_{i,h} + C_{R_i}.R_{i,h} \\
& + \sum_k \gamma_k \sum_h \sum_i (c_{p_i} \cdot p_{i,k,h} + c_{r_i} \cdot r_{i,k,h}) \\
\textbf{s.t.} \quad & P_{i,h} + R_{i,h} \leq P_i^+ \; Com_{i,h} && \forall i,h \\
& P_{i,h} + R_{i,h} \geq P_i^- \; Com_{i,h} && \forall i,h \\
& P_{i,h}, R_{i,h} \geq 0 && \forall i,h \\
& P_{i,h} - P_{i,h-1} \leq Ramp_i^+ && \forall i,h \\
& P_{i,h-1} - P_{i,h} \leq Ramp_i^- && \forall i,h \\
& \sum_i P_{i,h} + p_{i,k,h} + r_{i,k,h} = NL_{k,h} && \forall\, h,k \\
& 0 \leq r_{i,k,h} \leq R_{i,h} && \forall i,k,h \\
& 0 \leq p_{i,k,h} \leq p_i^+ && \forall i \in G_f,k,h \\
& p_{i,k,h} - p_{i,k,h-1} \leq Ramp_i^+ && \forall i \in G_f,k,h \\
& p_{i,k,h-1} - p_{i,k,h} \leq Ramp_i^- && \forall i \in G_f,k,h \\
& Com_{i,h} \in \{0,1\} && \forall i,k,h
\end{aligned}
\tag{2.27}
$$

The above SUC is a mixed integer program. In general, mixed integer programs are difficult to solve, although some classes of mixed integer programs can be solved, e.g., using MOSEK and CPLEX software [4]. Alternatively, we can relax the binary constraint, solve problem (2.27) which is a convex optimization problem after the binary constraints are relaxed, and then set $Com_{i,h} = 1$ for any i and h with highest $Com_{i,h}$. If we repeat this operation

until any $Com_{i,h}$ in the solution is either zero or one, we can obtain a feasible but sub-optimal solution for the original problem (2.27). We used this latter approach. Given the solution and the Lagrange multipliers corresponding to each constraint, the needed system parameters are calculated accordingly, as we have already explained at the end of Section **??**. Note that the above problem is solved in centralized fashion. We also note that, since the storage units are assumed to have no impact on prices, this optimization problem does not include any variable from the storage units.

2.6 List of Symbols, Chapter 2

h, t Indices for hours.

k Index of random wind generation scenarios.

K Total number of random wind generation scenarios

γ The weight/probability for different scenarios.

$\mathbb{E}$ Expected value operator.

P Storage bid in the day-ahead market for power.

R Storage bid in the day-ahead market for reserve.

p Storage bid in the hour-ahead market for power.

r Actual utilization of the storage reserve.

r^{max} The upper bound for reserve utilization.

CP Price value for energy in the day-ahead market.

CR Price for reserve in the day-ahead market.

cp Price for energy in the hour-ahead market.

cr Price for reserve utilization in the hour-ahead market.

Cl_{init} Initial charging level of the battery unit.

Cl_{full} Maximum charging capacity of the battery unit.

Cl_{min} Minimum charging capacity of the battery unit.

h_j^* The jth hour from the set of peak price hours.

$\mathcal{P}$ The total number of peak price hours.

Chapter 3

A Joint Bidding and Operation Strategy for Battery Storage in Multi-temporal Energy Markets

In this chapter, we provide a method to determine the optimal schedule and market bids of a battery storage, to maximize revenues from joint operation in day-ahead/ real-time markets. Our model considers financial risk of revenues in both markets and defines battery optimal bids in the two stages of the market, to obtain maximum profit with controlled risk by adapting the Markowitz portfolio selection theory. In the second stage of our framework, a receding horizon algorithm in real-time, updates the predictions of joint profit as well as financial value at risk, and improves the optimal battery schedule accordingly. Our approach has a key feature of tractability, as it is formulated as a convex problem, by several modelling and relaxation techniques. This model enables us to quantify the trade-off between revenues from each markets and the risk of revenues in return.

3.1 Introduction

In most ISO structures, there are opportunities for Energy Storage Systems (ESS), even for mid-sized batteries, to provide services, directly in the bulk market. These opportunities for ESS, and for battery storage in particular, when they attempt to offer services competitively in the market, as well as the challenges they face in defining bidding strategies

and operation schedules, yet needs to be further explored.

In the context of battery ESS, few works have looked into opportunities and challenges of offering services in energy markets jointly; i.e., few works addressed the question *"what are the possible revenues for a battery ESS in day-ahead, real-time markets, and how to optimally bid in both markets and operate battery ESS to maximize market profit?"* Several previous works (e.g., in [35–38]), try to obtain special unit commitment and dispatching plans for the ISO while ESS are present. In practice, ISO is not involved in operational constraints of each and every ESS technology.

A thread of papers, e.g. those in [39–43] have tied the ESS operation with a secondary generation source (e.g., a wind source or a gas turbine). In the authors viewpoint, however, the ESS operation and bidding should not necessarily be coupled with other units. An ESS can independently and modularly manage, operate, and offer services to the market, or third parties.

Additionally, all named papers, consider the operation of ESS only in either the day-ahead (DAM) or real-time (RTM) market. The cross market revenues, and the two-sided impact of RTM and the DAM operations, for Battery ESS, are not considered in such works. In this regard, the authors of [44, 45] developed a stochastic bidding strategy to account for next-day real-time operations and coordinate offers in advance, and obtained the best schedules of DAM. Their work, however, is limited to day-ahead schedules and they do not look into the reverse problem which is optimal operation in real-time market with consideration of previous commitments.

In this work, we aim to offer a complete framework, including the best offer strategies in both day-ahead and real-time markets, and coordinate the battery schedule accordingly. We propose to investigate an optimal operation and scheduling strategy for battery ESS to participate in the joint energy markets structure, i.e. day-ahead/ real-time markets. Based on these combined offers, optimal suggested schedule of battery ESS is obtained in real-time to attain the maximum revenues.

Fig.3.1 shows an example of DAM and RTM clearing prices. Participation across day-ahead and real-time markets with different price features is challenging. Although day-ahead and real-time markets are held separately, the goal of battery is to obtain the most revenues in both markets, since limited battery resources tie the operation in these two markets as the DAM and the RTM operations are jointly dependent.

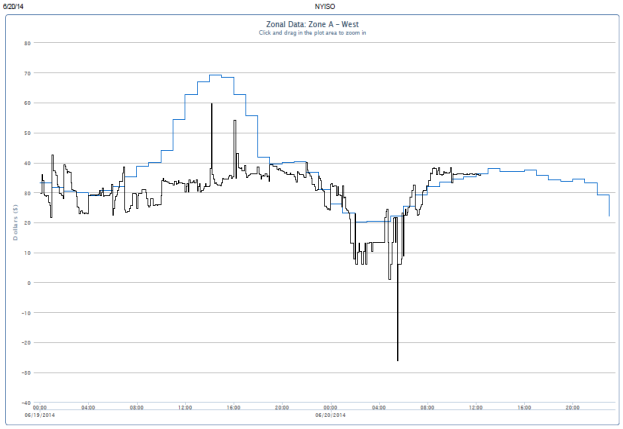

Figure 3.1: An example of day-ahead versus real-time market clearing prices in one zone of NY-ISO. Clearly prices have essential different features. Defining the battery ESS optimal bidding and operation strategy across the two markets with such prices, is the focus of this chapter.

In addition to the joint market optimization, a receding time horizon optimization, is derived that updates input information in the operating-day continuously as new forecasts, etc. becomes available and updates ESS decisions accordingly. In the presented framework, the Value-at-Risk of revenues due to errors in forecasts is calculated and controlled, throughout both stages of optimization in DAM and RTM.

Finally, all market formulation and battery modelling are convex and the problem can be solved effectively in real-time.

3.2 Storage Joint Market Operations

In this section we discuss the framework of the battery operations and bids/offers, based on joint markets revenues. In this design, battery ESS participate in both day-ahead and real-time markets to attain maximum revenues across both markets. Therefore, our design consists of two parts;

- A) In the day-ahead market operations, the battery ESS day-ahead problem is analysed and the optimal day-ahead market bids/offers are obtained. The objective here is to maximize the joint profit of ESS, including the forecast revenues in real-time market

which are stochastic. To account for uncertainty of such revenues, we restrict the Value at Risk (VaR) from those revenues.

- B) In the operating day, as the real-time market operations moves forward, the second part of our design continuously updates the ESS bids/offers in real-time market based on the most recent forecast of market price, using a receding horizon optimization. The optimal offers and battery schedule here is obtained by considering previous commitments of the ESS. Also the target VaR is updated to have limited risk of revenues at all times.

Fig. (3.2) shows an outline of the proposed framework for battery ESS joint market bidding and operation. The inputs to both modules of the ESS optimizer are the forecasts of DAM and RTM prices, and battery ESS parameters. Note the actual prices are not known at the time of decision. Hence, ESS utilizes any forecast of these prices available prior to its decision. In ESS day-ahead operations, battery decides over the optimal DAM offers, based on day-ahead forecasts of the RTM and DAM prices. From forecasts, we obtain revenues from future operations as well as current operations. Similarly, in operating-day, the ESS continuously updates its real-time forecasts of the RTM prices, and updates the ESS offers and schedule accordingly.

We should make this general notion that, all the discussions in this work assume that the battery ESS is a *price-taker*. Next, we discuss details of the two part proposed design separately in Sec. 3.3 and 3.4.

3.3 Day-ahead Market Operations

The bulk of energy sales are performed in day-ahead market. Each unit obtains the right to generate or consume the awarded quantity of energy in DAM, at day-ahead prices. Generating units however, can preserve a portion of their actual capacity to sell in the real-time market. A battery ESS unit can as well, participate in both markets and post bids for energy at different hours. The ESS revenues however, depends directly to the prices of the market. Market prices are not known at day-ahead. At day-ahead operation stage, both day-ahead prices and real-time prices are unknown. The ESS obtains forecasts of market prices, thereby forecast of revenues. Storage decides what is the best schedule for

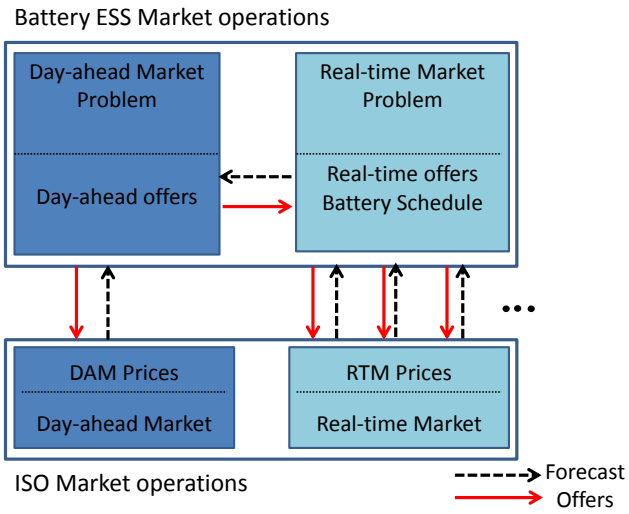

Figure 3.2: Illustration of joint market operations for battery ESS. Battery coordinates offers in day-ahead/real-time markets for most revenues in both markets. The day-ahead problem accounts for future real-time operations and future revenues based on day-ahead forecasts of RTM and DAM prices.

ESS and declares the DAM offers at different hours based on current forecast of prices. It also considers the possible real-time operations that may increase the battery ESS revenues. In the day-ahead operations, the battery ESS solves optimization (3.1) to obtain the optimal day-ahead bids/offers for energy, in hours $h = 1, ..., 24$ of the following day, denoted by vector of $\mathbf{P}_{DAM}$.

$$\begin{aligned} J^{f(DA)} = \underset{\mathbf{P}_{DAM}}{\mathbf{Max}} & \sum_{t=1}^{24} \Big(\ Rev.^{f(DA)}[t] - \ Cost[t] \Big) \\ \underset{\forall t \in \{1,\cdots,24\}}{\mathbf{S.\ t.}} & \quad ESS\ Operation\ Lmt.\ [t] \\ & \quad ESS\ Revenue\ Risk\ Lmt.^{f(DA)} \end{aligned} \tag{3.1}$$

ESS Revenue Risk Lmt.$^{f(DA)}$ denotes the risk in ESS revenues due to uncertainty of real-time operations. In an arbitrary time period, a positive $P_{DAM}[t]$ denotes a power generation offer, whereas a negative one denotes a power consumption bid. $\mathbf{P}_{DAM}$ is only a *financial binding offer*; i.e only defines ESS purchase/sell rights at DAM prices in the following day. The storage costs, is defined based on storage actual generation, which we denote by P_G. Similarly, storage operation constraints is dependent *only* on P_G.

3.3.1 Day-ahead Forecast of ESS Revenues

The ESS forecast revenues at time $[t]$ from both DAM and RTM operations can be obtained by:

$$Rev.^{f(DA)}[t] = P_{DAM}[t]\lambda^{f(DA)}_{DAM}[t] + P_{RTM}[t]\lambda^{f(DA)}_{RTM}[t] \tag{3.2}$$

To obtain ESS costs and operation constraints in (3.1), we used auxiliary variable $P_G[t]$. In each time period $[t]$, the following equality exists between the ESS day-ahead power bid/offer, real-time bid/offer, and the actual power injection:

$$P_G[t] = P_{DAM}[t] + P_{RTM}[t] \tag{3.3}$$

Therefore from (3.3) we substitute $P_{DAM}[t]$ and rewrite (3.2) as:

$$\begin{aligned} Rev.^{f(DA)}[t] &= (P_G[t] - P_{RTM}[t])\lambda^{f(DA)}_{DAM}[t] + P_{RTM}[t]\lambda^{f(DA)}_{RTM}[t] \\ &= P_G[t]\lambda^{f(DA)}_{DAM}[t] + P_{RTM}[t](\lambda^{f(DA)}_{RTM}[t] - \lambda^{f(DA)}_{DAM}[t]). \end{aligned} \tag{3.4}$$

In fact, the ESS joint revenues in (3.4) are decomposed into two terms; one obtained from providing actual generation at DAM prices. The second part is revenues from altering the ESS schedule due to price differences of DAM and RTM.

3.3.2 Day-ahead Forecast of Revenue Risk

Let us get back to the revenue forecasts of battery ESS in day-ahead problem, i.e. in (3.4). This equation actually denotes the average value of the revenues. However, the price forecasts of both day-ahead and real-time markets are uncertain values and random. Therefore, we actually have a *distribution function* for battery ESS revenues. Here, we assume that the forecasts of DAM prices are trusted much more, compared to the RTM price forecasts. In other words, we assume the forecast error of DAM prices in day-ahead are negligible compared to RTM price forecasts.

In finance, the Value at Risk (VaR) is a widely used measure, to asses and control the risk of loss on financial assets. Several prior studies have used this measure in other areas of energy management. The VaR function is defined as:

$$VaR_{\zeta}(Rev.) = inf\{\mathcal{R}_0 | Pr(Rev. > \mathcal{R}_0) \leq 1 - \zeta\} \tag{3.5}$$

where the $VaR_{\zeta}(Rev.)$ is the minimum revenue at probability $(1-\zeta)$. For a Gaussian distribution, we can obtain a simpler inequality in term of distribution function of revenues, e.g. if we have $\zeta = \%2$ we can write (3.5) as:

$$VaR_{\%2} = F^{-1}_{Rev.}(\zeta = 0.02) \approx \mu(Rev.) - 2\sigma(Rev.) \tag{3.6}$$

Therefore, here we assume that the forecast error of RTM prices are i.i.d Gaussian functions with $\mathcal{N}(0, \mathbf{\Lambda}^{f(DA)}_{RTM})$. Again, for simplicity and without loss of generality, we only limit the risk of stochastic revenues, considering that they have no cost for battery. In order to have a positive VaR we need to have the right hand side of (3.6) to be positive, i.e. we have:

$$\mathbf{P}^{\intercal}_{RTM}(\lambda^{f(DA)}_{RTM} - \lambda^{f(DA)}_{DAM}) - 2(\mathbf{P}^{\intercal}_{RTM}\mathbf{\Lambda}^{f(DA)}_{RTM}\mathbf{P}_{RTM})^{1/2} \geq 0 \tag{3.7}$$

3.3.3 ESS Costs

As pointed out earlier, the costs of generation in both day-ahead and real-time problems depend only on actual injection $P_G[t]$. The cost of providing energy in our model has two parts; cost of cycling, and cost of charging/discharging at high current rates. There are several complex non-linear models for wear costs of the battery. In order to preserve the tractability of the formulation, cost of battery is modelled as a peace-wise linear function to incorporate these two elements.

$$Cost[t] = \{ \begin{matrix} \alpha_1|P_G| & if \quad |P_G[t]| < P_{0.5C} \\ \alpha_1|P_G| + \alpha_2|P_G - P_{0.5C}| & if \quad |P_G[t]| \geq P_{0.5C} \end{matrix} \tag{3.8}$$

3.3.4 ESS Operation Limits

Storage operation limits in (3.1), depends on ESS actual injection $P_G[t]$. Therefore, for the optimization problem solved in both day-ahead and real-time, the following constraints should hold in all time intervals of $t \in \{1, \cdots, T\}$:

$$P_{DAM}, P_{RTM}, P_G[t] \in [P_{min}, P_{max}] \tag{3.9a}$$

$$SoC[t] \in [SoC_{min}, SoC_{max}] \tag{3.9b}$$

$$SoC[t] = SoC[t-1] - P_{dc}[t]\Delta t \tag{3.9c}$$

$$SoC[T] = SoC[0] + \Delta \tag{3.9d}$$

$$P_{dc}[t] = \mathbf{max}\{\eta_0 P_G[t], (1/\eta_0)P_G[t]\} \tag{3.9e}$$

Note that $P_{dc}[t]$ is an equality constraint in form of a convex function with respect to $P_G[t]$. However, in regular convex programming, a convex problem has only linear equality constraints, and all the non-linear constraints are in the form of $g(\mathbf{x}) \leq a$ where g is a convex function. Therefore, we relax the equality constraint by inequality constraints. We observe that the relaxation optimality gap is negligible in most cases.

3.4 Real-time Market Operations

ISO runs the real-time market continuously throughout the operating-day. In this work, we assume 1 *hour* intervals for real-time market. Battery ESS has the option to change its schedule throughout the day, when new forecasts of the current and future RTM prices becomes available. ESS solves its joint market problem again, when it receives new forecasts with less error, and corrects the optimal strategy accordingly.

Let us assume that ESS receives a new forecast of RTM price, at *every* hour h. Obviously, ESS cannot decide or change any of its previous activities; therefore, as the operating day auctions moves forward the number of variables decrease, i.e., the horizon recedes. In contrast, since the storage has the chance to alter future schedules, at each auction time interval h it only needs to submit offer for immediate next hour, i.e. $P_{RTM}[h]$.

At each hour, $P_{RTM}[h] = \mathbf{P}_{RTM}^{f(h)}(1)$, i.e. the first element of our optimization decision vector, which is best ESS schedule for all the time periods starting from and after $[h]$. Size of $\mathbf{P}_{RTM}^{f(h)}$ decrease as h increase; i.e. $\mathbf{P}_{RTM}^{f(h)} = [P_{RTM}[h], P_{RTM}[h+1], \cdots, P_{RTM}[T]]$. Optimization is continuously updated as we proceed in time. In each time h we have to solve for maximum $J^{f(h)}$ according to current forecasts:

$$\begin{aligned} J^{f(h)} = \underset{\mathbf{P}_{RTM}^{f(h)}}{\mathbf{Max}} & \sum_{t=h}^{T} \Big(Rev.^{f(h)}[t] - Cost[t] \Big) \\ \underset{\forall t \in \{h, \cdots, T\}}{\mathbf{S.\ t.}} & \quad ESS\ Opr.\ Lmt.\ [t] \\ & \quad ESS\ Rev.\ Risk\ Lmt.^{f(h)} \end{aligned} \tag{3.10}$$

where for instance $Rev.^{f(h)}[t]$ denotes the *forecast* of ESS joint revenues at time $[t]$, available at decision time $[h]$.

3.4.1 Real-time Forecast of ESS Revenues

Since ESS has already made some commitments in DAM, the real-time offers/bids are obtained directly, if ESS obtains the real-time decision on actual power generation $P_G[t]$. Therefore, we can formulate optimization (3.10) based on decision variable $\mathbf{P}_G^{f(h)}$, the real-time forecast in time $[h]$, of all ESS revenues, in the remaining horizon, i.e., $\forall t \in \{h, \cdots, T\}$ is obtained by:

$$\begin{aligned} Rev.^{f(h)}[t] &= P_{RTM}[t]\lambda_{RTM}^{f(h)}[t] \\ &= (P_G[t] - P_{DAM}^*[t])\lambda_{RTM}^{f(h)}[t] \\ &= P_G[t]\lambda_{RTM}^{f(h)}[t] + P_{DAM}^*[t](-\lambda_{RTM}^{f(h)}[t]) \end{aligned} \tag{3.11}$$

$P_{DAM}^*[t]$ is ESS optimal offer in day-ahead market, at time step $[t]$. Since the ESS day-ahead offers are already known in real-time market, the second term in (3.11) can be treated as a constant part of the objective function. However, as we will see shortly, $P_{DAM}^*[t]$ has impact on ESS revenue risk.

3.4.2 Real-time Forecast of ESS Revenue Risk

As mentioned, we limit the VaR in day-ahead market, from all revenues obtained from *future operations*, i.e., from P_{RTM}. Since our target level of *total revenues* risk is determined in DAM, we should define the risk constraints in real-time market in accordance with our original target risks.Similar to day-ahead, we assume an i.i.d Gaussian distribution with $\mathcal{N}(0, \mathbf{\Lambda}_{RTM}^{f(h)})$ for real-time forecast errors at any decision hour h. Next, we note that, as we proceed in time, part of our risk target constraint is set fixed and we have no control on it. Specifically, in the decision hour h we have:

$$[\mathbf{P}_{RTM}^{-h\intercal}, \mathbf{P}_{RTM}^{f(h)\intercal}][\lambda_{DIF}^{-h\intercal}, \lambda_{DIF}^{f(h)\intercal}]^\intercal - 2(\mathbf{P}_{RTM}^{f(h)\intercal}\mathbf{\Lambda}_{RTM}^{f(h)}\mathbf{P}_{RTM}^{f(h)})^{1/2} \geq 0 \tag{3.12}$$

where $\lambda_{DIF} = \lambda_{RTM} - \lambda_{DAM}$. $\mathbf{P}_{RTM}^{-h} = [P_{RTM}[1], \cdots, P_{RTM}[h-1]]^\intercal$ is the vector of all the past decisions on the real-time market offers up to hour h. Similarly, $\lambda_{DIF}^{-h} = [\lambda_{DIF}[1], \cdots, \lambda_{DIF}[h-1]]^\intercal$ is the difference of real-time market and day-ahead market prices up to hour h. Clearly, the prices which are already posted have no forecast error. Next,by separating the constant part from the variable terms in (3.12) and substituting $\mathbf{P}_{RTM}^{f(h)} = \mathbf{P}_G^{f(h)} - \mathbf{P}_{DAM}^*$, we have:

$$\begin{aligned} &2(\mathbf{P}_G - \mathbf{P}_{DAM}^{*\intercal})\mathbf{\Lambda}_{RTM}^{f(h)}(\mathbf{P}_G - \mathbf{P}_{DAM}^*)^{1/2} \\ &\quad - \mathbf{P}_G^{f(h)\intercal}\lambda_{DIF}^{f(h)} \leq \mathbf{P}_{RTM}^{-h\intercal}\lambda_{DIF}^{-h} - \mathbf{P}_{DAM}^{*\intercal}\lambda_{DIF}^{f(h)} \end{aligned} \tag{3.13}$$

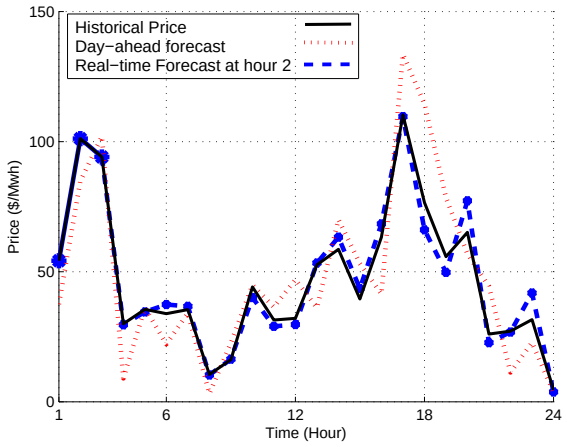

Figure 3.3: The day-ahead/ operating-day forecasts of RTM prices in a single zone of NYISO is simulated by adding a Gaussian error signal.

3.5 Numerical Studies

3.5.1 Input Data

In this section, we present some numerical studies performed to evaluate the proposed bidding/scheduling algorithm. To test the algorithm, the historical prices of both DAM and RTM, was obtained from New York Independent System Operator (NYISO) public data. The prices belong to January and May 2010 in three zones of NYISO.

Next, in order to create day-ahead and operating-day forecasts of the actual market prices, we added some random Gaussian noise with a specific (σ/μ) to the historical prices. Unless stated otherwise, day-ahead forecasts of the RTM, are added a noise with $(\sigma/\mu = 0.4)$. Operating-day forecasts are assumed to have variable forecast error. The forecast error signal in each decision hour of the operating-day has a Gaussian noise starting at $\sigma/\mu = 0.05$ for the same hour, and increase upto $\sigma/\mu = 0.2$ for the successive hours of the decision horizon. Fig.(6.3) shows a sample of RTM forecasts as well as the actual RTM price for a sample day.

The battery pack in this study is 2 MWh, 1.2 MW, operating between $20\% - 80\%$ of its capacity. The efficiency was assumed to be 80% and the cycle life was considered to be $7k$.

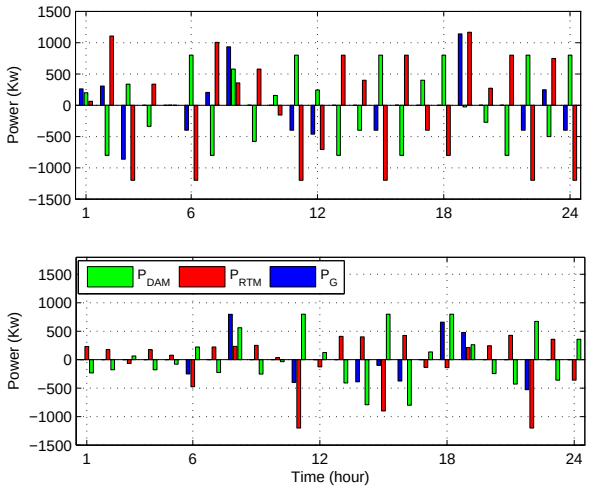

Figure 3.4: ESS optimal day-ahead forecast schedule and bids in DAM/RTM for two levels of uncertainty; (a) low forecast error ($\sigma/\mu = 0.3$), ESS relies more on the high prices of the RTM. (b) high forecast error ($\sigma/\mu = 1.3$), storage offers has decreased notably due to high risk with the same price curves.

3.5.2 Day-ahead Operations

Using the day-ahead forecast inputs, the ESS DAM optimizer determines the optimal DAM bids based on the predictions of the ESS operation schedule, and RTM offers of the next day. We observe in this stage, the market price differences across different hours of day-ahead market, different hours of real-time market, and the difference of price between DAM and RTM, all impact the ESS schedule and ESS profit.

The uncertainty in the price forecasts, i.e., the forecast error, has an important effect in our optimal schedule of ESS as well. For instance, in Fig. (3.4) for two different levels of uncertainty in RTM price, we have two distinct ESS schedule and market offers. Note that these values are predictions that ESS uses to set its DAM offer accordingly. Using the forecasts of RTM prices can help the ESS to increases its revenue, by reserving some of its resources for the real-time market. However, as the forecast error increase the ESS becomes more hesitant in utilizing the RTM forecast in the day-ahead market bids. In high risk of prices, ESS operation *prediction* will be more based on the day-ahead market prices and the revenues of ESS will decrease by forfeiting to utilize high-risk revenues.

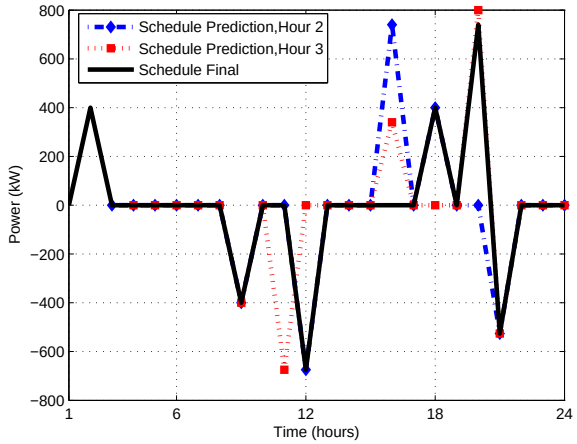

Figure 3.5: The ESS schedule in RTM is updated as new forecasts arrive. Here you see the final ESS schedule, and two predictions of the optimal schedule. The first element of every prediction, make the final solution over time.

3.5.3 Real-time Operations

As we mentioned in the formulation, ESS operation schedule, and real-time bid in the operating day, changes over time as new forecasts with new uncertainties become available. The result of operation schedule can be seen in Fig.(6.4) for a sample operating day. The final optimal schedule of ESS is shown alongside two predictions of the optimal schedule in two successive hours. Each prediction of optimal schedule, also consists of one point on the optimal final schedule, and the real-time market offer as well. Note that predictions of future hours operations are essential to determine the best decision/ market offer in the same hour. The difference of schedule prediction with final solution is due to different inputs, i.e., *prices*. Therefore, the predictions of optimal solution, fall closer to the final schedule due to less error in forecasts.

3.5.4 Impact on Revenues

Table 3.1 shows the profit values for the three sample days. It can be seen that the profit in day-ahead market only, could be a lot less than the profit of joint operation. In fact, as risk increases, i.e. the information on RTM decrease, the solution will rely less on RTM revenues. The least of joint revenues will be obtained when we have no certainty, or

no information at all about the RTM prices, or when we only participate in the day-ahead market. However, since the optimization relies on uncertain information, the actual profit could be less or more than what is predicted. The total revenues in the last column of Table 3.1 has two parts. The left-side value shows the day-ahead *prediction* of the total revenue, while the other shows the *realized* revenues from the real-time market optimizer.

Table 3.1: Comparison of revenues; joint operation vs. day-ahead market.

	DAM Rev.	Operation Cost	RTM Rev.	Total Rev.
Joint Operation				
Day 1	86	51	443	447/478
Day 2	90	63	467	425/494
Day 3	118	50	276	444/344
Day-ahead Only				
Day 1	61	40	0	23/ 21
Day 2	93	50	0	44/43
Day 3	79	43	0	35/35

3.6 Conclusion

In this chapter, we proposed a joint multi-temporal market optimization framework for battery ESS. We observed that the risk of stochastic revenues is an important factor in driving the ESS to utilise or forfeit the real-time market revenues, both in day-ahead and real-time market. We showed that risk-constrained joint market optimization can achieve more revenues compared to participation in risk-free market.

3.7 List of Symbols, Chapter 3

f_{DA} Indicator of variable forecast in day-ahead

f_h Indicator of variable forecast in operating-day,hour h.

$\mathrm{P_{DAM}}$ Day-ahead market power offer.

$\mathrm{P_{RTM}}$ Real-time market power offer.

P_G ESS actual energy generation/consumption.

$\lambda_{\boldsymbol{DAM}}$ Day-ahead market power price.

$\lambda_{\boldsymbol{RTM}}$ Real-time market power price.

$\lambda_{\boldsymbol{DIF}}$ Difference of real-time and day-ahead market power price.

$\boldsymbol{J}$ ESS joint profit in day-ahead/real-time markets.

Rev. ESS total revenues in day-ahead/real-time market.

$\mathcal{R}_0$ Revenue with probability of $(1-\zeta)$ or more.

$\boldsymbol{\Lambda}_{\boldsymbol{RTM}}^{f(\boldsymbol{DA})}$ RTM price forecast error covariance, day-ahead.

$\boldsymbol{\Lambda}_{\boldsymbol{RTM}}^{f(h)}$ Price forecast error covariance, real-time at hour h.

α_1, α_2 Appropriate wear cost coefficients in $Dolar/kWh$.

SoC Battery ESS state-of-charge.

P_{dc} Battery ESS absorbed/drained net power.

η_0 Battery ESS efficiency coefficient.

Δ Battery daily target state-of-charge.

Part II

Energy Storage Operation at the Distribution Grid

Distribution systems' planning grows to an ever challenging problem. One source of challenges arise from the growth of renewable resources such as solar photovoltaic as well as the increasing load from new devices such as electric vehicle chargers. All these new elements in the distribution systems have one factor in common as they are highly unpredictable. One of the key roles presumed for energy storage units in distribution grids, is the mitigation of fluctuations and time-variations of the contemporary elements such as renewable DGs and EV loads. Indeed, Energy Storage systems are expected to be an effective and cost-efficient solution in planning and support of distribution systems in order to prevent early investments. Optimal planning of storage units for reducing system costs should account for the impact of stochastic features of such elements on the operation of the distribution grids.

In our work as part of our efforts on formulating a tractable, computation effective, chance constrained stochastic formulation for optimal allocation of Energy storage systems for support of active distribution systems with uncertain resources, we develop and adapt a chance constrained stochastic formulation to manage the flow and voltage with deterministic resources in distribution networks with uncertainties.

Chapter 4

Data Synthesis to Model Power Distribution Networks

A key part of smart grid research is to use experimental data, both on the demand side and the generation side, to validate the results. There are currently various publicly available data sets for electricity prices, solar panels, wind turbines, and residential and commercial load profiles [46–48]. However, there are still some aspects, e.g., the charging load of electric vehicles, that is yet to be analyzed. Furthermore, there is still a need to combine various data sets in a unified modelling framework that is appropriate for various decision making processes. Next, we explain how one can synthesize a test data set for electric vehicles from non-electric vehicle traces. After that, we develop a data-driven model to integrate energy storage units in power distribution networks.

4.1 A Test Data Set for Electric Hybrid Vehicles

Due to the *still-insignificant* penetration of plug-in hybrid electric vehicles (PHEVs), there currently does not exist any detailed data set for large fleets of PHEVs. This has caused obstacles for smart grid researchers, who intend to investigate the challenges and opportunities that the PHEVs may introduce to power systems. Of course, more data is expected to gradually become available as more experimental PHEV projects are conducted over the next couple of years. However, for now, one option is to use the existing major *non-PHEV* vehicular data sets and combine them with the information and features of the recently emerged commercial PHEVs in order to *synthesize* new PHEV data sets that can be used

in a variety of smart grid research studies. Therefore, the central argument in this section is that, in the absence of a detailed database of PHEV loads, a *synthetic database* that includes the key pieces of information that are needed for PHEV-related smart grid research is highly useful. Developing such practical data set is our goal in this section.

In this section, we analyse the driving traces for 536 GPS-equipped non-PHEV taxi vehicles in [11] that are recorded for a duration of three weeks in San Francisco, CA. We then *combine* the results with the features and technical characteristics of four different PHEV brands that currently dominate the North American market: Chevrolet Volt [49], Honda Accord Plug-in [50], Ford Fusion Energi [51], and Toyota Prius Plug-in [52]. Our analysis has resulted in a new test data set to support PHEV-related smart grid research. It provides per-PHEV traces of states-of-charge (SoCs), per-PHEV traces of charging loads, per-PHEV information on SoC and charging deadline when the PHEV is parked at a charging station, and the detailed charging load at each of our three carefully identified charging stations.

The dataset that is developed in this section [53], can be used for various smart grid research projects. Some of the applications include investigating the impact of the increasing PHEV loads on power distribution feeders and substations, design, operation, and control of V2G systems based on vehicle arrival and departure data, charger sizing, design and optimal charger placement, and obtaining more precise statistics regarding the SoCs based on driving patterns, etc.

4.1.1 The Non-PHEV Driving Traces

Consider the non-PHEV vehicles data in [11]. This data set is widely used in over 100 vehicular research projects, ranging from vehicular movement prediction to vehicular communications, e.g., see [54–56]. However, the potential of this detailed vehicular movement data set has not yet been investigated in the context of electric hybrid vehicles and smart grid.

This data set includes the driving traces of 536 taxis in San Francisco, CA. The data recording starts on May 17, 2008 and ends on June, 10, 2008. For each taxi, each data record comprises a *time-stamp*, *latitude*, *longitude*, and a flag indicating whether or not the taxi has a passenger. The GPS tracking system is switched off every time that the vehicle is turned off. Recording resumes once the vehicle is turned on.

Since the taxis serve mainly the San Francisco area, most of the recorded GPS

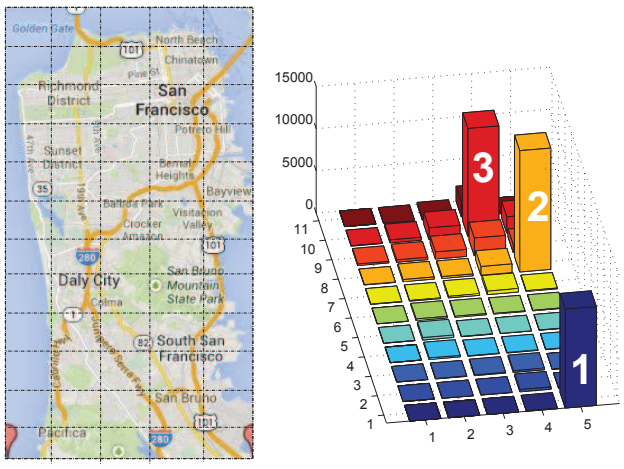

(a) (b)

Figure 4.1: By tracking the GPS locations of taxi vehicles in San Francisco, CA, we can identify the most frequent parking locations, based on our definition of a parking event: (a) The city map is divided into $5 \times 12 = 60$ regions based on latitude and longitude. (b) The number of parking events, i.e., the frequency of parking, in each region. The regions that are marked from 1 to 3 are the most common parking locations: Airport, Taxi Headquarters, Downtown.

coordinates are within latitudes 37.6 and 37.82 and longitudes -122.52 and -122.37. This rectangular area is shown in Fig. 4.1(a), where it is divided into $5 \times 12 = 60$ equal-area, rectangular regions.

As the first step in our analysis, we identify the number of times that a vehicle is *parked* in each of the 60 regions in Fig. 4.1(a). The parking events are important as they are later interpreted, under certain conditions on their location and duration, as PHEV *plug-in* events. Of course, not every stationary behaviour of a vehicle should be interpreted as a parking event. In many cases, heavy traffic can be the cause of no movement or a very slow movement. Similarly, some temporary stops are when the taxi is waiting for a passenger, etc. Therefore, we define a parking event based on both a *time duration threshold* and a *distance threshold*. In this regard, a parking event is a scenario where the vehicle traversed a distance of 500 meters or less in 15 minutes.

As for the distance travelled between the successive GPS readings, such distance is approximated by a straight path between each two coordinates. Such approximation is

reasonable for the purpose of our study since the reading intervals in [11] are fairly small. Let λ_1 and λ_2 denote the latitudes of two successive records of the GPS coordinates. Assume that ϕ_1 and ϕ_2 denote the longitudes of those coordinates. The direct distance traversed between the two points are calculated as

$$D_{1,2} = R\sqrt{\left((\phi_2 - \phi_1)cos\left(\frac{\lambda_1 + \lambda_2}{2}\right)\right)^2 + (\lambda_2 - \lambda_1)^2} \tag{4.1}$$

where R denotes the radius of the earth that is 6371 kilometres.

As we can see in the Fig. 4.1(b), most of the parking events are concentrated across *three* locations. We could identify these GPS locations on the San Francisco map in Fig. 4.1(a) as 1) Airport, 2) Taxi Depot and Headquarters, and 3) Downtown. Hence, it is reasonable to assume that if these taxis are replaced with PHEVs, then their charging stations must be placed in these three locations in order to provide them with charging service with minimum impact on their regular driving patterns. Accordingly, for the rest of this section, we assume that there are indeed three *Charging Stations* for the taxis exactly at these three regions as numbered in Fig. 4.1(b).

Next, we record and analyse the movements and parkings of each of the 536 vehicles for the entire three weeks of data traces in [11]. The results are shown in Fig. 4.2 for four sample vehicles over a time window of three days. Here, the value 1 on the y-axis indicates that the vehicle is parked at one of the three charging stations; and the value of 0 means otherwise. The index number of the charging station for each parking event is shown with numbers 1 to 3 on top of the curves. We can see in Fig. 4.2 that different taxis have different movement and parking patterns. Another interesting observation is that, as expected, the longest duration parking events are recorded at the second charging station, i.e., the Taxi Headquarters.

By putting together the detailed driving and parking traces of *all* vehicles, we can next calculate the number of vehicles that are parked at each station at any time of interest. The results are shown in Fig. 4.3. Here, the resolution is one minute. That is, we have calculated the number vehicles that are parked at each charging station during every one minute interval of each day. We can see that the parking patterns are quite different across different charging stations, depending on the dynamics of vehicles movements. For example, the number of stops vehicles that are parked at the Taxi Headquarters is at its peak during

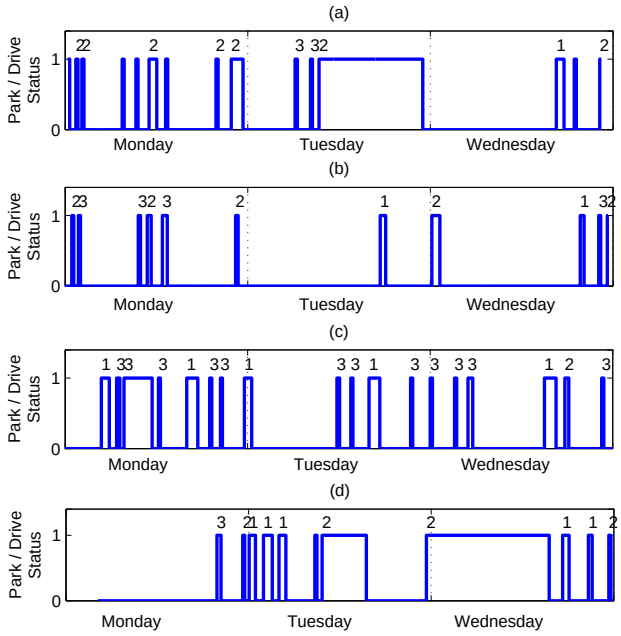

Figure 4.2: Examples of drive (0) versus park (1) intervals for four sample taxis during a three-days window: (a) taxi number 1, (b) taxi number 7, (c) taxi number 10, and (d) taxi number 17. The numbers on top of each park interval range from 1 to 3 and indicate the index of the charging station.

the night, when a large number of taxis return to the parking area. In contrast, there are few cars parking in the Downtown area at night. And of course, we see a completely different pattern at the Airport station , where the maximum number of vehicles are parked in late afternoon, when many flights arrive in the San Francisco area. The combination of the results in Fig. 4.3 with the stop duration and mileage driven by the vehicles could be the starting point for many useful information as we will discuss next.

The histogram of the parking event durations at each charging station is shown in Fig. 4.4. We can see that while most of the parking events at the Airport and Downtown stations have relatively short durations, there are several parking events that are one hour or longer at the Taxi Headquarters station. Similarly, the histograms for the distributions of the distance driven since departing the previous charging station for each vehicle that arrives at each of the three charging stations are shown in Fig. 4.5. This measure gives an

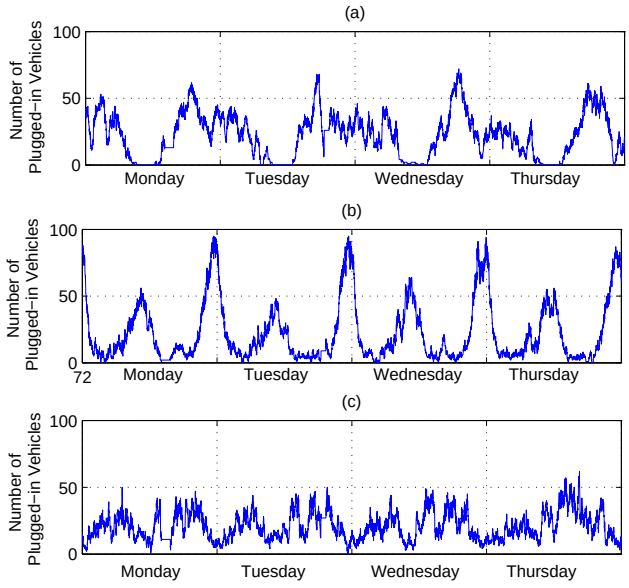

Figure 4.3: The number of taxis that are parked at the three charging stations during a sample four-days window: (a) Charging station number 1, Airport, (b) Charging station number 2, Taxi Headquarters, (c) Charging station number 3, Downtown. The parking patterns are different at different charging stations.

indication about how full or empty the battery of a PHEV could be when it arrives at a charging station, allowing us to calculate the initial state-of-charge for the PHEVs that arrive at a charging stations, once we also take into account the electric consumption patterns of various PHEVs into consideration. From the results in Fig. 4.5, we can see that the vehicles typically drive for longer distances when they arrive at the Airport charging station.

For all the results that we have presented so far, our focus has been solely on the driving and parking patterns of various vehicles. As is, these results were already insightful in various aspects as we explained throughout this section. However, these results would be even more useful, in particular for the purpose of smart grid research, if they are combined with some more analysis based on the specific operational and technical characteristics of various PHEVs, as we will see next.

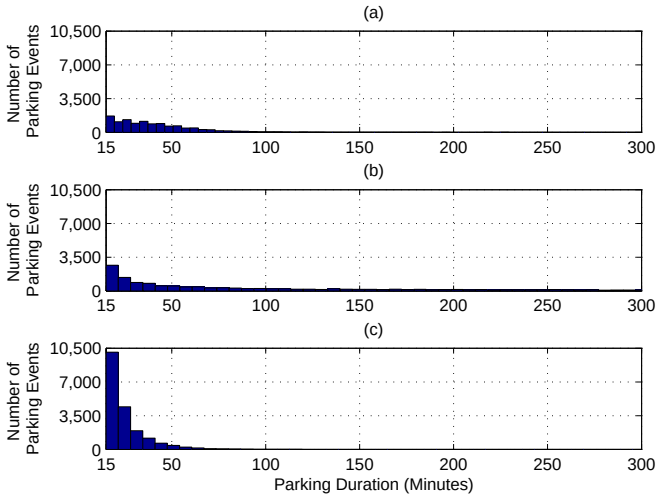

Figure 4.4: The histograms of the duration of parking for each parking event; (a) Charging station number 1, Airport, (b) Charging station number 2, Taxi Headquarters, (c) Charging station number 3, Downtown.

4.1.2 The Features and Characteristics of The Most Common PHEVs in the Market

In this section, we aim to combine the vehicles' movement and parking datasets that we generated in Section 4.1.1 with the nominal operation data of multiple PHEVs that dominate the present market. The goal is to obtain the charging patterns and SoCs of the vehicles with the same movement patterns, but different PHEV technologies. Here, we consider four PHEV brands: Chevrolet Volt, Honda Accord Plug-in, Ford Fusion Energi, and Toyota Prius. The main operational characteristics of these PHEVs are listed in Table 4.1 [57].

We can see that these vehicle brands are different in various operational characteristics. Characteristics such as available energy, maximum charge rate, vehicle efficiency, and vehicle power train, etc. All such characteristics have direct impact on the charging load, state-of-charge, and V2G potentials. With respect to the power train, we have divided our selected vehicles into two groups: *charge depleting*, and *charge blending*. The PHEVs in the first group use electric power as long as there is electric energy stored in the batteries. They switch to gas power only after the batteries are depleted. However, the PHEVs in the second

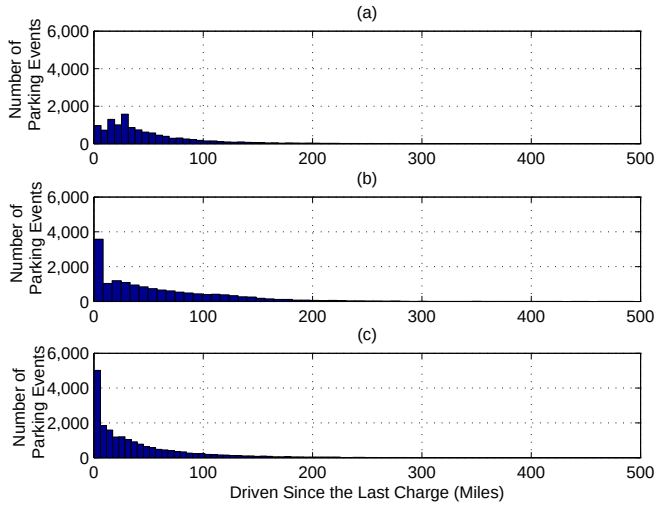

Figure 4.5: The histograms of the miles driven since departing the previous charging station: (a) Charging station number 1, Airport, (b) Charging station number 2, Taxi Headquarters, (c) Charging station number 3, Downtown.

group may blend the power sources and use the gas engine to increase the torque in high speed movements even if the battery is not completely depleted. As a result, the SoC for the second group of PHEVs depends on both the miles travelled and also the *travelling speed*. Here, we assume that the charge blending vehicles switch from electric power to gas power at a speed threshold, set to 60 mph. Finally, it is worth clarifying that while Ford Fusion is capable of using technology, it typically runs in all electric power mode [51]. Therefore, it is categorized within the charge depleting group.

Next, we transform the driving and parking trace information of vehicles into their SoC data sets. When a vehicle is plugged-in to a charging station, it is charged by a 240 V 32 A chargers [58]. However, the *actual* charge rate for each PHEV is limited by its own charger interface, as listed in Table 4.1. Therefore, we must calculate SoC during the charging period specifically based on the characteristics of each particular PHEV. Once a PHEV departs a charging station, its SoC will start to decrease based on its driving pattern and also its power train type, as we explained in the previous paragraph.

Four sample SoC trends for four representative taxis over a three-days time window are shown in Fig. 4.6. All the SoC curves in this figure are based on the Chevrolet Volt data.

Table 4.1: Operational Data of Four Common PHEVs

Brand	Chevrolet	Honda	Ford	Toyota
Model	Volt	Accord	Fusion	Prius
Battery Capacity (KWh)	16	6.6	7.6	4.4
Available Energy (KWh)	8.8	3.8	7.1	3.2
Ave. Electric Range (M)	37	13	21	11
Max Charge Rate (KW)	3.5	6.6	3.5	3.5
Electric Consumption *	36	29	34	29
Gas Consumption **	2.7	2.2	2.3	2
Power Train index ***	D	B	D	B

* KW/100 Miles
** Galons/100 Miles
*** D: Charge Depleting, B: Charge Blending

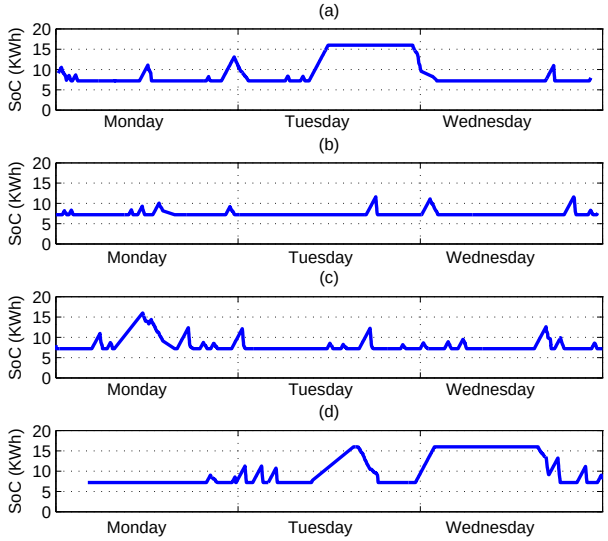

Figure 4.6: The state-of-charge traces for four sample vehicles over a three-days time window: (a) taxi number 1, (b) taxi number 7, (c) taxi number 10, and (d) taxi number 17. All vehicles are assumed to be Chevrolet Volt.

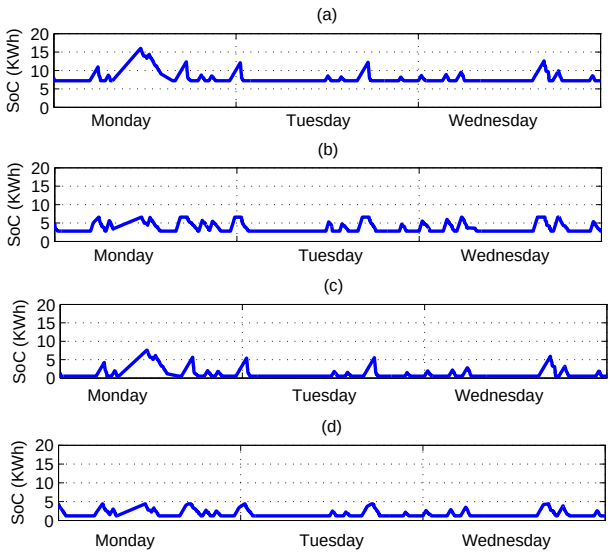

Figure 4.7: The state-of-charge traces for the same taxi, taxi number 10, but based on assuming four different PHEV types: (a) Chevrolet Volt, (b) Honda Accord Plug-in, (c) Ford Fusion Energi, (d) Toyota Prius Plug-in.

Recall that Chevrolet Volt has a charge depleting power train. It is interesting to compare the SoC curves in Fig. 4.6 with the drive and park intervals in Fig. 4.1. We can see that the SoC increases, following the charge rate of Chevrolet Volt, at every time that it is plugged-in to a charging station. Of course, if a charge interval is shorter than the time needed to fully charge the battery, then the vehicle leaves the charging station with a partially charged battery. Similarly, the SoC starts decreasing as the PHEV departs the charging station. We can see that, given the relatively small electric driving range of Chevrolet Volt, for a large portion of driving times, the SoC is at its minimum level 7.2 kWh, i.e., battery capacity 16 kWh minus available energy 8.8 kWh, indicating that the battery is depleted and the power train is switched to gas.

Next, we compare the SoC traces of different PHEVs brands. We focus on one taxi, taxi number 10, and generate its SoC traces based on the characteristics of different PHEVs. The results are shown in Fig. 4.7. Note that, the traces change from one car to another, not only during the charging periods, but also during the driving periods. For example, if the taxi of interest is a Honda Accord Plug-in, then then it can almost fully charge its rather small 6.6 kWh battery in several of its short duration stops at charging stations.

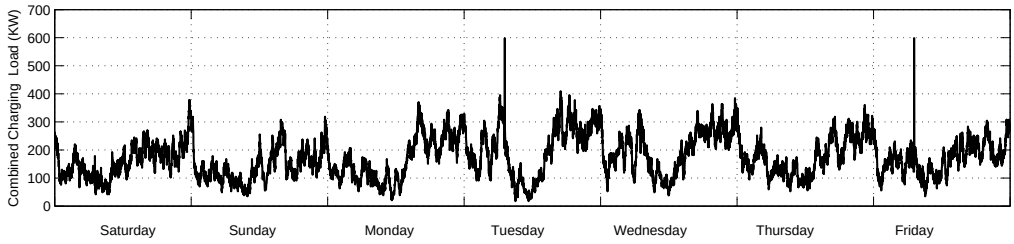

Figure 4.8: The combined charging load of all 536 vehicles and across all three charging stations for a period of one week starting on May 24th. The PHEVs are a mixture of different types as explained in the text. We can see that the total charging load highly fluctuates during each day and across different days.

4.1.3 Aggregate Data Sets at Charging Stations

In this section, we aggregate the data sets that we generated in Sections 4.1.1 and 4.1.2 and develop new data sets to provide useful information about the operation of charging stations. Recall from Section 4.1.1 that we identified three charging stations at the Airport, Taxi Headquarters, and Downtown. Our focus in this section is on calculating the *combined charging load* of all PHEVs as well as the total charging load at each charging station based on different PHEV types and during different hours of the day and different days of the week.

The combined charging load of all vehicles for a period of one week is shown in Fig. 4.8. The curve in this figure is the summation of the charging load of all the 536 PHEVs across all three charging stations. Therefore, it depends on not only the parking, charging, and driving patterns of each PHEV but also the exact specifications of the PHEVs. Here, we have assumed the following *mixture* of different PHEV brands:

- Chevrolet Volt: 161 vehicles,
- Honda Accord Plug-in: 125 vehicles,
- Ford Fusion Energi: 125 vehicles,
- Toyota Prius Plug-in: 125 vehicles.

We can see that the PHEV charging load curve in Fig. 4.8 fluctuates a lot. The average load during the considered week is 173.1 kWh, while the charging peak load is 598.5 kWh.

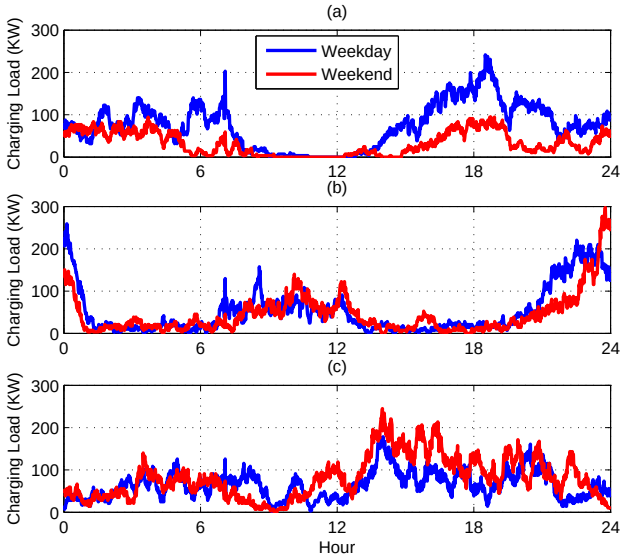

Figure 4.9: The charging load at each of the three charging stations during a weekday and also during a weekend: (a) Charging station number 1, Airport, (b) Charging station number 2, Taxi Headquarters, (c) Charging station number 3, Downtown. The load curves are obtained based on a *mixture* of different PHEV brands as explained in the text.

Therefore, the *peak to average ratio* (PAR) is 3.457.

Next, we separately plot the total daily charging load at *each* of the three charging stations. The results are shown in Fig. 4.9. The mixture of the PHEV brands is the same as the one in Fig. 4.8. We can see that the load patterns across different charging stations are very different. At Airport charging station, the peak load is during the afternoon, where many taxis wait for incoming passengers. As for the Taxi Headquarters charging station, the peak load hours are at night, where several taxis are parked at the headquarters overnight.

Another interesting observation is that the load profiles differ on a weekday and a weekend. This is particularly the case at the Airport charging station and to some extent at the Downtown and Taxi Headquarters charging stations.

It is interesting also to look at the changes in the charging load at different charging stations when we change the mixture of the PHEV brands and look at the scenarios where *all* PHEVs are of one brand. The results are shown in Fig. 4.10. We can see that the results are significantly different across some of the PHEV types because of the different features of

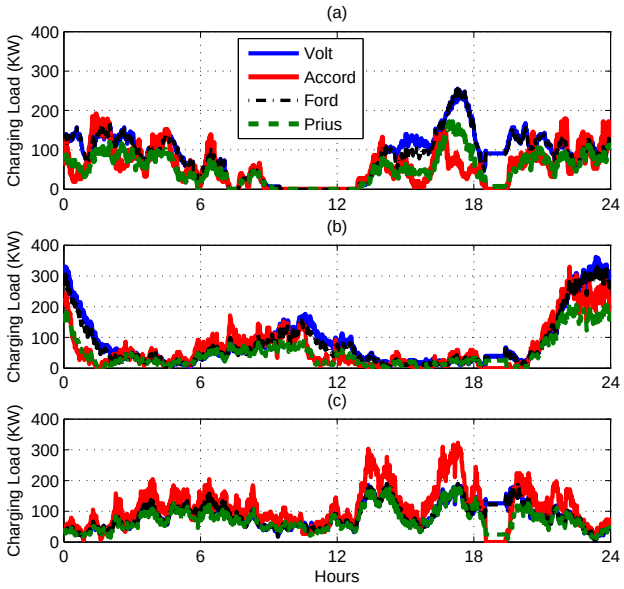

Figure 4.10: The PHEV charging load at each of the three charging stations based on the operational characteristics of four different PHEV brands.

these PHEVs. An interesting observation here is also about the differences between the four curves across the three charging stations. In particular, such differences are less significant at the second charging station, i.e., the Taxi Headquarters. This is because the duration of the parking events are longer at this station. Furthermore, it is notable that the curves in Fig. 4.10 for the cases of Chevrolet Volt and Ford Fusion are more or less similar. This can be tracked back by observing that the available charging energy and the charging rates of these vehicles are relatively close, as shown in Table 4.1.

Another point is that Honda Accord causes rather aggressive charging loads at short intervals, specifically at the Downtown charging station, where the parking durations are shorter. Therefore, in order to further examine charging patterns, we look at the total EV load for the two vehicle brands, i.e. Chevrolet Volt, and Honda Accord.

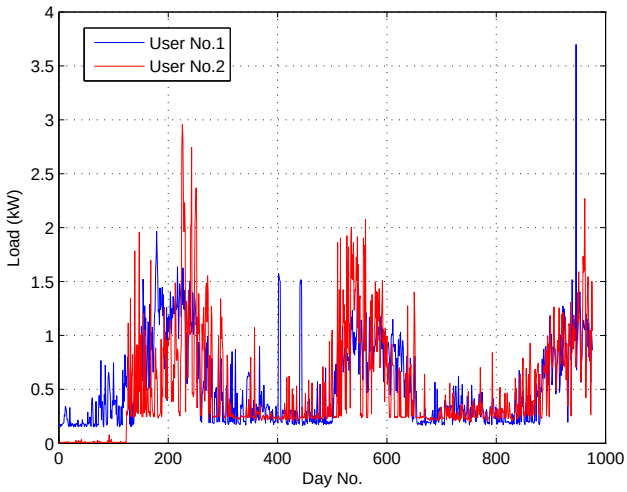

Figure 4.11: Metered load traces for two users at Hour=1 for over 900 days.

4.2 A Data Set for Residential Load Probability Distribution

Residential load is an essential part of stochastic modelling in distribution networks. In particular, for the purpose of storage planning at the distribution level, the uncertainty existing in the residential loads needs to be accounted. This calls for analysing the hourly and seasonal probability distributions of the household loads. To develop such probability distributions, the metered hourly loads of 600 residential consumers from PECON Street Database [13] were used. The individual household hourly metered loads, were then combined based on the topology information of the IEEE 13 bus standard test feeder, to from the hourly load traces of residential buses in the feeder. Finally, from time traces of residential load buses over the period of historical data, the hourly probability density functions are obtained in all residential load buses.

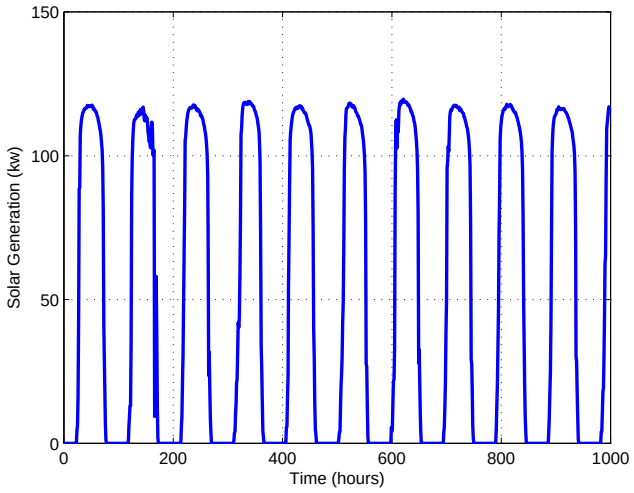

Figure 4.12: A sample of metered generation output traces of a solar panel.

4.3 A Data Set for Solar Generation Probability Distribution

To develop the hourly probability density functions of solar generation, the metered output generation of a solar panel with reasonable resolution, i.e. one hour or less, over a considerable period of time, a year or more, is required. In this project, such data is generated by applying the pair of metered solar irradiation and metered temperature, to the dynamic model of a 1,200 kW solar panel on Real-time Digital Simulator (RTDS) [59]. The solar irradiation/temperature historical data was obtained from the LLNL public database [12]. The historical data was extracted from LLNL database, with the resolution of 15 minutes over the period of five years, separately for every season. The hourly probability density functions of solar generation, were then obtained from the synthetic historical solar generation for each season.

Chapter 5

Energy Storage Planning in Active Distribution Grids: A Chance-Constrained Optimization with Non-Parametric Probability Functions

By considering the specific characteristics of random variables in active distribution grids, such as their statistical dependencies and often irregularly-shaped probability distributions, we propose a non-parametric chance-constrained optimization approach to operate and plan energy storage units in power distribution girds. In particular, we develop new closed-form stochastic models for the key operational parameters in the system. Our approach is analytical and allows formulating tractable optimization problems. Yet, it does not involve any restricting assumption on the distribution of random parameters, hence, it results in accurate modeling of uncertainties. Different case studies are presented to compare the proposed approach with the conventional deterministic and parametric stochastic approaches, where the latter is based on approximating random variables with Gaussian probability distributions.

5.1 Introduction

5.1.1 Motivation

Small and medium size Energy Storage Systems (ESS) have diverse applications in power distribution networks. For example, American Electric Power has recently installed a $1MW$ ESS to relieve pressure on a distribution-level transformer [60]. Distribution-level ESS installations can also relieve the fluctuations caused by generation of distributed generators (DGs) and/ or the charging load of electric vehicles (EVs) [61]. Such fluctuations are often more significant compared to typical baseloads [62]. The traditional distribution systems and their control equipment are not designed for compensating the excessive load / generation across their feeders, yet upgrading the existing system for such short periods of deficiency is not economical. In contrast ESS installations as a *multi-functional* resource, can maintain the system safe operation at low cost, if they are deployed and managed effectively.

Modelling uncertainty is different at distribution level versus at transmission level. For example, it might be reasonable to assume statistical independence and/or Gaussian distributions for the generation outputs of wind and/or solar farms that are scattered across a large transmission network [63]. However, these assumptions may not hold in a distribution grid with renewable DGs and EV charging stations that are confined to a relatively small geographical location due to the dependency in solar irradiance in proximate system buses [64] and the non-standard distribution of EV charging loads [65]. Also, the impact of some fluctuating elements may dominate the overall uncertainty in a distribution grid, making the typical use of the *central limit theorem* less practical. Therefore, a more general non-parametric approach (with no restricting assumption on the distribution of random parameters) could be more appropriate for ESS optimization at distribution level.

While non-parametric optimization has been adopted in a verity of problems in power systems, e.g. see [66–68], the aim of this chapter is to incorporate non-parametric stochastic modelling and optimization in power distribution systems, by addressing the specific characteristics of such systems to optimally operate and plan ESS for improved grid performance.

5.1.2 Comparison to Related Literature

With respect to the scope of this chapter, the related literature can be classified into several groups. First, some previous studies, e.g., in [69–72], are based on the assumption of *complete knowledge* of the hourly generation, demand, etc. Accordingly, despite their different design objectives and methodologies, they can all be classified as *deterministic* methods. In contrast, here, our focus is on stochastic optimization of ESS.

Second, there are studies, e.g., in [73–75], that *do* recognize uncertainties in ESS and distribution generation (DG) planning. However, they require fitting Gaussian or other parametric distributions into random variables. Accordingly, their design efficiency can degrade significantly if the Gaussian or other parametric distribution approximations are not accurate.

Third, there are studies, such as in [76–80], that address uncertainty *without* restricting the analysis to pre-determined parametric distributions of random variables; however, they account for uncertainties by defining *many instances* of each random variable. For example, the studies in [76, 77] use Monte-Carlo simulation methods. Accordingly, they must deal with a large number of scenarios. Such large-scale scenario generation is tractable if the focus is primarily on analysis, as opposed to on design and optimization. Other studies, e.g. in [78–80], utilize stochastic programing to address uncertainties which also involves scenario generation. Such methods are capable to incorporate non-linear but convex power flow equations by solving a deterministic problem over many samples of random variables; yet concerns do exist about the convergence and accuracy of the solution once the number of scenarios increases. In contrast, here in this chapter, we take an *analytical* approach where we improve modeling efficiency without exploding the computation workload, but of course with the limitation of linearizing the power flow equations.

Forth, there are studies, e.g. in [81–84], that use chance-constrained optimization for optimal operation and planning of resources, mainly in transmission systems. For example, in [81] a chance-constrained optimal power dispatch strategy is developed for transmission systems, using cumulant-based stochastic models. The Gram-Charlier expansion method is applied in [81, 85, 86] to approximate the distribution of state variables; however, it reduces the accuracy of stochastic modelling. Such reduced accuracy could be inevitable in large transmission systems; but it may not be acceptable at distribution level, which is where we focus on in this chapter. Also, the DC power flow equations used in [81–85] are

not appropriate to represent power distribution systems.

Last but not least, our design approach in this chapter is also fundamentally different from the fifth group of prior work, e.g., in [8, 87–90], where heuristics such as Genetic Algorithms are used to optimize ESS in distribution networks.

5.1.3 Technical Contributions

The contributions in this chapter are summarized as follows:

- We propose a new non-parametric chance-constrained optimization approach to operate and plan ESS in power distribution networks. Uncertainty from different sources of different stochastic nature, e.g. DGs, EVs, and residential baseloads are taken into consideration.

- Our analysis is based on developing new closed-form stochastic models for various key operational parameters of the distribution grid. This allowesd us to formulate optimization problems for ESS operation and planning that are in the form of tractable linear programs (LPs) or mixed integer linear programs (MILP). In principle, the developed closed-form stochastic models can be used also in other non-ESS distribution-level planning problems.

- Our ESS planning framework is customized for distribution grids, as opposed to some commonly used models that are based on Gaussian approximations of random variables that were originally intended for transmission systems. For example, our design accounts for the typical radial configuration of the distribution networks as well as the close proximity of distribution buses that causes statistical dependency across certain random variables.

- Several case studies confirmed the advantages of non-parametric chance-constrained optimization over deterministic and parametric chance-constrained optimization.

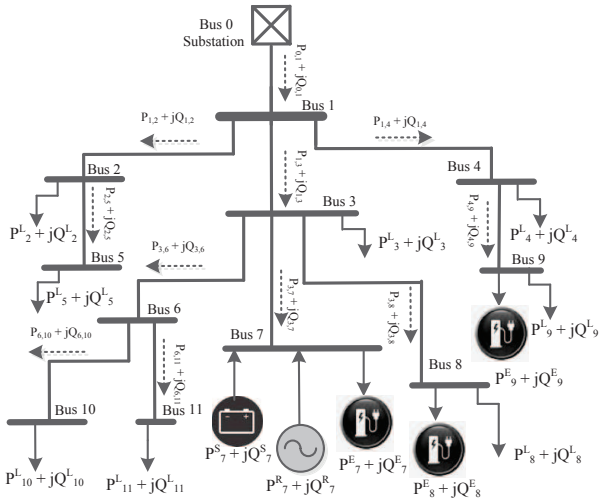

Figure 5.1: An example radial distribution network with 12 distribution buses.

5.2 Stochastic System Model

5.2.1 Notations and Power Flow Equations

Consider a radial distribution network, such as the one in Fig. 6.1. Let $\mathcal{N}$ denote the set of all buses, including *reference bus 0*. Also let $\mathcal{L}$ denote the set of all distribution lines. We define $\mathcal{N}^s$, $\mathcal{N}^e$, $\mathcal{N}^r$, and $\mathcal{N}^b$ as the sets of buses with storage units, EV charging stations, renewable DG units, and baseloads, respectively. At each bus i, we define $\mathcal{D}_i$ and $\mathcal{N}_i$ as the sets of direct descendant and descendant buses of bus i, where $\mathcal{D}_i \subseteq \mathcal{N}_i$. We also define $\mathcal{L}_{i,0}$ as the set of lines that connect bus i to bus 0. As an example, in Fig. 6.1, we have $\mathcal{N}^e = \{7, 8, 9\}$, $\mathcal{N}^r = \mathcal{N}^s = \{7\}$ and $\mathcal{N}^b = \{2, 3, 4, 5, 8, 9, 10, 11\}$. At bus 3, we have $\mathcal{D}_3 = \{6, 7, 8\}$ and $\mathcal{N}_3 = \{6, 7, 8, 10, 11\}$. Set $\mathcal{L}_{7,0} = \{(0, 1), (1, 3), (3, 7)\}$.

Suppose the operation time is divided into T time slots. For each line (i, j), let $P_{(i,j)}[t]$ and $Q_{(i,j)}[t]$ denote the line active and reactive power flows at time slot t. The voltage at bus i at time slot t is denoted by $V_i[t]$. At each bus i, the active power draw at time slot t is denoted by $P_i^s[t]$, $P_i^e[t]$, $P_i^r[t]$, and $P_i^b[t]$, for storage units, EV charging stations, renewable DG units, and baseloads, respectively. A negative power draw means power injection. The notations $Q_i^s[t]$, $Q_i^e[t]$, $Q_i^r[t]$, and $Q_i^b[t]$ are defined similarly for reactive power.

Next, we model power flows in the distribution grid using the linearized DistFlow equations, which are widely used in the literature, e.g., see [91–93]. For all non-reference

buses $i \in \mathcal{N}\backslash 0$, and all distribution lines $(i,j) \in \mathcal{L}$ we have:

$$\tilde{P}_{(i,j)}[t] = P_j^s[t] + \tilde{P}_j^b[t] + \tilde{P}_j^e[t] + \tilde{P}_j^r[t] + \sum_{l \in \mathcal{D}_j} \tilde{P}_{(j,l)}[t] \tag{5.1}$$

$$\tilde{Q}_{(i,j)}[t] = Q_j^s[t] + \tilde{Q}_j^b[t] + \tilde{Q}_j^e[t] + \tilde{Q}_j^r[t] + \sum_{l \in \mathcal{D}_j} \tilde{Q}_{(j,l)}[t] \tag{5.2}$$

$$\tilde{\mathrm{v}}_i^2[t] - \tilde{\mathrm{v}}_j^2[t] = 2R_{(i,j)}\, \tilde{P}_{(i,j)}[t] + 2X_{(i,j)}\, \tilde{Q}_{(i,j)}[t], \tag{5.3}$$

where $\mathrm{v}_0 = 1$ and the tilde sign indicates *random* variables. Bus 0 serves as a slack bus with infinite supply capability. Note that, the DistFlow model is originally non-linear and non-convex. Certain convex relaxation techniques are proposed, e.g., in [94], that are exact under certain deterministic formulations. However, those techniques are not applicable in chance-constrained programming. See Section 5.4.6 for additional discussions on the impact of the DistFlow model linearzation.

For the ease of notation, for the rest of this chapter we denote:

$$V \triangleq \mathrm{v}^2. \tag{5.4}$$

Given the above one-to-one relation, we refer to V as voltage, even though it is technically voltage squared. Obtaining all characteristics of v from V is straightforward.

5.2.2 Stochastic Representation of Key Operational Parameters

We classify the parameters and variables in a distribution grid into three groups: First, the *key operational parameters*, i.e., the voltages at all buses and the power flows at all lines; second, all *random variables*, i.e., baseloads, EV charging loads, and renewable DG outputs at all buses; third, our *decision variables*, i.e., the charge and discharge powers of all ESS units. Using the recursive relationships in (5.1)-(5.3), we can describe the key operational parameters in the first group in terms of the variables in the second and the third groups:

$$\tilde{P}_{(i,j)}[t] = \sum_{k \in \mathcal{N}_j} P_k^s[t] + \sum_{k \in \mathcal{N}_j} \left(\tilde{P}_k^b[t] + \tilde{P}_k^r[t] + \tilde{P}_k^e[t] \right), \tag{5.5}$$

$$\tilde{Q}_{(i,j)}[t] = \sum_{k \in \mathcal{N}_j} Q_k^s[t] + \sum_{k \in \mathcal{N}_j} \left(\tilde{Q}_k^b[t] + \tilde{Q}_k^r[t] + \tilde{Q}_k^e[t] \right), \tag{5.6}$$

and

$$\begin{aligned}\tilde{V}_i[t] = 1 &- \sum_{(k,j)\in\mathcal{L}_{i,0}} \Big(2R_{(k,j)}\, P_{(k,j)}[t] + 2X_{(k,j)}\, Q_{(k,j)}[t]\Big) \\ = 1 &- \sum_{(k,j)\in\mathcal{L}_{i,0}} \sum_{l\in\mathcal{N}_j} \Big(2R_{(k,j)}\, P_l^s[t] + 2X_{(k,j)}\, Q_l^s[t]\Big) \\ &- \sum_{(k,j)\in\mathcal{L}_{i,0}} \sum_{l\in\mathcal{N}_j} \Big[2R_{(k,j)} \left(\tilde{P}_l^b[t] + \tilde{P}_l^r[t] + \tilde{P}_l^e[t]\right) \\ &\qquad +2X_{(k,j)} \left(\tilde{Q}_l^b[t] + \tilde{Q}_l^r[t] + \tilde{Q}_l^e[t]\right)\Big].\end{aligned} \tag{5.7}$$

We can see that each line power flow or each bus voltage is formulated as a sum of a *deterministic* term and a *stochastic* term. The former is a linear combination of ESS injection *decision variables* while the latter is a linear combination of power draw from random variables at different buses.

Given the expressions in (5.5), (5.6), and (5.7), at each time slot t, we can define the Cumulative Distribution Functions (CDFs) for the distribution line active power flows as

$$\begin{aligned}F_{(i,j)}^P[t](p) &\triangleq \Pr\Big\{\tilde{P}_{(i,j)}[t] \le p\Big\} \\ &= \Pr\Big\{\tilde{\phi}_{(i,j)}^P[t] \le p - \psi_{(i,j)}^P[t]\Big\},\end{aligned} \tag{5.8}$$

and for reactive power flows and voltages as

$$F_{(i,j)}^Q[t](q) \triangleq \Pr\Big\{\tilde{\phi}_{(i,j)}^Q[t] \le q - \psi_{(i,j)}^Q[t]\Big\}, \tag{5.9}$$

$$F_i^V[t](v) \triangleq 1 - \Pr\Big\{\tilde{\phi}_i^V[t] \le 1 - v - \psi_i^V[t]\Big\}, \tag{5.10}$$

where

$$\tilde{\phi}_{(i,j)}^P[t] \triangleq \sum_{k\in\mathcal{N}_j} \left(\tilde{P}_k^b[t] + \tilde{P}_k^r[t] + \tilde{P}_k^e[t]\right), \tag{5.11}$$

$$\tilde{\phi}_{(i,j)}^Q[t] \triangleq \sum_{k\in\mathcal{N}_j} \left(\tilde{Q}_k^b[t] + \tilde{Q}_k^r[t] + \tilde{Q}_k^e[t]\right), \tag{5.12}$$

$$\tilde{\phi}_i^V[t] \triangleq \sum_{(k,j)\in\mathcal{L}_{i,0}} \Big(2R_{(k,j)}\, \tilde{\phi}_{(k,j)}^P[t] + 2X_{(k,j)}\, \tilde{\phi}_{(k,j)}^Q[t]\Big), \tag{5.13}$$

and

$$\psi_{(i,j)}^P[t] \triangleq \sum_{k\in\mathcal{N}_j} P_k^s[t], \qquad \psi_{(i,j)}^Q[t] \triangleq \sum_{k\in\mathcal{N}_j} Q_k^s[t], \tag{5.14}$$

$$\psi_i^V[t] \triangleq \sum_{(k,j)\in\mathcal{L}_{i,0}} \Big(2R_{(k,j)}\, \psi_{(k,j)}^P[t] + 2X_{(k,j)}\, \psi_{(k,j)}^Q[t]\Big). \tag{5.15}$$

Note that, the expressions in (5.11)-(5.13) depend solely on random variables and the expressions in (5.14)-(5.15) depend solely on the decision variables of the storage units.

At each bus i and time slot t, the Probability Density Function (PDF) for baseload, EV charging load, and renewable generation is denoted by $f_i^b[t](\cdot)$, $f_i^e[t](\cdot)$, and $f_i^r[t](\cdot)$, respectively. These random variables are represented by discrete empirical distributions *with no specific mathematical expressions*. Also, $f_{(i,j)}^P[t](\cdot)$, $f_{(i,j)}^Q[t](\cdot)$, and $f_i^V[t](\cdot)$ denote the PDFs of the system operational parameters at each line and each bus.

Next, we *group* the random variables based on their *statistical dependence*. For example, the outputs of all solar panels are dependent due to their proximity, given the relatively small size of distribution grids. Accordingly, such outputs can be grouped such that they can all be represented in terms of *solar irradiance* as the independent random variable. Other grouping can be done for other renewable DGs of the same type.

Without loss of generality, suppose solar panels are the only DG types on the distribution grid. Let $\tilde{U}[t]$ and $\tilde{H}[t] = \kappa^u[t]\,\tilde{U}[t]$ denote the active and reactive power outputs of a solar panel at time slot t, where κ^u is a constant of the solar panel and its power electronics interface [95]. The PDF of the random variable $\tilde{U}[t]$, i.e. *a unit of solar panel active power output*, is expressed by $f^u[t](\cdot)$. At each bus $i \in \mathcal{N}^r$, we have:

$$\tilde{P}_i^r[t] = \lambda_i^u\,\tilde{U}[t], \quad \tilde{Q}_i^r[t] = \lambda_i^u\,\kappa^u[t]\,\tilde{U}[t], \tag{5.16}$$

where λ_i^U is a constant that is set for the the DG installation at bus i. Random variable $\tilde{U}[t]$ solely depends on solar irradiance. *Statistical dependency* also exists among active and reactive power injections at each bus [96]. Therefore, at each bus i, we assume that $\tilde{Q}_i^b[t] = \kappa_i^b[t]\tilde{P}_i^b[t]$ and $\tilde{Q}_i^e[t] = \kappa_i^e[t]\tilde{P}_i^e[t]$, where κ_i^b depends on the type of loads and their power electronics interfaces and κ_i^e depends on the EV chargers.

Theorem 1 *The CDFs in (5.8)-(5.10) are obtained as*

$$F_{(i,j)}^P[t](p) = G_{(i,j)}^{\phi^P}[t]\Big(p - \psi_{(i,j)}^P[t]\Big), \tag{5.17}$$

$$F_{(i,j)}^Q[t](q) = G_{(i,j)}^{\phi^Q}[t]\Big(q - \psi_{(i,j)}^Q[t]\Big), \tag{5.18}$$

$$F_i^V[t](v) = 1 - G_i^{\phi^V}[t]\Big(1 - v - \psi_i^V[t]\Big), \tag{5.19}$$

where G^{ϕ^P}, G^{ϕ^Q}, and G^{ϕ^V} are some CDFs that have the following probability density functions:

$$g_{(i,j)}^{\phi^P}[t](z) \triangleq \zeta_{(i,j)}^u \Bigg(\mathop{\ast}_{k\in\mathcal{N}_j} f_k^b[t] * f_k^e[t](z)\Bigg) * f^u[t]\big(\zeta_{(i,j)}^u z\big), \tag{5.20}$$

$$g^{\phi^Q}_{(i,j)}[t](z) \triangleq \frac{\zeta^u_{(i,j)} \prod_{k\in\mathcal{N}_j} \left(\kappa^b_k[t]\kappa^e_k[t]\right)}{\kappa^u[t]} f^u[t]\left(\frac{\zeta^u_{(i,j)} z}{\kappa^u[t]}\right) * \left(\mathop{\circledast}_{k\in\mathcal{N}_j} f^b_k[t]\left(\frac{z}{\kappa^b_k[t]}\right) * f^e_k[t]\left(\frac{z}{\kappa^e_k[t]}\right)\right), \tag{5.21}$$

$$g^{\phi^V}_i[t](z) \triangleq \gamma^u_i[t] \prod_{l\in\mathcal{N}} \left(\gamma^b_{(l,i)}[t]\gamma^e_{(l,i)}[t]\right) f^u[t]\left(\gamma^u_i[t]z\right) * \left(\mathop{\circledast}_{l\in\mathcal{N}} f^b_k[t](\gamma^b_{(l,i)}[t]z) * f^e_k[t](\gamma^e_{(l,i)}[t]z)\right). \tag{5.22}$$

The proof of Theorem 1 and the definition of coefficients $\zeta^u_{(i,j)}$, $\gamma^b_{(l,i)}[t]$, $\gamma^e_{(l,i)}[t]$, and $\gamma^u_i[t]$ are given in Appendix I. Here, we do not make *any* assumption about the distribution of random parameters. Specifically, we do *not* assume any pre-determined PDF, such as Gaussian distribution. The discrete convolution in Theorem 1 can be calculated efficiency, e.g., using the methods in [97]. A brief discussion on the computational complexity of these convolution operations is given in the Section 5.4.6.

5.2.3 Design Implications

The results in Theorem 1 can be used to analytically, yet accurately, model the complex probability distributions of line power flows and voltage buses. An example is shown in Fig. 2. Here, we compare two methods. First, the proposed analytical method where we obtain the non-parametric distributions of operational parameters from the numerical convolution in Theorem 1. Second, the Monte-Carlo Simulation (MCS) method, where *extensive scenario generations* from the original random variables are applied to the power flow model in (1)-(3). We can see that the PDFs obtained from Theorem 1, achieve the same results as the MCS method. However, the computation complexity of our analytical method is much less than that of the MCS method, see Section 5.4.6.

5.3 Optimal Operation and Deployment of Energy Storage Units

The analytical approach in Section 5.2 can also be used to find the best charge and discharge schedules for the ESS in an optimization-based framework, as we will see in details next.

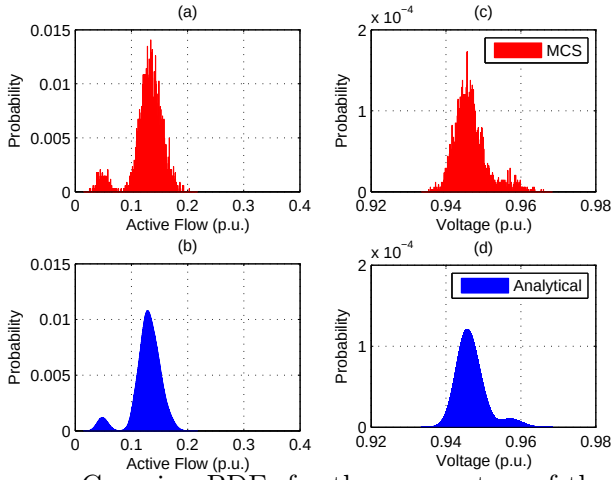

Figure 5.2: Example non-Gaussian PDFs for the parameters of the network in Fig. 1: (a) and (b) power flow in line $(6, 10)$; (c) and (d) voltage at bus 10.

5.3.1 Bus Voltage Violation Chance Constraints

At each time slot, the probability of under- and over- voltage violations must be less than a certain threshold $\epsilon > 0$:

$$\begin{aligned} \Pr\Big\{V_i[t] \le \underline{v}\Big\} < \epsilon \quad &\Rightarrow \quad F_i^V[t](\underline{v}) < \epsilon, \\ \Pr\Big\{V_i[t] \ge \overline{v}\Big\} < \epsilon \quad &\Rightarrow \quad 1 - F_i^V[t](\overline{v}) < \epsilon. \end{aligned} \tag{5.23}$$

From (5.19), we can rewrite (5.23) as

$$\begin{aligned} G_i^{\phi^V}[t]\Big(1 - \underline{v} - \psi_i^V[t]\Big) > 1 - \epsilon, \\ G_i^{\phi^V}[t]\Big(1 - \overline{v} - \psi_i^V[t]\Big) < \epsilon. \end{aligned} \tag{5.24}$$

Since, by definition, $G_i^{\phi^V}[t]$ is a non-decreasing function, we have unique equivalents for (5.24) as follows [98]:

$$\begin{aligned} 1 - \underline{v} - \psi_i^V[t] > \sup\{\phi | G_i^{\phi^V}[t](\phi) \le 1 - \epsilon\}, \\ 1 - \overline{v} - \psi_i^V[t] < \inf\{\phi | G_i^{\phi^V}[t](\phi) \ge \epsilon\}. \end{aligned} \tag{5.25}$$

The right-hand sides in (5.25) are known, as long as $G_i^{\phi^V}[t]$ is known. Since $\psi_i^V[t]$ is a linear function of the ESS active and reactive power variables, the constraints in (5.25) are linear.

5.3.2 Line Active Power Flow Violation Chance Constraints

Next, we set the constraints to limit the probabilities of violating line thermal limits based on the line power flows:

$$\begin{aligned} &\Pr\Big\{P_{(i,j)}[t] \geq \overline{p}\Big\} < \epsilon \;\Rightarrow\; F^P_{(i,j)}[t](\overline{p}) > 1-\epsilon, \\ &\Pr\Big\{P_{(i,j)}[t] \leq \underline{p}\Big\} < \epsilon \;\Rightarrow\; F^P_{(i,j)}[t](\underline{p}) < \epsilon, \end{aligned} \tag{5.26}$$

and with the same analogy of Section 5.3.1, we arrive at

$$\begin{aligned} &\overline{p} - \psi^P_{(i,j)}[t] > sup\{\phi | G^{\phi^P}_{(i,j)}[t](\phi) \leq 1-\epsilon\}, \\ &\underline{p} - \psi^P_{(i,j)}[t] < inf\{\phi | G^{\phi^P}_{(i,j)}[t](\phi) \geq \epsilon\}. \end{aligned} \tag{5.27}$$

5.3.3 Energy Storage System Operation Constraints

The energy that is discharged from an ESS into the grid at a certain time slot must be first charged into the ESS at some earlier time slots. Let $E^s_i[t]$ denote the energy that is stored in the ESS at bus i during time slot t. We must have:

$$\begin{aligned} &\sum_{\tau=1}^{t} E^s_i[\tau] \leq K^{up}_{cp} Ah_i \quad \forall i \in \mathcal{N}_S, \forall t \in \{1, \cdots, T\}, \\ &\sum_{\tau=1}^{t} E^s_i[\tau] \geq K^{dw}_{cp} Ah_i \quad \forall i \in \mathcal{N}_S, \forall t \in \{1, \cdots, T\}. \end{aligned} \tag{5.28}$$

The ESS power output constraints can be expressed as:

$$-I^s_i \leq P^s_i[t] \leq I^s_i, \tag{5.29}$$

where I^s_i denotes the rating of its interface.

5.3.4 Energy Storage System Efficiency Constraints

The efficiency of the storage unit can be modelled as [99]:

$$E^s_i[t] = max\{\eta_0 P^s_i[t], 1/\eta_0 P^s_i[t]\}\Delta t. \tag{5.30}$$

5.3.5 Energy Storage System Deployment Constraints

If we seek to select the best location(s) to install the storage unit(s), then we need to also define a variable $d_i \in \{0, 1\}$ which indicates whether or not an energy storage unit is

installed at each bus i. Hence, the following constraints must hold:

$$Ah_i \leq d_i \cdot \overline{Ah}, \tag{5.31}$$

$$I_i^s \leq d_i \cdot \overline{I^s}, \tag{5.32}$$

$$\sum_{i \in \mathcal{N}} Ah_i \leq \overline{Ah}, \tag{5.33}$$

$$\sum_{i \in \mathcal{N}} I_i^s \leq \overline{I^s}, \tag{5.34}$$

$$\sum_{i \in \mathcal{N}} d_i = N_{ESS}. \tag{5.35}$$

5.3.6 Energy Storage System Design Objective

Various design objectives can be considered when it comes to installing energy storage units on a distribution grid, e.g., see [78]. However, since the focus in this chapter is on understanding the impact of using non-parametric stochastic optimization in energy storage planning, we account only for a typical design objective. Specifically, we seek to minimize

$$\sum_{i \in \mathcal{N}} \left(\sum_{t=1}^{T} \pi_{opr} \cdot |E_i^s[t]| \right) + \pi_{cap} \cdot Ah_i + \pi_{inv} \cdot I_i^s. \tag{5.36}$$

The first term is related to the *operation* cost, i.e., the wear cost, which is proportional to the charge/discharge level at each time slot. The second and third terms are related to the *installation* cost, which are proportional to the size of the ESS.

5.3.7 Optimization Summary

In brief, the ESS optimization problem is formulated as:

$$\begin{aligned} &\underset{P_i^s[t], E_i^s[t], Ah_i}{\textbf{Minimize}} && (5.36) \\ &\textbf{Subject to} && (5.25), (5.27), (5.28), (5.29), (5.30), (5.31), (5.32), (5.33), (5.34), (5.35). \end{aligned} \tag{5.37}$$

All the constraints in Sections 5.3.1, 5.3.2, and 5.3.3 are linear. The absolute-value function in the first term of the objective function in (5.36) can be replaced by linear constraints using auxiliary variables, c.f. [100]. Therefore, depending on whether the constraints in Sections 5.3.5 and 5.3.4 are taken into consideration, the formulated optimization problem is either a *linear program* or a *mixed-integer linear program*.

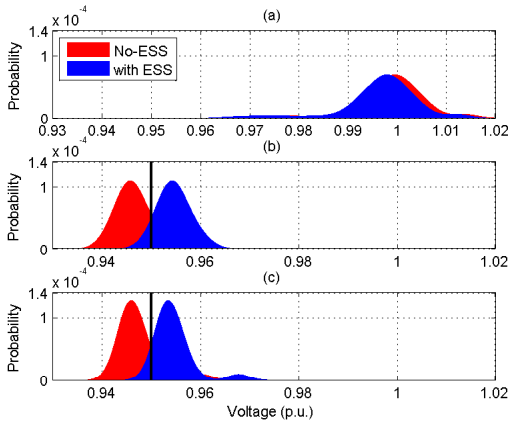

Figure 5.3: The pdf of voltage at bus 10 with and without installed ESS: (a) The ESS is charged during time slot 8, which is an off-peak hour, and this has resulted in some tolerable drop in voltage; (b) The ESS is discharged during time slot 22, which is a peak hour, and this has resulted in some desirable increase in voltage; (c) The ESS is discharged also during time slot 24, which is another peak hour, and this has resulted in some desirable increase in voltage. The probability of violating the minimum threshold at hour 22 reduces from 0.7 to only 0.1 when the ESS is being used.

5.4 Case Studies

Again, consider the 13-bus distribution feeder in Fig. 6.1. It is assumed to be balanced. The baseload is synthesized by aggregating the metered hourly loads of 633 residential consumers in the PECON project [13], from January 2012 to August 2014. This is done such that the average combined load at each bus roughly matches its original feeder load in [101]. The generation output of a solar panel is synthesized by applying the metered pair of solar irradiation and temperature to a detailed dynamic model of a 1.2 MW solar panel in PSCAD [102]. The solar irradiation and temperature data was obtained from the LLNL database over six years form 2008 to 2013 for the months of May and June [12]. The hourly load of EV charging stations are from [65]. Given the focus of this chapter, we take the PDFs of the random variables, e.g., solar generation, baseload, EV charging, etc. as given. These PDFs are obtained using the above historical hourly data.

The cost of battery is calculated for WB-LYP1000AHA lithium ion 1000 Ah battery modules with 3.2V discharge voltage [34]. The batteries operate between 20% to 80% of their nominal capacity. The rated lifetime of these batteries is 12,000 cycles and the current

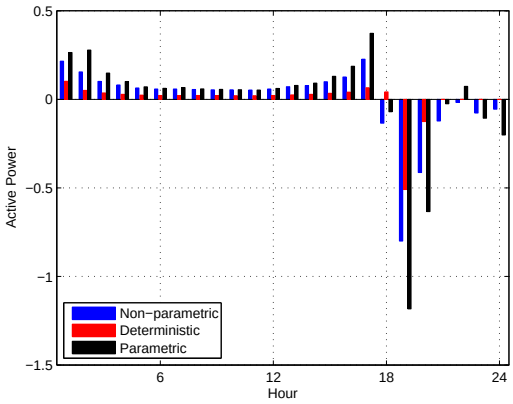

Figure 5.4: The hourly ESS operation schedule based on three optimal designs.

market price is \$1,660 per module. Therefore, by dividing the module price by

$$2 \times Ah \times volts \times cap(\%) \times N_{cycle}, \tag{5.38}$$

we can estimate the battery wear cost as 36 \$/MWh per cycle.

5.4.1 Parametric versus Non-Parametric Design

We compare our Non-Parametric Chance-Constrained (NPCC) approach with two other approaches in ESS planning: 1) Deterministic, where all random variables are represented by their mean values; 2) Parametric chance-constrained (PCC), where all random variables are represented by their Gaussian approximations, i.e., based on their mean and variance.

We start off our analysis based on a simplified problem set up, where the line power flow limits are not enforced, and only the bus voltage limits are considered. The minimum voltage threshold is assumed to be 0.95 per unit. The acceptable probability of violating the minimum voltage threshold is $\epsilon = 0.1$ or less. We consider the typical scenario where the battery system does not provide reactive power support. The location of the storage unit is assumed to be fixed at bus 7.

The probability mass functions of voltage at bus 10 are shown in Fig. 6.3, where there is severe voltage drop at peak hours prior to using ESS. The voltage distributions in one off-peak hour, hour 8, and two peak hours, hours 22 and 24 are shown prior and after ESS compensation. We can see that the use of ESS reduces the probability of violating the

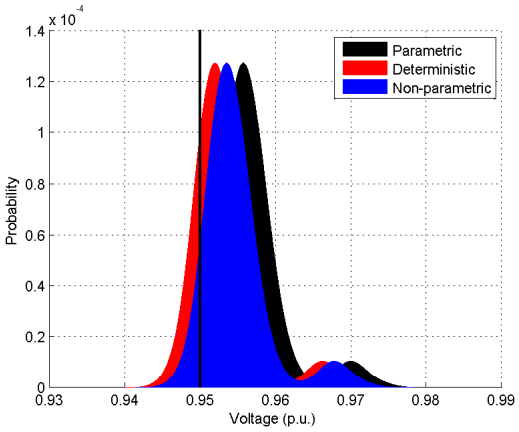

Figure 5.5: The pdf of voltage in bus 10 at hour 24, under three different design approaches for the case study in Section 5.4.1.

minimum threshold at peak hours. The probability of violating $\underline{v} = 0.95$ in bus 10 at hour 22 prior to ESS installation is 0.7. Such probability reduces to only 0.1 once the ESS is installed.

Next, we show the ESS operation schedules for various designs in Fig. 5.4. We can see that different designs lead to significantly different charge and discharge schedules. Accordingly, the obtained optimal size of the ESS is also different for each design. Based on the deterministic approach, it is presumed that the system constraints are met most of the time, thus *under-estimating* the potential for voltage violations. Accordingly, the size of the ESS unit is under-estimated and the allocated ESS unit is not used extensively. On the contrary, the PCC approach *over-estimates* the potentials for voltage violations. As a result, the ESS utilization based on PCC approach is higher than the NPCC approach in most peak hours. The required ESS capacity is also larger. Note that, the optimal ESS size based on the deterministic, PCC, and NPCC design approaches are 1.05, 3.57, and 2.69 MWh, respectively.

The voltage distributions for the deterministic, PCC, and NPCC designs are shown in Fig. 5.5. We can see that the deterministic approach compensates for the voltage less than the NPCC approach, whereas the PCC approach compensates more than the NPCC approach at this hour. The probability that the voltage distribution falls below $\underline{v} = 0.95$ is 0.21, 0.093, and 0.018 for the deterministic approach, the NPCC approach, and the PCC approach, respectively.

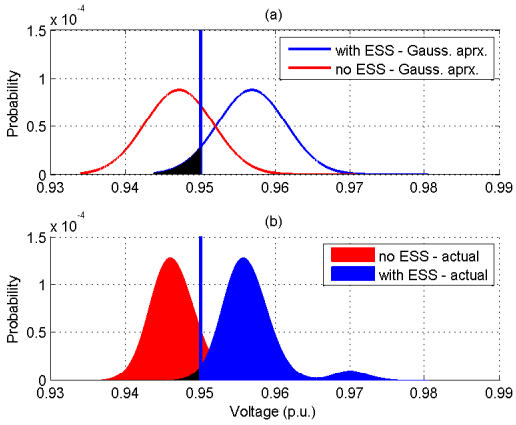

Figure 5.6: Voltage compensation at hour 24 based on the PCC approach: (a) the Gaussian approximation of the voltage pdfs; (b) the true voltage pdfs.

Additional details about the ESS operation during time slots 22 and 24 based on the PCC approach are given in Fig. 5.6. Here, the Gaussian approximations of the voltage probability functions with and without ESS unit are compared with the empirical pdf curves. The approximated probability of voltage violation, i.e., the black shaded area in Fig. 5.6(a), is 0.07. However, the empirical probability of voltage violation is only 0.02 in Fig. fig:gaussian(b). This confirms our previous observation that a PCC approach often over estimates the probability of voltage violation; thus, requiring a ESS size larger than what is actually needed. The inaccurate estimation of the probability of violating the voltage constraints is the main reason for the difference between the PCC approach and the NPCC approach.

5.4.2 Compensation on System Operational Limits

In this section, we discuss another factor that further shows the advantages of NPCC over PCC. First, we note the fact that an ESS cannot increase the voltage or decrease the power flow at a certain hour, *unless it decreases the voltage and increases the power flow at another hour*. Therefore, the distribution network must originally be capable of tolerating bus voltage decreases or line power flow increases during certain hours; otherwise the ESS is *not* the solution for alleviating the system undesirable states. Therefore, next, we examine the system operational bounds under different ESS design approaches.

Unlike in Section 5.4.1, where the minimum threshold for voltages was pre-set

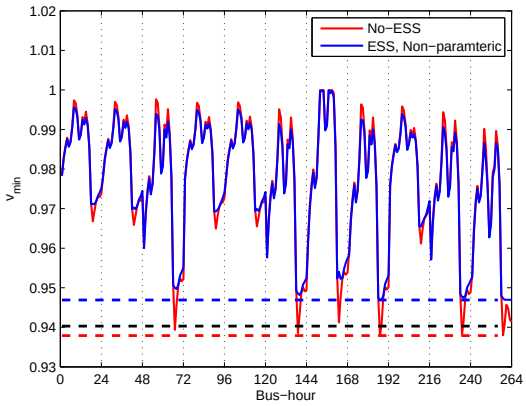

Figure 5.7: The best minimum voltage bounds achieved during $11 \times 24 = 264$ bus-hour instances under NPCC approach.

to $\underline{v} = 0.95$, and the required ESS capacity was obtained using different approaches, in this section, we instead assume that the ESS storage capacity is fixed to $2MWh$ and we rather obtain the best voltage operation thresholds using non-parametric and parametric approaches. Same as in Section sec:Ilust, we assume that $\epsilon = 0.1$.

To examine the system operational bounds, we introduce some slack variables to all chance constraints. That is, we treat the acceptable system state bounds in Sections 5.3.1 and 5.3.2 to be decision variables. Instead, we set the ESS capacity to be fixed. We also introduce a new *regulatory* term $K_{reg} \max_{i,t}\{\underline{v}_i[t]\}$ into the objective function in (5.36), where K_{reg} is a large weight factor. The purpose of adding this regulatory term is to make all chance constraints binding so that we can obtain the best bounds achievable for each state.

Fig. 5.7 shows the tolerable bounds for the case of bus voltage compensation when the proposed NPCC approach is used. The blue dashed line shows the minimum of such bounds across all locations and all time slots. Here, we also show the similar minimum bounds for the PCC and the No-ESS case. In this figure, if the minimum bound is 0.94 p.u. with at least 90% probability at all times, then the PCC approach gives an *infeasible solution* with 2 MWh of ESS at bus 8.

A similar analysis can be done to assess the tolerable bounds for line power flow compensation. Here, we must minimize the power flow on the most congested line. To

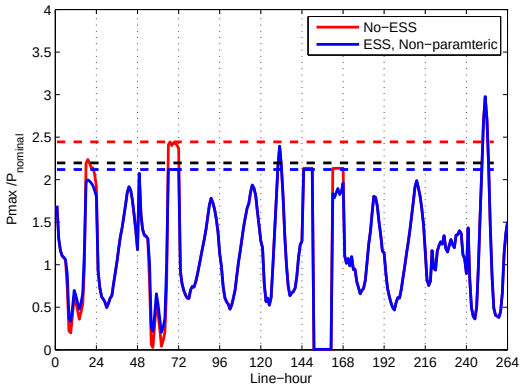

Figure 5.8: The best maximum active power flow bounds achieved during $11 \times 24 = 264$ line-hour instances under NPCC approach.

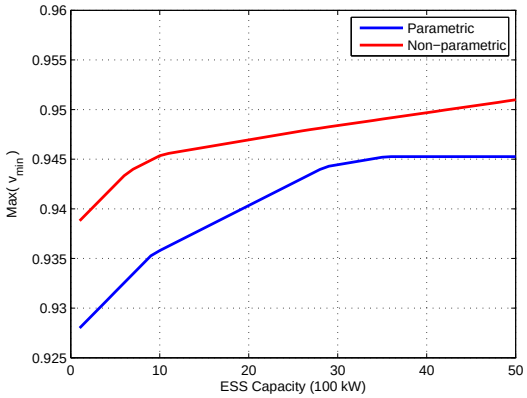

Figure 5.9: The maximum lower thresholds bounds achieved in all buses for different ESS capacities under NPCC and PCC design approaches.

do so, we shall minimize the maximum of $\overline{p}/p_{nominal}$ for each line. The results are shown in Fig. 5.8. We can see that the ESS compensation brings down the highest power flow limit. However, the ESS may affect only the lines that lie on the path from the ESS to the substation bus. Therefore, the ESS location is of importance if we intend to lower the power flow on a particular line. For each ESS capacity, this figure also shows how much the maximum power flow can be reduced by the ESS among the lines that *have the possibility of improvement based on the ESS location.*

The best minimum voltage bounds achieved in 24 hours at all buses as a function of ESS capacity under NPCC and PCC stochastic design approaches are shown in Fig. 5.9.

First, we note that both curves are continuous, piecewise linear, concave, and monotonic increasing, c.f. [103, Lemma 2]. Second, we can see that the NPCC approach can always enforce higher minimum voltage, regardless of the capacity of the ESS.

5.4.3 Impact of Location

Next, we take a closer look at the impact of the ESS location on improving the system tolerable bounds that we introduced in Section 5.4.2. This also brings up the question on optimizing the location, when there are multiple ESS units. We observe in Fig. 5.10 that

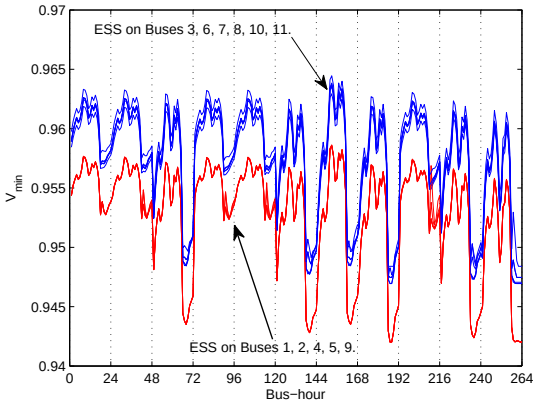

Figure 5.10: The Impact of ESS location on voltage improvement at each bus.

installing an ESS at either of buses 1, 2, 4, 5, and 9 does not significantly improve the minimum voltage bounds. Therefore, at least for the purpose of voltage improvement, these buses are *not* suitable locations for ESS installation. Note that, we do not suffer from over-voltage issue of PV injections at end buses since the grid is heavy-loaded.

Based upon a similar analysis as in Section 5.4.2, Fig. 5.11 shows the normalized maximum active power flow bound reduction in each line, i.e. $\Delta\overline{p}$ for the cases of *with* and *without* ESS installation. We can see that installing the ESS at each bus improves the active power flow only on certain lines in the path between the ESS bus and the reference bus. Since the back current issue is not considered, installing an ESS is always preferred in the end buses of a heavy-loaded line.

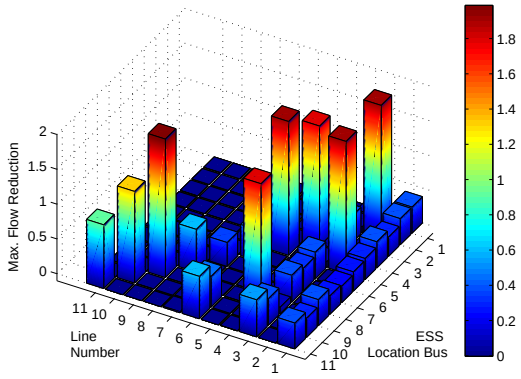

Figure 5.11:The impact of ESS location on active flow improvement at each line.

5.4.4 Optimal Locations and Sizes of Multiple ESS Units

Recall that in in sections 5.4.1 to 5.4.3, only a single ESS unit was deployed and the optimization did not involve choosing the location of the ESS. As we illustrated in Section 5.4.3, however, the location of the ESS unit can have a significant impact on its ability to improve the system operational parameters. Additionally, the *locations of uncertain resources* in the distribution system can also have impact on the ESS requirements for the system. Therefore, we obtained the optimal ESS locations and sizes for the base-case as well as for several additional test cases, where the location of some random resources are changed in the test distribution system of Fig. 6.1. The results of the optimal deployment solutions for the NPCC and PCC approaches are given in Table 5.1 for two ESS units (i.e. $N_{ess} = 2$). Note that, the ESS units are deployed in order to maintain the voltage violation probabilities within 10% of the thresholds as in Section 5.4.1.

Table 5.1: Optimal locations and sizes for two ESS units

Case Number	PV Bus	EV Chargers Buses	Optimal ESS Plan			
			Capacity (MWh)		Bus Location	
			NPCC	PCC	NPCC	PCC
1	7	7,8,9	1.6,0.33	0.12, 3.2	8, 11	8,10
2	3	2,4,11	0.29, 0.03	0.31,0.02	8,10	8,10
3	4	2,3,6	0.38, 0.08	0.5,0.3	8,10	10,11
4	1	4,5,7	0.32, 0.01	0.13,0.21	8,10	7, 8

From the results in Table 5.1, we can make several observations. First, the NPCC method achieves a better solution in terms of a lower deployed ESS capacity to maintain the same voltage thresholds. The overall ESS capacity deployed by NPCC is 1.93 MWh, whereas PCC requires the deployment of 3.32 MWh ESS capacity. Second, the deployed capacity with multiple ESS units and in the optimal locations is smaller both in NPCC and PCC approaches compared to Section 5.4.1 where the location of the single ESS was arbitrarily selected. Third, the choice of the design method, i.e., NPCC or PCC, in representing the random variables can have an impact on the optimal locations of ESS unit as well. Specifically, from case numbers 2-4 in Table 5.1, it is also observed that the required ESS capacity as well as the optimal ESS locations are greatly affected by the locations of the random resources on the distribution system. In Case 1, the placement of those resources at the end buses has led to more voltage drops and hence more ESS capacity requirements. In contrast, in Cases 2 to 4, we have less ESS requirements, because several random resources are placed in up-stream buses of the distribution grid. Finally, the design objective towards which the ESS deployment is optimized, e.g. better voltage compensation, lower line power flow reduction, and/or reverse flow prevention, has great impact on the choices of the ESS capacity and locations.

5.4.5 Comparison with Scenario-Based Stochastic Optimization

In this section, we compare the performance of our proposed NPCC approach with that of the methods that rely on sampling of input random variables. To this aim, we approximate the chance constraints in (25) and (27) with some convex bounds in the form of their expected values, specifically by using the Markov Bounds [104]. We then compare the two approaches for the same set-up and objectives of Section 5.4.1.

Table 5.2: Optimal locations and sizes for two ESS units to mitigate the voltage violation.

Method	Decision Vars. Num.	ESS Cap. (MWh)	Voltage Violation Worst Probability
NPCC	97	2.69	0.105
SBO(50)	55800	6.25	0.112
SBO(100)	217800	5.5	0.086
SBO(500)	1M+	4.1	0.073

The optimal ESS capacity deployed by each approach to maintain the system voltage within the 90% tolerable range is compared for each approach, and the results are shown

in Table 5.2. Here, the scenario-based optimization (SBO), solved with 50 scenarios, converges roughly within the same time that our proposed approach converges, including its distribution processing time. However, the deployed ESS capacity to maintain the voltage violations within the probability threshold, is much higher for SBO than the NPCC approach, which means a *better resource management* for our proposed NPCC approach.

We also compared the actual numerically-obtained probability of voltage violation for each method using Monte-Carlo simulation with 10,000 random scenarios. The worst probability of voltage violation across the system buses and at different hours is shown in Table. 5.2. We observe that SBO with 50 scenarios leads to even a higher probability of violation, even with a larger ESS capacity deployed. We also see in Table 5.2 that the performance of SBO indeed improves with a larger number of scenarios. However, such improvement is obviously at the expense of higher computational complexity. Another observation was that increasing the number of scenarios is not *easy*, because as we increase the number of scenarios, the performance of the scenarios-based optimization approach either becomes dependent to the choice of solver software or all solvers face *numerical issues* to reach a solution.

We note that, there exist techniques, e.g those in [105–107], to decompose and / or improve the computation efficiency of scenario-based optimization approaches. They often are applicable to a wide range of optimization problems, including our intended problems, and are independent of the inherent computation burden of solving the optimization problem under many instances of the random variables. However, those techniques are *not* always guaranteed to convergence.

5.4.6 Computational Complexity and Accuracy

Finally, we assess the impact of the common DistFlow model linearization on the result accuracy. Fig. 5.12 compares the empirical voltage PDFs obtained from Theorem 1 and that of a Monte-Carlo Simulation that is based on *non-linear power flow equations*. We can see that due to ignoring the line losses, the analytical voltage PDFs are slightly different from the empirical PDFs. Thus, there is a small over estimation in the voltage PDFs when the linear flow model is used. However, the significantly lower computation complexity of our analytical method compensates its slight inaccuracy. For example, in Fig. 5.12, we perform only 12 convolution operations to obtain the voltage PDF in each bus, whereas

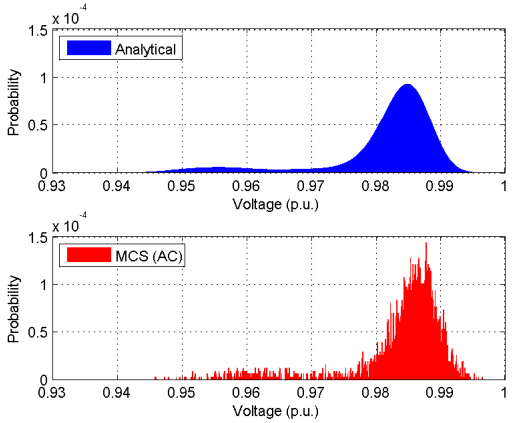

Figure 5.12:Power flow linearization impact on a voltage distribution at hour 17.

more than 60, 000 scenarios are generated to construct the empirical PDF.

Next, we examine the impact of considering the transverse distribution line parameters, e.g. the capacitances of coaxial cables, on the probability distribution of operational parameters, e.g. bus voltages. Note that, all the results in Sections 5.4.1 to 5.4.5 are obtained by neglecting the impact of transverse line parameters. However, it is still possible to consider the impact of transverse line parameters as constant power elements connected to buses. This is done in Fig. 5.13, where we compare the results of bus voltage distribution at bus 11 and hour 17, for two cases. The first case is where the impact of transverse line parameters are neglected. The second case is where we did model such parameters. The results are obtained from MCS with 60,000 scenarios. The AC power flow equations are solved by applying second-order cone programming, c.f. [94].

We see in Fig. 5.13 that the voltage distribution inaccuracy due to neglecting the line suscpetance is *not* significant. The reactive power injections from the lines shunt capacitors are well below $8{\times}10^{-4}$ p.u. in all buses. It is presumed the results inaccuracy due to *inability* of Distflow model in representing lines constant impedance capacitance, instead of constant power, is even *less* significant.

We also compared the computation efficiency of our proposed approach with those of the two existing approaches. The results are shown in Table 5.3. Note that, our proposed approach consists of two parts: first, an analytical stochastic representation of the operational parameters, i.e. bus voltages and line active and reactive flows; and second, a chance-constrained optimization approach based on the results in the first part. The com-

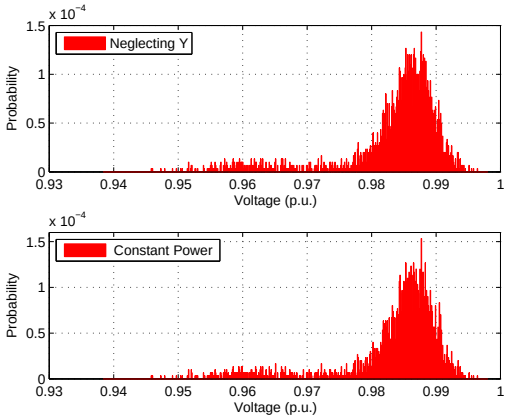

Figure 5.13: The voltage distribution at bus 11 and hour=17, which are obtained using MCS with 60,000 scenarios and AC power flow model: (a) the line transverse parameters (Y) are neglected; (b) Those parameters are modelled as constant power shunt elements.

putation time required for the first part is compared to that of the Monte-Carlo simulation method discussed in section 5.2.3 with 60,000 scenarios to produce comparable resolution of operational parameters probability density functions. The amount of computation time required for MCS is more than 500 times that of our proposed analytical approach. The overall runtime of our proposed approach, i.e. for the first as well as the second part mentioned earlier, is also compared with that of scenario-based stochastic optimization (SBO), discussed in section 5.4.5, with a mere 100 scenarios. Clearly, in order to increase the accuracy of the scenario-based optimization approach, the required computation time increases significantly. The runtime obtained for all the methods above is based on a single 2.67 GHz processor.

Table 5.3: The computation time required form Different Methods.

Method	Analytical	Monte-Carlo	NPCC	SBO
Runtime (min.)	37	20000	90	225

The convolution operations required to obtain *each* operational parameter is at most equal to the number of independent random variables. It does *not* depend on network size. Also, for a practical system, we may not need the PDFs of all operational parameters, but just for a few important ones. To assess the computation efficiency, in the data preparation process, the hourly PDFs of more than 500 individual residential users with length of 60 for each vector, i.e., 12,000 operations in total, was convolved in only few minutes using a single processor.

5.5 Additional Remarks and Extensions

5.5.1 Modeling Chance-Constraints Based on Line Currents

In section 5.3.2, the chance-constraints related to line flows were expressed in terms of power. However, in practice, for lines below 36 kV, this value is often expressed in terms of current. If one chooses to use a current-based model, he/she needs to transform our power-limit constraints to current-limit constraints, e.g., in form of $I^2 < I^2_{max}$. Since $I^2 = S^2/V$, such constraint can then be transformed into $S^2 \leq I^2_{max}V$. If we neglect the changes in voltage, then after replacing S^2 with its active and reactive power terms, we have:

$$\Big\{P^2_{i,j} + Q^2_{i,j} < S^2_{max}.\Big\} > 1 - \epsilon. \tag{5.39}$$

If the ESS power injection is given, then we can obtain the distributions of $P_{i,j}$, $Q_{i,j}$, and $S_{i,j}$ in terms of ESS injections. But even in that case, the above family of constraints will not be convex. Note that, since $P_{i,j} = \psi^P_{i,j} + \phi^P_{i,j}$, for the square variable, we will have multiplication of random variables and decision variables, which renders the optimization non-convex when we use non-parametric distributions. Of course, a tractable chance-constraint on the current of the transmission line can still be *approximated*, possibly by using several independent linear constraints on active and reactive power flow of the line. However, addressing this issue is beyond the scope of this chapter. This could be a pointer for a future work.

5.5.2 Impact of Slack-Bus Voltage Variations

In order to study the stochastic representation of the model in Section 5.2, we assumed that the voltage on the slack bus is fixed. However, in practice, this value might fluctuate as a function of the state of the upstream grid. The impact of slack bus voltage fluctuations may as well be treated as a stochastic random variable, independent of the nodal power injections. By considering the slack bus voltage as a random variable with probability density function of f^{V_0}, we can write (9) as

$$F^V_i[t](v) \triangleq 1 - \Pr\Big\{\tilde{\phi}^V_i[t] - \tilde{V}_0 \leq -v - \psi^V_i[t]\Big\}, \tag{5.40}$$

which will result in the following CDF of voltage distributions:

$$F^V_i[t](v) = 1 - G^{\phi' V}_i(-v - \psi^V_i). \tag{5.41}$$

Here $G_i^{\phi'^V}$ is the CDF corresponding to density function

$$g_i^{\phi'^V}(z) = -g_i^{\phi^V}(z) * f^{V_0}(-z). \tag{5.42}$$

5.6 Conclusions

A non-parametric chance-constrained optimization approach was proposed for energy storage operation and planning in power distribution networks. The analysis was done by introducing new closed-form stochastic models for various key operational parameters, with no restricting assumption on the probably distribution of random parameters. Uncertainties from different sources of different nature, such as DGs and EVs, were considered. Several case studies confirmed the advantages of the proposed design method compared to the conventional deterministic and parametric (based on Gaussian approximation) chance-constrained optimization frameworks. In future, the developed closed-form stochastic models can be used in other non-ESS distribution-level planning problems.

Chapter 5, Appendix: Proof of Theorem 1

From the properties of linear transformations on density functions, c.f. [108], if $Y = a_1X_1 + \cdots + a_NX_N$, then

$$\begin{aligned} f_Y(y) =& f_{a_1X_1}(y) * \cdots * f_{a_NX_N}(y) \\ =& \left(\frac{1}{a_1} \cdots \frac{1}{a_N}\right) \cdot f_{X_1}(y/a_1) * \cdots * f_{X_N}(y/a_N). \end{aligned} \tag{5.43}$$

Therefore, the expression in (5.20) results directly from (5.11) and (5.16), where the coefficient $\zeta_{i,j}^u$ is defined by tracking all the DGs that are on descendants of the intended node:

$$\zeta_{(i,j)}^u \triangleq 1/\left(\sum_{k\in\mathcal{N}_j} \lambda_k^u\right). \tag{5.44}$$

We can show (5.21) similarly. Note that, since $\tilde{Q}_k^b = \kappa_k^b \tilde{P}_k^b$ and $\tilde{Q}_k^e = \kappa_k^e \tilde{P}_k^b$, we have

$$\begin{aligned} f_k^{Q^b}(z) &= (1/\kappa_k^b) f_k^b(z/\kappa_k^b), \\ f_k^{Q^e}(z) &= (1/\kappa_k^e) f_k^e(z/\kappa_k^e). \end{aligned} \tag{5.45}$$

Therefore, from (5.12), (5.16) , and (5.43), we can obtain (5.21).

To derive (5.22), we note that the distributions $\phi^P_{k,j}$ across $(k,j) \in \mathcal{L}_{i,0}$ are not independent. The distributions of $\phi^Q_{k,j}$ across $(k,j) \in \mathcal{L}_{i,0}$ are not independent either. Thus, we can rewrite (5.13) in terms of the original independent random variables f^b_k, f^e_k, and f^u. Specifically, from (5.11)-(5.13), we have:

$$\gamma^b_{(l,i)}[t] \triangleq 1 \Big/ \left(\sum_{(j,k)\in\mathcal{L}_{i,0}\cap\mathcal{L}_{l,0}} 2(R_{(j,k)} + X_{(j,k)})\kappa^b_l[t] \right), \tag{5.46}$$

$$\gamma^e_{(l,i)}[t] \triangleq 1 \Big/ \left(\sum_{(j,k)\in\mathcal{L}_{i,0}\cap\mathcal{L}_{l,0}} 2(R_{(j,k)} + X_{(j,k)})\kappa^e_l[t] \right). \tag{5.47}$$

For renewable DGs, since they are all assumed to depend on the similar solar irradiance, we combine the coefficients of all the DG's that share a path with the intended node:

$$\gamma^u_i[t] \triangleq 1 \Big/ \left(\sum_{l\in\mathcal{N}^s} \sum_{(j,k)\in\mathcal{L}_{i,0}\cap\mathcal{L}_{l,0}} \lambda^u_l \big(2(R_{(j,k)} + X_{(j,k)})\kappa^u_l[t]\big) \right) \tag{5.48}$$

5.7 List of Symbols, Chapter 5

$\mathcal{N}, \mathcal{L}$ Set of all buses, and all distribution lines.

$\mathcal{N}_i$,$\mathcal{D}_i$ Set of descendants and direct descendants of bus i.

$\mathcal{L}_{i,0}$ Set of lines on the path from bus i to bus 0.

s Superscript indicating storage.

e Superscript indicating charging station.

r Superscript indicating renewable generator.

b Superscript indicating baseload.

u Superscript indicating solar panel.

i, j, k, l Subscripts indicating bus numbers.

(i,j) Distribution line connecting buses i and j.

V, P, Q Functions for voltage, active and reactive power.

v, p, q Values for voltage, active power, and reactive power.

U, H Active, and reactive power output of a solar panel.

ϕ Random part of an operational parameter.

ψ Decision variable part of an operational parameter.

$t, \Delta t$ Index of time slot, duration of a time slot.

R, X Line resistance and reactance.

f, g Probability density function.

F, G Cumulative probability distribution function.

κ Reactive to active power ratio for an energy resource.

λ Number of solar panels.

ζ Scale of a random input at power flow distributions.

γ Scale of a random input at voltage distributions.

$*_{i=1}^{N}$ Convolution integral over N functions.

ϵ Probability target for a chance constraint.

E Drawn energy from battery storage system.

η_0 Efficiency coefficient of energy storage system.

Ah Installed capacity of energy storage system in a bus.

N_{ESS} Number of total installed energy storage systems.

π Scale factor for installation or operation costs.

K_{cp} Scale factor for capacity to available energy.

$\overline{(\cdot)}, \underline{(\cdot)}$ Indicators of maxima and minima of variables.

Part III

Distributed Generation and Demand Response Planing at the Distribution Grid

Chapter 6

Distributed Generation Planning to Profit Both Utility and DG investors

Most current regulations allow small-scale electric generation facilities to participate in distributed generation (DG) with few requirements on power-purchase agreements. However, in this chapter, it is shown that distribution companies can alternatively encourage DG investors into DG contracts that can significantly benefit the utility network. In this regard, a new algorithm is proposed to determine the best sites, sizes, and optimal payment incentives under such special contracts for committed-type DG projects to offset distribution network investment costs. On one hand, the aim is to allocate DGs such that the present value profit gained by the distribution company is maximized via procuring power from DGs and the market at a minimum expense. On the other hand, each DG unit's individual profit is taken into account to assure that private DG investment remains economical. The algorithm is verified in various cases and the impacts of different factors are accordingly studied.

6.1 Introduction

The increasing growth in electric load has made the traditional vertically integrated power systems inefficient due to the significant investment cost of transmission and

distribution systems expansion. Therefore, there is a growing interest towards a distributed generation (DG) paradigm to provide small-scale generation opportunities close to consumer sites. Furthermore, DG systems can benefit from short lead time and low investment risk, small physical sizes, and flexibility in locations. For example, they can be installed nearly everywhere without the land availability challenges of traditional power plants. Due to these and many other advantages, DG is expected to play a significant role in the power grid's operation, structure, design and upgrading planning [109, 110].

There exists a wide range of algorithms in the literature for the purpose of distribution planning incorporating DGs. One thread of research focuses on optimization-based approaches with a *single* objective function, e.g., with respect to power losses, voltage profile, and total generation or distribution costs. In [111], the authors proposed an algorithm to determine the optimum locations of DGs to minimize power losses. In [112], an optimal planning framework is introduced to minimize the total system planning costs for DG investment, operation, maintenance, as well as the cost of purchased power and system losses. In [113], the Artificial Bee Colony algorithm is applied to determine the optimal size, power factor, and location of DGs to minimize the total real power loss in the system. Another thread of research in DG planning involves optimization-based approaches with *multiple* objectives. For example, a particle swarm optimization algorithm is introduced in [114] to determine the location and size of DGs considering voltage profile, total harmonic distortion reduction and losses on distribution lines. Another multi-objective algorithm is developed in [115] to minimize the losses, investment cost in new facilities and distribution lines, and the number of faults and the lengths of interruption times. A heuristic approach for DG investment planning is proposed in [116] that aims to minimize the distribution company (DISCO)'s investment costs, operation costs and the costs related to system losses. It works by searching for a set of DGs that can have their marginal benefits greater than their overall installation and operation cost. Finally, in [117], a multi-objective approach is proposed to determine the optimal size and location of DG units, considering various implementation challenges, using the particle swarm optimization.

Most of the previous studies, such as those in [111–119], focus on reducing the investment and running costs of DISCO, including the cost for installing new DG units. In this regard, they implicitly assume that the DISCO is solely responsible for the *investment* and *operation* of the DG units. However, in many practical scenarios, distribution companies purchase power from *independent* DG owners without being directly involved in

investment or operation [120]. To address this issue, in [121], the authors apply the concept of local marginal prices (LMPs) to distribution generation to maximize the social welfare between DISCO and DG providers. Similarly, in [122], DG units are positioned based on LMPs, power loss reduction, and voltage improvement criteria. However, unlike the wholesale electricity markets, the distribution systems are *not* fully decentralized and a single utility company usually operates across a region. Finally, in [123], increasing economic benefits for DG investors is addressed, but there is no consideration of achieving the optimal utility network performance or maximizing DISCO's profit. Therefore, a major challenge for a DISCO while implementing purchase-based procurement of power is to enforce optimal system performance across several independently owned and operated DGs. The key question that needs to be answered is: *How can a DISCO encourage the DG investors and operators into special contracts which can benefit the utility and enforce optimal overall grid performance?* Answering this challenging question is the main focus of this chapter. Our contributions can be summarized as follows.

- First, a detailed economic model is developed for DG installation in distribution networks. Our model determines the optimum location, capacity, generation amount in different load levels (namely at on-peak and off-peak periods), as well as retail power procurement prices for each DG unit in each period of time.
- A new optimization problem is developed to maximize the total profit gained by the distribution company while *maintaining the investment attractive* for independent DG owners and operators by keeping DG profitable.
- Our design takes into account various parameters: the network upgrade costs, including the costs for expanding line segments and transformers, the value of released capacities, DG's lead time, different investment conditions in each bus which could be due to different land value or environmental standards, different daily load levels, future demand growth, power losses, and voltage profile.

6.2 Problem Formulation

6.2.1 Problem Description and Background

Many Independent System Operators (ISOs) have already established policies to facilitate integration of on-site efficient generation, in accordance with their country/state administration objectives in supplying renewable and distributed generation. For example, in many countries, the Renewable Portfolio Standards (RPS) and Renewable Obligation Orders (RO) mandate electricity providers to serve a portion of their load from renewable resources. Although these regulations help the growth of DGs, they do not attempt to optimize the operation and expansion of the distribution networks. As a result, while utilities have to operate in accordance with RPS regulations, they are individually responsible to ensure economic procurement of power. Furthermore, despite the supportive regulations and policies, it is still the case that sometimes the DG investors may find the long-term payback time of the project uneconomical [123–125].

Tackling the above problems is our focus in this chapter. Our system model is within the framework of some existing DG structures in the United States. For instance, consider the Sacramento Municipal Utility District in California, where the feed-in contracts are available for renewable generating units up to 5 MW, including Combined Heat and Power (CHP) Units with a certain required level of pollution standards. These contracts are to sell generation at different periods of time, such as on-peak or off-peak hours, under long-term 10, 15, or 20-years power purchase agreements [126]. The prices offered by the DISCO are usually set to be fixed at different buses and for the whole duration of the contract, depending on the start date of project. Similarly, in this chapter, it is assumed that the DISCO offers standard agreements for DGs, which may include CHP units, and the DISCO has to pay the contracted DG owner at the minimum standard rate in every bus.

Within the practical framework described above, one option to reduce the costs of utilities and to make the investment more attractive, is to encourage certain DG projects that are strategically located with financial benefits for lowering the distribution costs. In other words, distribution companies may increase the offered price to even more than standard tariffs for certain DG projects at certain buses, considering the location, size, technology, and potential external costs (e.g., impacts of the gas infrastructure and real-estate aspects) in order to encourage investors into providing desired on-site generation in desired locations. The DG units considered are the CHP units capable of operating at base load to provide

committed generation. In the rest of this section, the focus is on formulating a new optimization problem to find the best allocation for the DG sites, sizes, and prices to maximize the DISCO's profit while attractive investment for the DG owners is guaranteed. The algorithm needed to solve the formulated optimization problem will be developed later in Section 6.3.

6.2.2 Optimization Problem

The objective of the proposed optimization problem is to maximize the DISCO's profit; while maintaining positive profit for each *individual* DG in the system to assure DG investment attractive. Profit is evaluated in terms of Net Present Value (NPV), a concept in finance that takes into account all the capital investment costs, variable costs during the term of a project, as well as the revenues gained during the planning term. In this regard, the NPV indicates the net present total profit gained with a target interest rate [127]. The optimization problem can be formulated as follows:

$$\begin{aligned} &\textbf{maximize} && NPV_{DISCO} \\ &\textbf{subject to} && NPV_{DG_i} \geq 0, \qquad i = 1, \ldots, n_{DG}, \end{aligned} \tag{6.1}$$

where for the ith DG, NPV_{DG_i} can be obtained in terms of present values for benefit and cost:

$$NPV_{DG_i} = PVB_{DG_i} - PVC_{DG_i}. \tag{6.2}$$

The present value of DG's costs can be written as:

$$\begin{aligned} PVC_{DG_i} = &\left(\frac{(i_f+1)^{n_{end}}-1}{i_f.(i_f+1)^{n_{end}}}\right).\left(\frac{i_f.(i_f+1)^{PEL}}{(i_f+1)^{PEL}-1}\right) \\ &\times \lambda_i.C_{capital}(T_{DG_i}).I_{DG_i} \\ &+ \sum_{j=n_{start}}^{n_{end}} \frac{1}{(i_f+1)^j}\left(\sum_{k=1}^{n_{periods}} P_{DG_i}(k).H(k)\right. \\ &\left.\times \Big[C_{fuel}(T_{DG_i}) + C_{O\&M}(T_{DG_i})\Big]\right). \end{aligned} \tag{6.3}$$

To reach (6.3), all the cash flows that the ith DG receives or pays are discounted back to their present values before they are added together in the summation term. Note that, the present value (PV) of DG's future annuities during the contract is obtained with respect to a future value (FV) in period n as:

$$PV = \frac{FV}{(1+i_f)^n}\ , \tag{6.4}$$

where the nominal interest rate i_f is usually greater than the real interest rate that an investor expects to receive. The nominal interest rate is obtained from the real interest rate, r, by considering inflation rate p, according to:

$$i_f = r + p + r.p \ . \tag{6.5}$$

Here, r is set to the Minimum Acceptable Rate of Return ($MARR$) for DG investors. Clearly, if the NPV_{DG} considering $MARR$ becomes negative, then the DG investment fails to meet the minimum expectation and becomes uneconomical.

The payment period in (6.3) is assumed to be one year and the payments are made at the end of each year. For investments with PEL greater than n_{end}, obtaining the present value requires two steps. First, the capital cost is distributed evenly across the future annuities during the project's economic life. Then the present value of these annuities are added together for the duration of contract. The capital investment for DG is determined regarding its installed capacity, while its variable costs are defined according to each period's generating level (e.g. on-peak or off-peak periods), and the duration of each period. Both capital and variable costs depend on the classified type or technology of the DG. The capital costs also depend on the location of DG which are represented in (6.3) by λ_i. Finally, note that the variable costs begin at the start time of project, which depends on the DG installation lead time.

Following similar discussions as above, the present value of benefits that the ith DG gains can be obtained as:

$$PVB_{DG_i} = \sum_{j=n_{start}}^{n_{end}} \frac{1}{(i_f+1)^j} \sum_{k=1}^{n_{Periods}} \left(P_{DG_i}(k).H(k).C_{offer}(i,k) \right) \ . \tag{6.6}$$

Finally, the NPV of all the cash flows for the DISCO is:

$$\begin{aligned} NPV_{DISCO} = & \sum_{j=1}^{n_{end}} \frac{1}{(i_f+1)^j} \sum_{k=1}^{n_{periods}} \left(P_{load}(j,k)H(k)C_{retail}(k) \right) \\ & - \sum_{j=1}^{n_{end}} \frac{1}{(i_f+1)^j} \sum_{k=1}^{n_{periods}} \left(P_{net}(j,k)H(k)C_{market}(k) \right) \\ & - \sum_{i=1}^{n_{DG}} PVB_{DG_i} + CRB \ . \end{aligned} \tag{6.7}$$

Note that, the revenue of the DISCO is provided by selling power to the retail customers. Of course, the load level may change during different daily and seasonal periods and the total demand may also experience an annual growth. Therefore, both P_{load} and P_{net} may take different values over the years and in different time periods. Since P_{net} also includes the network losses; therefore, reducing the losses means reducing the total amount of procured power. In (6.7), the expenses considered for the DISCO include the payments to the DGs and the cost of procuring the excess power from the wholesale market. While the market price is changing during the day, the customer rates are normally constant; in the optional time of use programs, limited tiers of price rates in summer or winter season (e.g. two rates in SMUD) are considered [126]. The payment of DISCO to the DGs is equal to the total revenue that all DGs will have, thereby is the sum of PVB_{DG_i}.

It is worth mentioning that the DISCO expenses may also include the investment costs for upgrading the network transformers and line segments in order to meet the growing demand in the upcoming years. Installing DG may lower these expenses by releasing the network capacity and hence postponing the network upgrade. The benefit gained from delaying the network upgrades, which is referred to as Capacity Release Benefit (CRB), is obtained by calculating the network expenses of the upgrades during the planning term, when a particular set of DGs are installed, and subtracting from the network upgrade costs when no DG is installed. By performing power flow in the successive years of the planning term and in different load levels, the anticipated year in which each line segment or transformer will be over loaded is obtained and the costs related to its upgrade is discounted back to present. By replacing (6.2)-(6.7) in (6.1), the formulation of the proposed optimization problem is complete. However, in order to have a practical and implementable design, there is also a need to include some other constraints in the optimization problem which are explained in detail in the next sub-section.

6.2.3 Additional Optimization Constraints

- **Active and reactive power balance equations:** The sum of active and reactive power flows injected into a node should match the power flows extracted from that node. Note that $P_G(i)$ in buses which include distributed generation also includes P_{DG_i}. Furthermore, note that P_{net} is equal to, the power injection in the first bus,i.e.

$P_G(1)$. A similar statement is true for the reactive power injection.

$$\begin{aligned} &P_G(i) - P_D(i) = \\ &V_i. \sum_{j=1}^{n_{nodes}} \left[V_j.\big(G_{ij}.\cos(\delta_i - \delta_j) + B_{ij}.\sin(\delta_i - \delta_j)\big)\right] , \end{aligned} \tag{6.8a}$$

$$\begin{aligned} &Q_G(i) - Q_D(i) = \\ &V_i. \sum_{j=1}^{n_{nodes}} \left[V_j.\big(G_{ij}.\sin(\delta_i - \delta_j) - B_{ij}.\cos(\delta_i - \delta_j)\big)\right] . \end{aligned} \tag{6.8b}$$

- **Bus voltage limit:** Bus voltages must remain within the acceptable range of levels in all periods:

$$V_i^{min} < V_i < V_i^{max} \tag{6.9}$$

- **Transmission injected power limit:** Regardless of distribution substation upgrades, the transmission system may have a limited capability in supporting the distribution substation. Therefore, with growing demand $P_{net}(j,k)$, i.e., the difference between load and local provided generation should be lower than a maximum value.

$$P_{net}(j,k) < P_{max} \quad \forall j,k \ . \tag{6.10}$$

- **Generating unit capacity:** The limited generating capacity of the units cannot be violated at any time.

$$\begin{aligned} &0 < S_{DG_i}(k) < I_{DG_i} \qquad i = 1, \ldots, n_{DG} \ , \\ &S_{DG_i}(k) = \frac{P_{DG_i}(k)}{PF_{nominal}(T_{DG_i})} \ . \end{aligned} \tag{6.11}$$

- **Offered price limit:** Each electrical corporation has to obey the standard tariffs by purchasing electricity from small-scale electric facilities at the price set by the Commission, which is known as Market Price Referent (MPR) and reflects the market price. Therefore, the contract purchase prices should be at least as high as the MPRs:

$$C_{offer}(i,k) \geq MPR(k) \quad k = 1, \ldots, n_{periods} \ . \tag{6.12}$$

Together, equations (6.1)-(6.12) formulate our proposed optimization problem. Once solved, the optimal solution allocates the distributed generation sites, sizes, and prices, such that the DISCO's profit is maximized, all DG owners' individual profits are guaranteed, and the solution is assured to be implementable in practical scenarios. Next, in the next section it is showed how the problem (6.1)-(6.12) can be solved numerically.

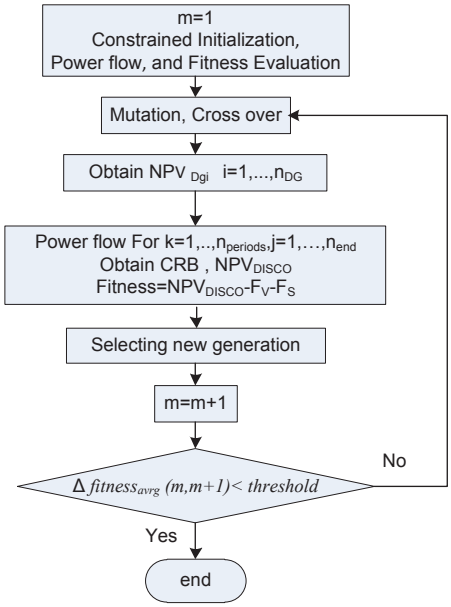

Figure 6.1: The flowchart of the proposed DE algorithm to solve problem (6.1)-(6.12).

6.3 The Optimal Allocation Algorithm Using Differential Evolution

The optimization problem formulated in (6.1)-(6.12) is very challenging as it cannot be solved using classic optimization techniques, such as the linear or convex programming methods [128,129]. Therefore, here, it is proposed to solve (6.1)-(6.12) using the Differential Evolution (DE) algorithm, which was originally proposed to solve non-convex discontinuous optimization problems [130–132]. Here, DE is used over a continuous space optimization. Our other modifications of the DE algorithm include applying some individual constraints in initialization and also after cross over. The flow chart of proposed DE algorithm to solve optimization problem (6.1)-(6.12) is depicted in Fig.6.1. In the DE algorithm, the population individuals or vectors evolve under algorithm operators, mutation, and cross over, to generate new populations with better objective values. This evolution continues until the objective values of the population get close to each other and to that of previous generations. The implemented algorithm has three main elements to be described in the next three sub-sections.

6.3.1 Initialization phase

Differential evolution is a population-based algorithm, where a population of individuals, each consisting of a particular arrangement of control variables, is seen as a possible solution to the optimization problem of interest. In each generation, a new set of solutions are generated to find a better fitness, a greater objective value, i.e. a higher overall profit. The first step in utilizing a DE algorithm is to define the control variables. In our model, each individual or vector from each generation m consists of the following variables:

$$\begin{aligned} \mathbf{x_{n,m}} &= [I_{DG_i}, P_{DG_i}(k), C_{offer}(i,k)] \\ i &= 1, \ldots, n_{DG} \ , \quad k = 1, \ldots, n_{Periods} \ . \end{aligned} \tag{6.13}$$

From (6.13), the control variables in each node consist of the installed capacity, the committed generating level in different periods, and their associated offered price tariffs. Since the number of candidate DG locations are limited compared to the DG capacities and given the fact that the choice of location can significantly change the outcome of the objective function, it is better to make sure that the program examines *all* candidate locations at which a DG can be sited. Therefore, since each vector in (6.13) contains the active power generation in each available node of the distribution system; we set n_{DG} in the initialization phase to be equal to the network's available locations. Note that, although the DG units are initially placed in all locations, quite a few of the DG units will remain in the successive generations until the optimum solution is obtained and the generation in many nodes will gradually be eliminated. While I_{DG_i} takes integer values between available DG types, $P_{DG_i}(k)$ and $C_{offer}(i,k)$ are continuous variables. The initial value of the control variables are determined using randomization to assign each parameter of the n^{th} vector, a value within its upper and lower bounds. Such initialization is done for all elements in each $\mathbf{x}_n$. The population size is considered as four times the number of control variables. In order to avoid calculating the fitness for infeasible solutions and to reduce computational complexity, the initial values of parameters related to $x_{n,1}$ should meet:

$$\sum_{i=1}^{n_{DG}} P_{DG_i} < P_{load}(k) \ , \qquad k = 1, \ldots, n_{periods} \ . \tag{6.14}$$

Otherwise, the solution is infeasible and must be replaced. It should also be verified that with the determined generation levels and price tariffs, whether the unit operation will be economical. To do this, for each $\mathbf{x}_n$, all NPV_{DG_i} with the pre-set price tariffs and generating

levels are determined. Note that, NPV_{DG_i} must be positive. Furthermore, generating in each period under the associated price tariffs should be beneficial. That is, it should be more than the current revenue gained by generating at peak hours in post-contract life of DG, assuming the unit has a limited total hours of efficient operation and it can generate later under standard contracts. This constraint is checked at all periods for each DG unit. If the generation levels in all periods for DG_i are zero or if NPV_{DG_i} is negative, then the DG_i capacity is set to zero and the DG is eliminated.

6.3.2 Power Flow and Fitness Evaluation

For each $\mathbf{x}_n$, the power flow is performed in every period of each year during the planning stage. The voltage violations and line flows are obtained for every year, as well as the excess power to be procured from the network. Then, the CRB is calculated according to Sec. 6.2.2 and the NPV_{DISCO} is as in (6.7). The fitness function is obtained as:

$$Fitness(\mathbf{x}_n) = NPV_{DISCO} - F_V - F_S \tag{6.15}$$

where

$$\begin{aligned} F_V = K_V . \sum_{l=1}^{n_{end}} \sum_{k=1}^{n_{Periods}} \sum_{j=1}^{n_{nodes}} max(0, V_{min}(l,k,j) \\ - V_j, V_j - V_{max}(l,k,j) \end{aligned} \tag{6.16}$$

and

$$F_S = K_S . \sum_{l=1}^{n_{end}} \sum_{k=1}^{n_{Periods}} max(0, S_{net}(l,k) - S_{max}) \tag{6.17}$$

denote the penalty functions related to violating the voltage profile tolerance or violating the transmission capacity limit. Here K_V and K_S usually take large values to eventually remove an infeasible solution from the next generations.

6.3.3 Applying the DE Operators, Obtaining the New Generation

Once the fitness functions are obtained, we apply the DE operators of *mutation*, *cross-over*, and *selection*. The details on how these operators are applied can be found in [130–132]. Note that, here, the mutant vector is obtained as

$$\mathbf{v}_{n,m} = \mathbf{x}_{r_1,m} + \zeta(\mathbf{x}_{r_2,m} - \mathbf{x}_{r_3,m}) \ , \tag{6.18}$$

where r_1, r_2, and r_3 are random integers to choose different random vectors from the current population. The control parameter ζ is chosen within [0.5, 1]. Smaller values of ζ are usually used for larger population sizes. Here, we set $\zeta = 0.7$ by experiment. In fact, it was observed that the lower values of ζ may help the algorithm converge faster. However, in small population sizes, this may cause the algorithm to reach a local minimum, rather than a near global optimum, confirming the trade-off between DE optimality and convergence speed [132]. For our design, a uniform cross-over is used. In our analysis, $Cr \in [0, 1]$ the parameter that controls the fraction of parameters copied from the mutant vector is set at 0.3. [130]. The three steps of mutation, cross-over, and selection are repeated for each generation until the termination criteria is met, i.e., the difference between the average fitness values of successive generations drop below a pre-determined level. A maximum number of generations are also considered as an additional criterion for termination. Once the algorithm converges, the optimal solution of problem (6.1)-(6.12) is achieved.

6.4 Case Studies

The modified IEEE 37-bus distribution system which is an actual feeder located in California has been used to test the functionality of the proposed algorithm [133]. The graph diagram of this network, with renumbered branches and nodes, is depicted in Fig. 6.2. This system serves a total demand of 2.63 MW and 1.55 MVAR reactive power. The distribution transformer capacity is 3200 kVA with a rough value of $50,000. The characteristics of different cable types, used in line segments and their rough per meter prices, as well as their maximum allowable currents are shown in Table. 6.1 [134]. The demand curve takes different values during the day. The load level considerably changes from the morning to the afternoon and at night. The demand also slightly varies at each hour of these periods. Therefore, the load curve can be approximated to several periods with an average level of demand in each period. The simplified load curve that has been used for this study is shown in Fig. 6.3. A demand growth of 6.5% has been considered during the term of planning. The customer price rates are defined in two periods: on-peak and off-peak. The on-peak price is set to be $0.21/kWh and the off-peak price is set at $0.10/kWh [135].

To develop a robust market for distributed resources, there is a need for uniform

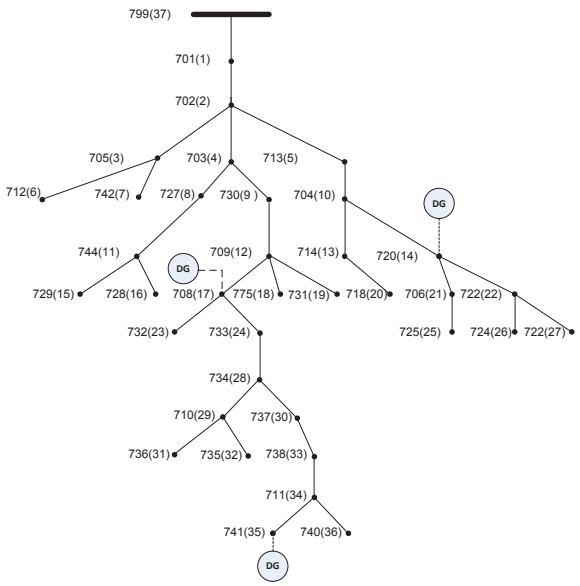

Figure 6.2: The IEEE 37 bus distribution system with renumbered buses.

technical inter-connection standards on a national or state-wide basis. Currently, there are certain limits in existing standards for connection of DG resources into the distribution networks. Therefore, in our study, the capacity of DGs is assumed to be between 50-1500 kW. The contract term, decided by the DISCO, may take different values between 5-20 years. Without loss of generality, the contract term in this study is assumed eight years, since it is stated in [124] that a payback period of less than eight years is essential for DG penetration. Therefore, we set any NPV_{DG_i} after eight years to be positive to attract investment. It is assumed that DGs can benefit from standard power purchase agreements afterwards.

We assume that the DG technologies in the system operate as CHP units. The non-renewable DGs are often not efficient enough to make the project economical unless process heat can be captured and re-used. Recoverable heat is valued at the cost of natural gas delivered to end-users. Only the least-cost DG technologies capable of operating at base-load are considered. The CHP technologies are divided into three classes based on application size: 50-500 kW, 500-1000 kW, and 1-1.5 MW. The characteristics of these classes are depicted in Table 6.2 [124]. The current tariff provides the buyer with the right to terminate service if seller has not achieved operation in 18 months from the execution date [136]. This requires the commercial operation of units to be less than 18 months. In

Table 6.1: Underground Cable Line Configuration Data.

Config.	Cable(AWG)	Conductor size (mm^2)	Ampacity (A)	Price($/m)
721	1000AA,CN	3×500	550	213
722	500AA,CN	3×240	385	161
723	2/0AA,CN	3×70	200m	64
724	2# AA,CN	3×35	135	41

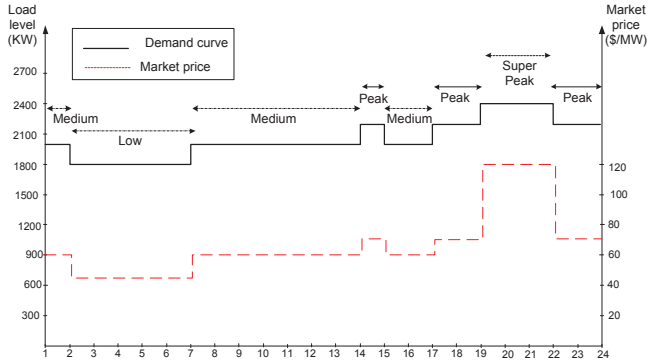

Figure 6.3: Approximated daily load and market daily price in the case studies.

this work, for gas engine and gas turbine units, a rough installation lead time of 12 months is assumed. For micro-turbine units, the installation lead time is assumed insignificant.

The weekly average natural gas spot prices in California for the fourth quarter of 2009 are used from [137]. The DG penetration and offered prices are obtained with different gas prices in the range of $3.5-6/MMBTU. The average daily value of energy in this study was considered $65.8/MWh; while the hourly values vary in the range of $45-120/MWh from the low period to super-peak period. The off-peak period consists of the low and medium load periods and the on-peak period consists of the peak and super-peak periods. The minimum offered price MPR to DG facilities is set to $0.06/kWh for off-peak periods and $0.065/kWh for on-peak periods.

Given the above simulation setups, next we obtain the optimum size, site and

Table 6.2: The Characteristics of Different Types of CHP Units.

System Type	Micro Turbine	Gas Engine	Gas Turbine
Applicable Size (kW)	50-500	500-1000	1000-1500
Heat rate (BUT/kWh)	9,477	9,382	9,605
Recovered Heat (BTU/kWh)	2,748	3,096	3,746
Turnkey Cost ($/kW)	915	690	950
O&M Cost ($/kWh)	0.011	0.009	0.005
Project economic life	10 Years	15 Years	15 Years
Recoverable Heat Used (%)	70%	70%	80%

prices in two scenarios. First, we obtain the optimum solution considering all the introduced constrains. Second, for a better understanding of the results, a hypothetical case is studied where the DISCO's investment costs and voltage profile limits are neglected.

6.4.1 Simulation Scenario I

In this scenario the results of best locations, capacities and generating level in each period with the optimum price tariffs are obtained, taking into consideration *all* the constraints that we introduced in Section 6.2. The impact of an increase in spot gas prices and bilateral contracts are also studied. First, we assume that the gas price for DGs is \$3.5/MMBTU. The results for best locations, generating levels in different periods and the prices are shown in Table 6.3. The locations of DG units are also depicted in Fig. 6.2. We can see that the offered price for the first two units is set to the minimum allowable value *MPR*. However, for the third unit with a relatively smaller capacity, the offered price needs to be more than *MPR* to maintain investment economical. The first two units are of type-2 with lower investment and maintenance costs where the generation can be still economical with lower FiT prices. Here in this scenario, the average cost of energy procurement from DG units is lower than the market price; therefore, the DISCO tends to utilize the DGs as much as possible. total optimal NPV_{DISCO} in this scenario becomes \$3,372,600.

Next, we show the impact of an increase in gas prices on the optimal solution in Table 6.4. Note that, gas price have significant effects on both DGs' and DISCO's profits, since higher gas prices increase the cost of generation. When the price increase from \$3.5

Table 6.3: DGs optimal sites, generating levels and fit prices in each period in Scenario I with $3.5 for the gas price.

DG Bus	P_{DG} (kW)		C_{offer} ($/kWh)		NPV_{DG}
	on-peak	off-peak	on-peak	off-peak	
720	700	655	0.065	0.060	57770
708	900	800	0.065	0.060	57988
741	400	345	0.0723	0.060	235

to $4.5, the optimal choice of locations and generating levels do not change. However, the offered prices in on-peak period has to increase in order to maintain NPV_{DG_i} positive for all DGs. Note that the DGs' profits are notably lower when the gas price is $4.5, compared to when the gas price is $3.5. However, we can see that the average cost of DGs' energy procurement is still slightly lower than the market price . Therefore, the DISCO still benefits from utilizing NPV_{DISCO} and we have $3,230,300.

Table 6.4: Comparison of the solutions with different gas prices.

Fuel cost	Generation Levels(kW)		offered prices(cents/kWh)	
$/MBTU	on-peak	off-peak	on-peak	off-peak
3.5	700-900-400	655-800-345	6.5-6.5-7.2	6.0-6.0-6.0
4.5	700-900-400	655-800-345	7.08-7.3-9.06	6.0-6.0-6.0
6	800-700	800-658	7.62-7.34	7.0-7.03

Next, consider the case where the gas price increases to $6. Clearly, this will lead to a major increase in the generation cost and will require a significant increase in the offered price of electricity to maintain DG investment economical. However, in this case, the average cost of DGs becomes higher than the market price. This makes the DISCO less interested in distributed generation, which results in decreasing the total amount of DG capacities. Note that, NPV_{DISCO} in this case is $2,956,800 and the DISCO investment cost is $87,893. If the DISCO were to use no DG, the corresponding NPV_{DISCO} would become $3,003,000 with DISCO investment cost of 200,026$ which is still higher than the profit gained by DISCO from utilizing DGs. However, to avoid the installation of a new transformer with the capital cost of $50,000 and to prevent the technical difficulties related to transmission injected power limit and voltage profile, the DISCO decides not to procure the power solely

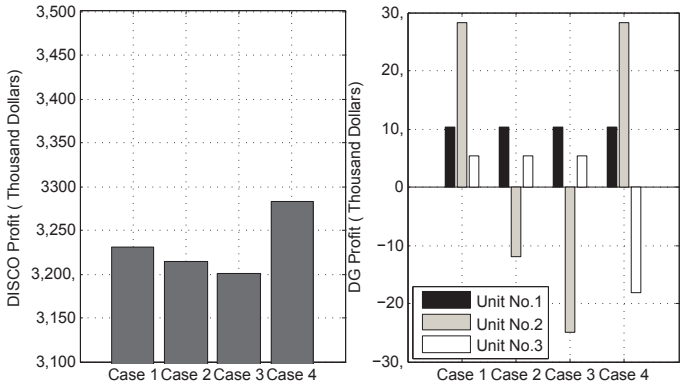

Figure 6.4: The impact of project start time on the DISCO's and the DGs' profits.

from the market. In this case, in order to maintain the DG investment profitable in presence of the minimum offered prices, the multiple local generation units have to be merged into fewer but bigger units. For this purpose, the algorithm optimally increases the capacity in bus 741 to a larger unit and disconnects one of the DGs from bus 720.

Next, we show the impact of start date of the projects on the net profits of both DG units and the distribution company. So far, we have assumed in the numerical studies that the DGs start generation right after their installation time has completed. Now we consider four cases when the start dates of the DG projects are postponed. In Case 1, all units are installed in the first year and depending on the project installation time, they start generation in the first or the second year. In Case 2 and 3, we assume that the installation of the second unit is postponed one year and two year, respectively. We also consider another case where the generation of the smallest unit is postponed for two years. We can see in Fig. 6.4 that the net profit of the DG units decrease as they delay the start time of the project , and with the same offered prices, considering the time value of cash flows and relatively high interest rate, the projects will not remain profitable. However, postponing the DG projects start time may serve the DISCO in terms of net profit, depending on the average purchase price to be offered by the DG unit. We can see that the profit of DISCO from postponing the start time of the largest DG unit decreases, while the profit rather increases when the generation time of the smallest unit with a higher purchase price is delayed.

Finally, the optimum solution for the case that a portion of DISCO's required

Table 6.5: The optimal solution of dg sites and sizes with 800 kW bilateral contract and 3.5$ gas price .

DG Bus	P_{DG} (kW)		C_{offer} ($/kWh)		NPV_{DG}
	on-peak	off-peak	on-peak	off-peak	
708	800	650	0.065	0.060	27,786
741	400	350	0.0717	0.060	141

energy is procured through bilateral contracts is shown in Table 6.5. The capacity to be procured through bilateral contract is 800 kW with the price of $0.065/kWh. We can see that the NPV_{DISCO} in this case is still higher than the case where all energy is procured from the market. However, the total amount of DG's generation capacity decreases in this case as well as their associated profits since the DISCO has to obtain the power from the network. The results on NPV_{DISCO} as well as the summation of NPV_{DG_i} for all DGs *with* and *without* bilateral contract is shown in Table 6.6. We also see that NPV_{DISCO} decreases in presence of bilateral contracts compared to the case with no such contracts, where more energy is procured from DGs. In this case, although the bilateral price is less than market average price, less power is procured from the DGs with an average price of less than $0.065. Moreover, since the total power to procure from DGs has decreased, the DISCO has offered higher prices in bus 741 in order to maintain the investment attractive, causing an increase in the average price of energy procurement from DGs.

Table 6.6: Comparison of profits with and without bilateral contract.

Bilateral Contract	NPV_{DISCO}	$Sum(NPV_{DG_i})$	NPV_{total}
0	3,372,600$	115,993$	3,488,593$
800 kW	3,301,820$	29,060$	3,330,880$

6.4.2 Simulation Scenario II

The second scenario is defined by removing the network upgrade costs and voltage profile limits from the optimization problem formulation such that the design objective becomes limited to just finding the allocation that best suits DISCO with minimum power procurement cost. Our intention to study Scenario II is to gain insights with respect to the

prominent factor in choosing the optimal allocation. Thus, the results here complement those already obtained for the case of Scenario I.

Table 6.7: DGs Optimal Sites, Generating Levels and FIT Prices in Each Period in Scenario II without distribution investment costs.

DG Bus	P_{DG} (kW)		C_{DG} (\$/kWh)		NPV_{DG}
	on-peak	off-peak	on-peak	off-peak	
720	1000	1000	0.065	0.060	107,880
734	1000	800	0.065	0.060	29,218

The optimization results for the case of Scenario II are shown in Table 6.7. The number of units has been decreased to two such that we can integrate more power generation to be able to procure power with lower prices. Furthermore, by increasing the generation level of unit-2, the DG has been moved upward to prevent the flow back of current. We can see that the DISCO utilizes the DGs in the off-peak period despite the fact that the average market price in this period is lower than the MPR. Note that, the increase in the generation levels are indeed required in order to decrease the on-peak price of DGs such that we can maintain NPV values positive. In other words, since a DG unit with on-peak period generation cannot maintain economical with \$0.065/kWh; the DISCO should also procure the power from DGs in off-peak period with a loss of about \$0.005/kWh so that it can purchase the power in the on-peak period with a profit about \$0.0237/kWh. In this way, DISCO procures more overall power at less overall price.

The results in this section show that apart from the capacity release benefits that DISCO may have from utilizing DGs, a proper choice of DG size and offered price can lead to increased benefits for DISCO in procuring the energy. This factor motivates the DISCO to merge the DG units into bigger sizes to make it possible for lower prices for energy procurements. However, network constraints and network upgrade costs motivate the DISCO to distribute the DG units. The combination of these competing factors leads to an optimal trade-off between the size and offered price which is achieved using the proposed optimization-based algorithm.

6.5 Conclusion

In this chapter, a novel optimization-based approach is presented to determine the best sites, generation levels in different periods of time, and the Feed-in-Tariff incentives in distributed generation systems. The design goal is to maximize the DISCO's profit while maintaining investment attractive for each individual DG owner. A detailed economical model was proposed that takes into account different factors related to the DISCO's and DGs' profits, including gas price and the total MW of bilateral contracts. A differential evolution algorithm is proposed to effectively solve the formulated optimization problem. The performance of algorithm is verified in various cases. Simulation results show that despite the lower value of average market price in off-peak period, if the DG sites, sizes, and prices are allocated optimally, the DISCO can utilize and coordinate the DGs to gain more profit compared with purchasing the power only from the grid, while the DGs can assure positive profits and attractive investments.

The results in this chapter can be extended in several directions. First, given the observation that some factors, such as gas price, may change the optimal solution for DG sizes and offered prices, the models can be adjusted to incorporate the presence of such risks to maximize the profit with minimum risk. Second, the DG units considered in this chapter of committed types. However, it is likely that a DG unit has a force outage; therefore, the costs that DISCO might incur from loss of load in these conditions need to be further investigated. Finally, integrating renewable DGs in the proposed optimization framework remains as an interesting open problem.

6.6 List of Symbols, Chapter 6

n_{DG} Number of DG units

n_{start} Year of starting generation in DG contract

n_{end} Year of ending generation in DG contract

$n_{periods}$ Number peak periods in DG contract

PVB_{DG_i} Present value benefit for ith DG

PVC_{DG_i} Present value cost for ith DG

$H(k)$ Total number of hours in kth peak period

$P_{DG_i}(k)$ Active power of ith DG in kth period (kW)

$S_{DG_i}(k)$ Apparent power of ith DG in kth period (kVA)

$PF_{nominal}$ Nominal power factor of ith DG

$P_{load}(j,k)$ Load in kth period of jth year (kW)

$P_{net}(j,k)$ Power procured in kth period of jth year (kW)

$C_{offer}(i,k)$ Tariff rate for ith DG in kth period (kWh)

$C_{capital}$ DG capital investment cost (\$/kW)

C_{fuel} DG fuel cost (\$/kWh)

$C_{O\&M}$ DG operation & maintenance cost (\$/kWh)

C_{market} Wholesale market price (\$/kWh)

C_{retail} Price rate for retail customers (\$/kWh)

i_f Nominal interest rate

PEL Project's economic life

λ_i Installation cost coefficient of ith DG.

T_{DG} Classified type of DG

I_{DG} Installed capacity of DG (kVA)

P_G Total injected active power at a node (kW)

Q_G Total injected reactive power at a node (kW)

P_D Active power demand at a node (kW)

Q_D Reactive power demand at a node (kW)

V_i Voltage magnitude of ith bus

δ_i Voltage angle of ith bus

K_V Penalty for violating voltage tolerance

K_S Penalty for violating transmission capacity

$\mathbf{x}_{n,m}$ nth member vector of mth generation

$\mathbf{v}_{n,m}$ nth mutant vector of mth generation

Cr Cross over probability ratio

ζ Differential variation control parameter

Chapter 7

Challenges and Opportunities in Large-Scale Deployment of Automated Energy Consumption Scheduling Systems in Smart Grids

Recent studies have shown that the lack of knowledge among users on how to respond to time-varying prices and the lack of effective home automation systems are two major barriers for fully utilizing the advantages of real-time pricing. Therefore, there has been a growing interest over the past few years towards developing automated energy consumption scheduling (ECS) devices to constantly monitor the hourly prices and schedule the operation of users' controllable load to minimize their energy expenditure. While the prior results in using ECS devices are promising, all prior work are limited to *small-scale* deployment of ECS devices. For example, in most cases, the users that are equipped with the ECS devices are assumed to be part of a microgrid or a feeder connected to a sub-station. In this chapter, we rather investigate *large-scale* deployment of ECS devices in a power grid with several buses and generators. The price of electricity at each bus is set according to the locational marginal price (LMP) at that bus. We show that a key challenge in large-scale deployment of ECS devices is *load synchronization*. However, we propose to use a moving

average smoothing mechanism for LMPs that can fix the load synchronization problem and stabilize the system. Furthermore, we show that the proposed large-scale ECS system has a close to optimal performance in terms of reducing peak-to-average-ratio in load demand, minimizing the total power generation cost, and lowering users' electricity bills.

7.1 Introduction

Real-time and time-of-use electricity pricing models can potentially lead to several economic and environmental advantages compared to the current commonly used flat rates. In particular, they can provide power consumers with the opportunity to reduce their electricity expenditure by responding to pricing that varies at different times of day and is higher at peak load hours [138]. Furthermore, they can help utilities and independent system operators to reduce the *peak-to-average-ratio* (PAR) in aggregate load demand which can lead to minimizing the need for building new power generation capacities [139].

Despite several advantages that real-time, time-of-use, and other non-flat pricing models can offer, recent studies have shown that the lack of knowledge among users about how to respond to time-varying prices and the lack of effective home automation systems are two major barriers for fully utilizing the benefits of non-flat electricity pricing tariffs [140, 141]. In fact, most of the current residential load control activities are operated manually. This makes it difficult for users to optimally schedule the operation of their appliances in response to the hourly updated pricing information they may receive from the utilities in a non-flat pricing program. For example, the experience of the real-time pricing program in Chicago, IL has shown that although the price values were available via telephone and the Internet, only rarely did households actively check prices as it was difficult for the participants to constantly monitor the hourly price values to respond properly [142].

To tackle the problems with manual load control, there has been a growing interest recently towards using automated energy consumption scheduling (ECS) device [143–152], similar to the one shown in Fig. 7.1. In this setup, each user is equipped with an ECS devices, e.g., in its smart meter, which is assumed to be connected to a smart power distribution system with a two-way digital communication capability through computer networking [153, 154]. Based on the updated pricing signals that the ECS device receives from the utility through the available communications infrastructure, and also given the users' personal energy needs, the ECS device optimally schedules the energy consumption for the users'

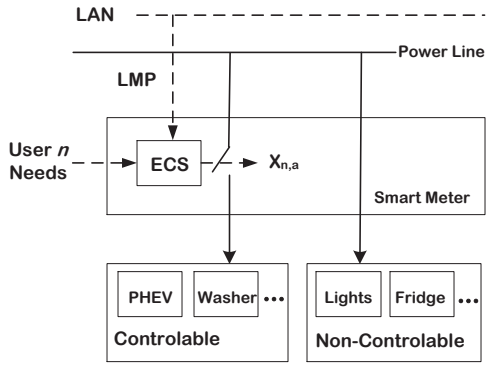

Figure 7.1: An automated energy consumption scheduling device in a smart meter. The prices are obtained through a communications infrastructure.

controllable load such that it can minimize the users' daily or monthly electricity expenses. The use of ECS devices is recommended not only for residential consumers [143] but also for industrial consumers [155]. Furthermore, there have been companies that have already started offering commercial ECS devices for home automation products, e.g., see [156].

While the prior results in using automated ECS devices in smart grids have been very promising, all prior work along this line of research have been limited to small-scale deployment of the ECS devices. For example, in most cases, the users that are equipped with the ECS devices are assumed to be part of a microgrid or part of a small feeder in a distribution line that is connected to a single generator or a sub-station. Therefore, in this chapter, we investigate large-scale deployment of ECS devices in power grid such as the one shows in Fig. 7.2. The price of electricity at each bus in this system is assumed to be set according to the locational marginal price (LMP) at that bus. Note that, most existing deregulated electricity markets in the United States currently use LMPs to settle various bulk sale and ancillary service transactions [157]. Although setting retail prices according to LMPs is still not a common practice in most regions, it is recently shown that by reflecting the prices in the wholesale market to the consumer side, users will be better encouraged to consume electricity more efficiently [158].

We will show that a key challenge in large-scale deployment of ECS devices is *load synchronization*. This problem can be explained as follows. Every time the electricity prices, i.e., the LMPs, are set, the ECS devices move their load from high-price hours to low-price hours in an attempt to minimize their energy expenditure. However, this will in turn

overload low-price hours, making them high-price hours in the next iteration, and underload high-price hours, making them low-price hours in the next iteration. This causes constant fluctuations in the electricity prices and makes the system unstable. To tackle this problem, we propose to use a moving average smoothing mechanism for LMPs. Our simulation results show that the proposed approach works well and can assure system stability. Furthermore, we show that the proposed large-scale deployment of ECS devices has a very close to optimal performance in terms of reducing PAR in the aggregate load demand, minimizing the total power generation cost in the system, and reducing each user's individual electricity bill payments.

7.2 System Model

Consider a power grid system, such as the IEEE 24-bus system in Fig. 7.2(a). Let $\mathcal{B}$, with cardinality B, denote the set of buses in the system. For each bus $i \in \mathcal{B}$, let $\mathcal{N}_i$, with cardinality $\mathcal{N}_i$, denote the set of users connected to bus i. Clearly, in bus i is not a load bus, then we have $N_i = 0$. For each load bus, we assume that all users are equipped with an ECS device. An example for the case of bus 8 with N_8 users is shown in Fig. 7.2(b). The price of electricity at each load bus is set according to the locational marginal price at that bus. Let LMP_i^h denote the locational marginal price at load bus i at hour h. Consider an $H > 1$ hours ahead energy consumption scheduling problem for a user $n \in \mathcal{N}_i$ connected to bus i. Note that for day-ahead planning, we have $H = 24$. Given the following $H \times 1$ price vector

$$\mathbf{LMP}_i = [LMP_i^1, LMP_i^2, \ldots, LMP_i^H], \tag{7.1}$$

the ECS device in user n's smart meter is responsible for scheduling the operation of all user n's controllable load such that user n's daily energy expenditure is minimized.

For each user n, let $\mathcal{A}_n$ denote the set of all appliances that have controllable / shiftable load. Examples for such appliances may include washer, dryer, dishwasher, and plug-in hybrid electric vehicles. For each appliance $a \in \mathcal{A}_n$, we define an energy consumption scheduling vector as

$$\mathbf{x}_{n,a} = [x_{n,a}^1, x_{n,a}^2, \ldots, x_{n,a}^H]. \tag{7.2}$$

Let $E_{n,a}$ denote the total energy needed to finish the operation of appliance a. For example,

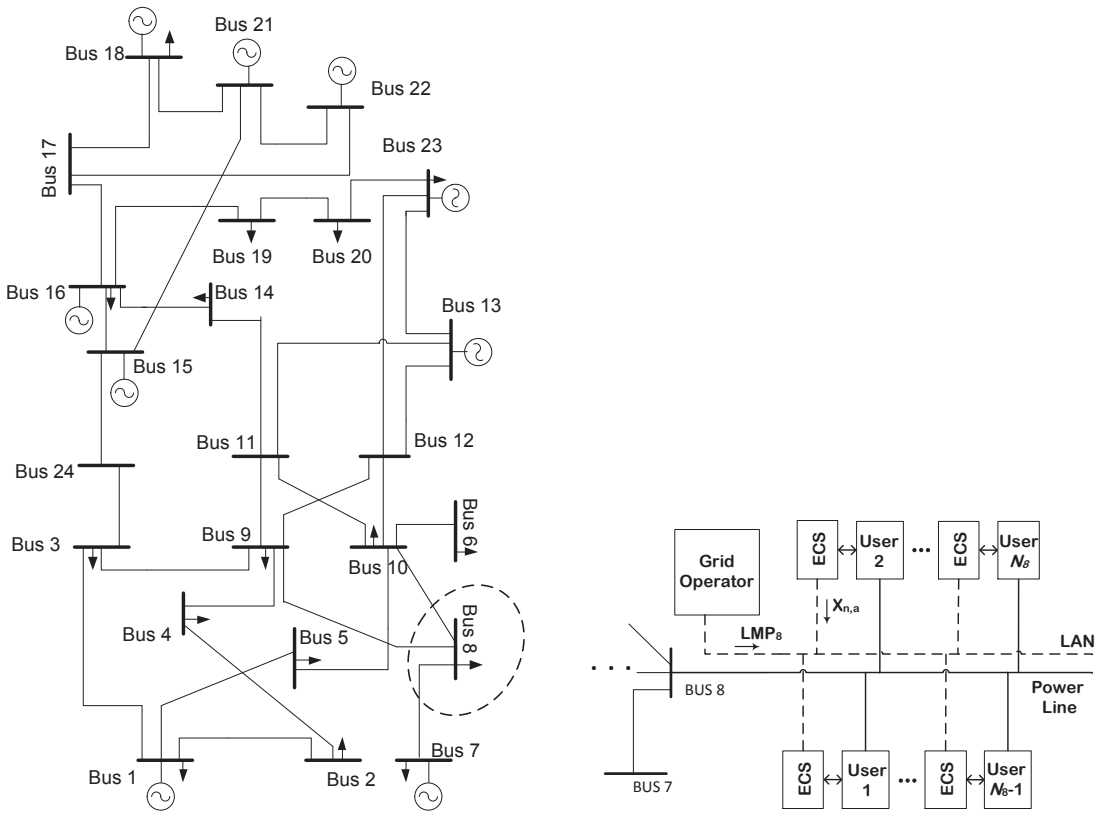

Figure 7.2: An example for large-scale deployment of automated ECS devices: (a) An IEEE 24-bus power system with 16 load buses. (b) The set of N_8 users, equipped with ECS devices, that are connected to bus 8. The retail price of electricity at each bus is set according to the LMP at that bus.

$E_{n,a} = 16$ kWh for a sedan electric car with 40 miles daily driving range [138]. Furthermore, for each appliance a, the operation needs to be scheduled within a time frame $[\alpha_{n,a}, \beta_{n,a}]$, where $1 \leq \alpha_{n,a} < \beta_{n,a} \leq H$. These parameters are set by user n based on his energy consumption needs for each appliance. For example, user n may set $\alpha_{n,a} =$ 1:00 PM and $\beta_{n,a} =$ 5:00 PM for the operation of a dishwasher after lunch table and before diner. Of course, the time duration $\beta_{n,a} - \alpha_{n,a}$ must be larger than or equal to the time needed to finish the normal operation of appliance a. To assure on time operation of appliances, it is

required that user n's ECS device fulfills the following constraints

$$\sum_{h=\alpha_{n,a}}^{\beta_{n,a}} x_{n,a}^{h} = E_{n,a}. \tag{7.3}$$

Furthermore, it is required that

$$x_{n,a}^{h} = 0, \quad \forall\, h \in \mathcal{H}\backslash\mathcal{H}_{n,a}, \tag{7.4}$$

where

$$\mathcal{H} = \{1, \ldots, H\}, \quad \text{and} \quad \mathcal{H}_{n,a} = \{\alpha_{n,a}, \ldots, \beta_{n,a}\}. \tag{7.5}$$

Finally, we note that some appliances may have some minimum standby power $\gamma_{n,a}^{\min}$ and/or some maximum supported power $\gamma_{n,a}^{\max}$. In that case, it is also required that

$$\gamma_{n,a}^{\min} \leq x_{n,a}^{h} \leq \gamma_{n,a}^{\max}, \quad \forall\, h \in \mathcal{H}_{n,a}. \tag{7.6}$$

For notational simplicity, for each user n, we introduce a new vector $\mathbf{x}_n$, which is formed by stacking up energy consumption scheduling vectors $\mathbf{x}_{n,a}$ for all appliances $a \in \mathcal{A}_n$. In this regard, we can define a *feasible* energy consumption scheduling set corresponding to user n as follows:

$$\begin{aligned} \mathcal{X}_n = \{\mathbf{x}_n \;\mid\; & \textstyle\sum_{h=\alpha_{n,a}}^{\beta_{n,a}} x_{n,a}^{h} = E_{n,a}, \\ & x_{n,a}^{h} = 0, \qquad\qquad \forall\, h \in \mathcal{H}\backslash\mathcal{H}_{n,a}, \\ & \gamma_{n,a}^{\min} \leq x_{n,a}^{h} \leq \gamma_{n,a}^{\max}, \quad \forall\, h \in \mathcal{H}_{n,a}\}\,. \end{aligned} \tag{7.7}$$

An energy consumption schedule calculated by the ECS unit in user n's smart meter is valid only if we have $\mathbf{x}_n \in \mathcal{X}_n$.

For each user $n \in \mathcal{N}_i$ at bus i, the total electricity bill within the scheduling horizon of interest is calculated as

$$\sum_{h=1}^{H} LMP_i^h \times \left(L_n^h + \sum_{a \in \mathcal{A}} x_{n,a}^{h} \right), \tag{7.8}$$

where L_n^h denotes the total load of user n at hour h due to his appliances that have non-controllable load. Examples for such appliances may include lights, refrigerator, television and other entertainment devices. Note that the operation of appliances with non-controllable load is *not* scheduled by ECS devices. To minimize user n's energy expenditure, the ECS

Figure 7.3: Interactions between the grid operator and the ECS devices. (a) The electricity prices are set based on the original LMPs. (b) The electricity prices are set based on a smoothed version of LMPs in order to enforce stability.

device in user n's smart meter should solve the following optimization problem across appliances that have controllable load:

$$\underset{\mathbf{x}_n \in \mathcal{X}_n}{\textbf{minimize}} \sum_{h=1}^{H} LMP_i^h \times \left(L_n^h + \sum_{a \in \mathcal{A}} x_{n,a}^h \right). \tag{7.9}$$

Note that the above optimization problem can capture the behavior of each user's ECS device. Next, we investigate the interactions between the ECS devices and the grid operator when the ECS devices are deployed in a large scale.

7.3 Operator-User Interactions

If the ECS devices are deployed only in small scales, e.g., in a microgrid or in a single distribution feeder as in [143–152], the operation of ECS devices may not have any impact on the LMPs. However, if the ECS devices are deployed in a larger scale and at several buses, such as in the power system in Fig. 7.2, then the operation of the ECS devices may have a significant impact on the LMPs at different buses as we explain next.

Let X_i^h denote the total load at bus i at hour h. Once all ECS devices set the load by solving problem (7.9), we have

$$X_i^h = \sum_{n \in \mathcal{N}_i} \left(L_n^h + \sum_{a \in \mathcal{A}_n} x_{n,a}^h \right). \tag{7.10}$$

Using the standard power system dispatch control model in [159], at each hour h, the grid

operator can solve the following optimization problem to calculate the LMPs at each bus:

$$\underset{G_i^h, \forall i}{\textbf{minimize}} \quad \sum_{i=1}^{B} C_i\left(G_i^h\right) \tag{7.11a}$$

$$\textbf{subject to} \quad \sum_{i=1}^{B} G_i^h - \sum_{i=1}^{B} X_i^h = 0 \tag{7.11b}$$

$$\sum_{i=1}^{B} f_{k,i} \times (G_i^h - X_i^h) \leq F_k^{\max}, \quad \forall\, k \in \mathcal{K} \tag{7.11c}$$

$$G_i^{\min} \leq G_i^h \leq G_i^{\max} \quad \forall\, i \in \mathcal{B}, \tag{7.11d}$$

where G_i denotes the amount of dispatched power generation at generator bus i at hour h, $C_i(\cdot)$ denotes the cost function for the generator at generator bus i, $\mathcal{K}$ denotes the set of all transmission lines in the system, $f_{k,i}$ denotes the [160] injection shift factor to transmission line k from bus i, and $F_k^{\max}$ denotes the transmission limit of transmission line k. Finally, $G_i^{\min}$ and $G_i^{\max}$ denote the minimum and maximum generation range for the generator at bus i. Clearly, if bus i is not a generation bus, then we have $G_i^{\min} = G_i^{\max} = 0$. Assuming that power loss is negligible on transmission lines, the formulation of LMP at bus i can be written as [161, 162]:

$$LMP_i^h = \lambda + \sum_{k=1}^{K} f_{k,i} \times \mu_k, \tag{7.12}$$

where K denotes the number of transmission lines, i.e., the cardinality of set $\mathcal{K}$, λ denotes the Lagrange multiplier corresponding to the energy balance constraint in (7.15b), and μ_k denotes the Lagrange multiplier corresponding to the line capacity constraint in (7.15d) for transmission line $k \in \mathcal{K}$.

7.3.1 Decentralized Model

The interactions between the grid operator and ECS devices can be analyzed under the real-time pricing framework in [163]. Given the price values, i.e., vector $\mathbf{LMP}_i$ at each bus i, the ECS devices schedule the load based on the optimal solution of problem (7.9). In turn, if the updated load profiles are plugged in optimization problem (7.11), the resulted LMPs can become different from the original values. This is shown in Fig. 7.3(a). Note that, the message exchanges are supported through the two-way digital communications capability which is expected to be available in the future smart grid [138]. The key question

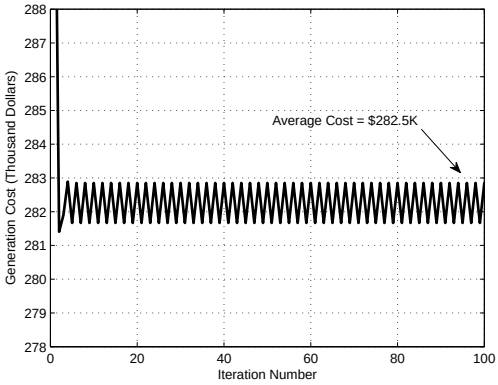

Figure 7.4: The fluctuation in total power generation cost in the system when the electricity prices are set based on the original LMPs as in Fig. 7.3(a).

is: *Do the back and forth iterations between the grid operator and the ECS devices converge to any fixed point?*

To answer this question, we perform a simulation based on the power grid topology in Fig. 7.2. The detailed simulation setup is explained in Section 7.4. As shown in Fig. 7.4, the objective value of the generation dispatch problem (7.11), i.e., the total cost power generation in the system, does not converge. The fluctuations in this figure can be explained as follows. Every time the prices are set, the ECS devices move their load from high-price hours to low-price hours. This will in turn overload low-price hours, making them high-price hours in the next iteration, and underload high-price hours, making them low-price hours in the next iteration. This problem is referred to as *load synchronization* [143]. While load synchronization does not have a major impact on electricity prices when the ECS devices are deployed only in a small scale, large-scale deployment of the ECS devices can cause significant instability in the price signals as well as the aggregate load profiles, as it is evident from the simulation results in Fig. 7.4.

Next, we propose a moving average smoothing mechanism for LMPs to resolve the load synchronization problem. Let $\mathbf{LMP}_i[t]$ denote the locational marginal price vector at bus i that is obtained by solving optimization problem (7.11) at iteration $t \geq 1$. We introduce a smoothed version of $\mathbf{LMP}_i$ at iteration t, denoted by $\bar{\mathbf{LMP}}_i[t]$, to be calculated as follows:

$$\bar{\mathbf{LMP}}_i[t+1] = (1-\eta_t)\bar{\mathbf{LMP}}_i[t] + \eta_k \, \mathbf{LMP}_i[t], \tag{7.13}$$

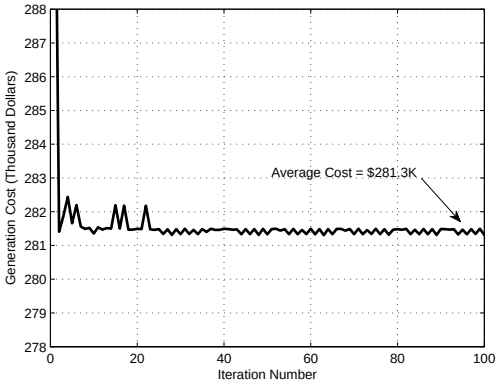

Figure 7.5: The total power generation cost in the system when the electricity prices are set based on the smoothed version of LMPs as in Fig. 7.3(b).

where $0 \leq \eta_t \leq 1$ is an iteration-dependent step-size. Choosing a diminishing step-size can particularly assure convergence to a fixed point. Therefore, we select η_t as

$$\eta_t = \frac{t_0}{t_0 + t - 1}, \tag{7.14}$$

where $t_0 \geq 1$ is a fix parameter. As iteration number $t \to \infty$, step-size $\eta_t \to 0$. In the new model, the interactions between the grid operator and the ECS device becomes as in Fig. 7.3(b). The simulation results in this case are also shown in Fig. 7.5. Note that, once the price signals sent to the ECS devices converge to a fixed point, the load profiles will also stop changing and the whole system reaches an equilibrium.

7.3.2 Centralized Model

Before we conclude this section, it is worth emphasizing that the interaction between the grid operator and the ECS devices shown in Fig. 7.3 is due to the fact that the utility / grid operator does not usually have any centralized control over the operation of users' personal appliances. In fact, for each user, the ECS device in his smart meter does not follow the utilities commands. Rather it solely responds to the price signals sent by utilities and aims to minimize the energy expenditure specifically for its corresponding user. However, if the grid operator does have direct control over the operation of ECS devices, e.g., as in a direct load control (DLC) framework [164], then the interactions between the grid operator and the ECS devices would no longer be based on Fig. 7.3. Instead, the operator would solve the following global optimization problem and it would send the obtained

optimal energy schedules as a command signal to each corresponding ECS device to enforce optimal energy consumption scheduling:

$$\begin{aligned}
&\textbf{minimize} && \sum_{i=1}^{B} C_i\left(G_i^h\right) && \text{(7.15a)}\\
&\substack{G_i^h,\ \forall i,\\ \mathbf{x}_n \in \mathcal{X}_n, \forall n} && && \\
&\textbf{subject to} && \sum_{i=1}^{B} G_i^h - \sum_{i=1}^{B} X_i^h = 0 && \text{(7.15b)}\\
& && X_i^h = \sum_{n\in\mathcal{N}_i}\left(L_n^h + \sum_{a\in\mathcal{A}_n} x_{n,a}^h\right) && \text{(7.15c)}\\
& && \sum_{i=1}^{B} f_{k,i} \times (G_i^h - X_i^h) \le F_k^{\max}, \quad \forall\, k \in \mathcal{K} && \text{(7.15d)}\\
& && G_i^{\min} \le G_i^h \le G_i^{\max} \quad \forall\, i \in \mathcal{B}, && \text{(7.15e)}
\end{aligned}$$

where X_i^h acts as an auxiliary variable. Recall that, in (7.11), X_i^h was a known constant. The centralized design in (7.15) is not the focus of this chapter as it may not be practical as users could be reluctant to relinquish full control of their load to utilities. Nevertheless, the solution of optimization problem (7.15) can provide a benchmark to assess the performance of our proposed distributed design in Section 7.3.1, when it comes to minimizing the total cost of power generation in the system.

7.4 Performance Evaluation

To evaluate the proposed approach on an illustrative system, the IEEE 24-bus standard test system is selected [32]. This system has a total 2650 MW maximum consumption in any hour. In order to alleviate the computation burden of the problem and to better see the impact of energy consumption scheduling in the overall power system, the scale of the users' load is assumed to be relatively high, such as major industrial loads. The total load is distributed among 100 users located at load buses. Each user has a fixed or uncontrollable portion of consumption as well as some shiftable load as discussed in Sec. 7.2. We also defined four specific tasks with known total consumption for each task that users will have at least two or more of these tasks during the day.

7.4.1 Peak Shaving

In order to develop a natural load profile, we assumed that users will select the deadlines for their daily tasks, i.e. $\alpha_{n,a}$ and $\beta_{n,a}$ randomly. However this selection follows some normal distribution for each task, around some specific time period of the day, e.g. one task might be concentrated at some time intervals during the evening. For the Base case, with no ECS units installed, the users will start their consumption with the maximum capacity for each task right after the start time, $\alpha_{n,a}$, until the task is done. This results in the load curve shown in Fig. 7.6 with the PAR of 1.58.

In the distributed scheduling of the ECS units, The controllable portion of the users consumption is shifted from the peak hours, leading to a more even load profile and a reduced PAR. This is shown in Fig. 7.6 with the aggregate consumption curve for 50% controllable load. The PAR in this case is 1.32.

We can also see that in the distributed mode, we reach to a very similar curve to the load profile for centralized scheduling of the ECS units which is the best case the grid can achieve with PAR of 1.23. Therefore, the proposed large-scale distributed ECS deployment system can significantly reduce the peak-to-average ratio (PAR) in the aggregate load demand.

7.4.2 Reducing Total Power Generation Cost

We solved the problem to obtain the optimal schedule and minimum cost for different penetration levels of controllable load.i.e. different ratios of $E_{n,a}$ to the total load of each user. The fixed portion of the load,i.e. L_n^h is assumed to have the same pattern of the base case. The optimal cost of generation for different percentage of controllable load is shown in Fig.7.7. From this figure, we can say that although the proposed large-scale distributed ECS deployment system cannot achieve the same performance as a in benchmark centralized energy consumption scheduling scenario, its performance is close to optimal and significantly better than the case with no ECS deployment, as far as minimizing the total power generation cost in the system is concerned.

7.4.3 Benefit to Users

The average bill of the users for the whole day is shown in Fig.7.8 at some different buses when 50% of the load is shiftable. It is evident that, users will individually benefit

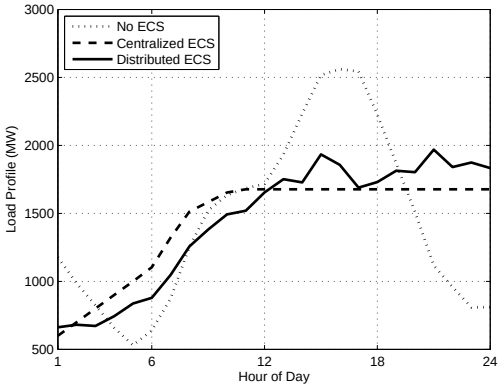

Figure 7.6: The daily load profile for various ECS deployment scenarios.

from participating in the proposed large-scale distributed ECS deployment system, beside their contribution in reducing the peak to average ratio of the system load.

7.4.4 Collected Revenue by Utility

Fig.7.9 illustrates the collected revenues from the users based on the smoothed LMPs sent to the users, in different levels of controllable load, as well as the Intended revenues based on actual LMMs of the unit commitment problem. The revenues are calculated for the whole day. Here, although we change the prices from original LMPs to smoothed LMPs, the intended revenue and the collected revenue are very close and sometimes the collected revenue is even slightly higher than the intended revenue. Therefore, the proposed large-scale distributed ECS deployment system is beneficial to utilities.

7.5 Conclusion and Future Work

This chapter represents the first step towards understanding the challenges and opportunities in large-scale deployment of automated energy consumption scheduling systems in smart grids. To gain insights, we considered an IEEE 24 bus reliability test system with nine generator buses and 16 load buses. We assumed that all users connected to each load bus are equipped with an ECS device to obtain the updated price information from the smart grid and accordingly schedule the operation of the user's controllable load to minimize

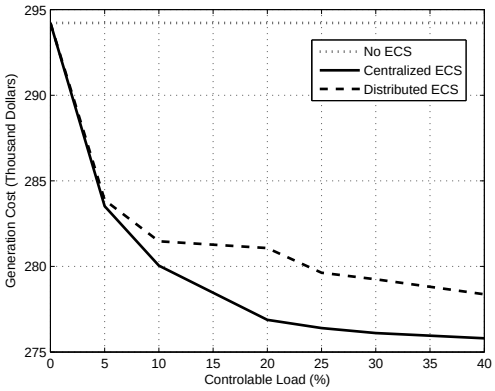

Figure 7.7: The total power generation cost in the system versus the portion of controllable load for various ECS deployment scenarios.

the user's daily electricity bill. We showed that unlike the case when only a few users are equipped with ECS devices, the large-scale deployment of ECS devices can directly impact the electricity prices. In particular, the phenomenon of load synchronization can cause fluctuations and instability in locational marginal prices at different buses. We proposed to fix this problem using a moving average smoothing mechanism for LMPs. We showed that once this mechanism is applied, the interactions between the grid operator and the ECS devices can be coordinated such that a very close to optimal performance is achieved in terms of reducing peak-to-average-ratio in load demand, minimizing the total power generation cost in the system, and lowering all users' electricity bill payments.

The results in this chapter can be extended in several directions. First, in addition to using a smoothing mechanism, new pricing models can be examined to enforce stability. Second, larger grid topologies as well as the presence of intermittent renewable power generators can be considered. Finally, while we assume that users are price taker and ignore the impact of their load profiles on LMPs, one can extend the results to the case when users are price anticipator. The interactions among users in this case can be studied, e.g., using game theory.

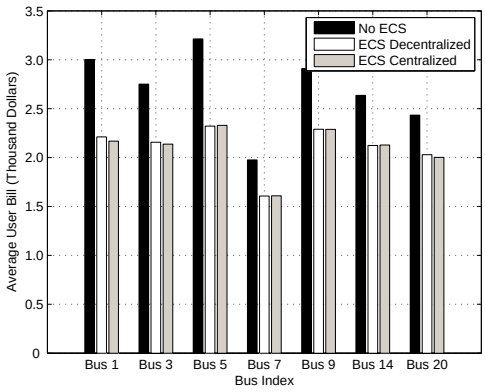

Figure 7.8: The average user bills for various ECS deployment scenarios.

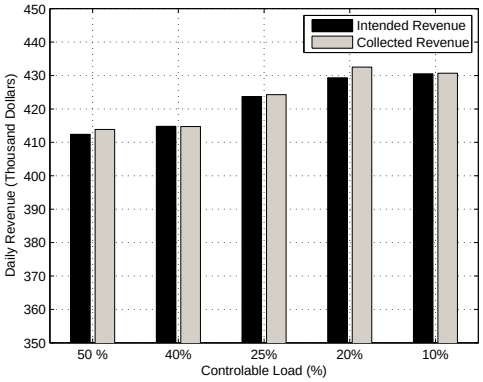

Figure 7.9: The intended revenue based on original LMPs versus the collected revenue based on smoothed LMPs in distributed ECS deployment scenario.

Chapter 8

Conclusions and Future Work

8.1 Conclusions

In this thesis we investigated various optimization and modeling techniques for the operation and planning of the energy storage systems at the transmission and distribution grid. We also designed planning and pricing schemes to facilitate the distributed generation and automated demand response integration in the context of smart grids. In the first part of the thesis, we obtain novel mathematical methodologies and algorithms to tractably formulate and solve the independent energy storage unit problem of bidding and operating in the energy and ancillary service markets. In the second part of the thesis, we propose stochastic optimization and modelling formulations for energy storage operation and planning to enable the integration of renewable generation and EV loads at the distribution grids. In the third part of the thesis, we develop an optimization framework to integrate incentivized distributed generation with minimum cost for the utility operators and investigate the impact of large penetration of automated demand response on the operation of the system. Next, we will summarize the observations and conclusions driven in each part of this thesis.

8.1.1 Conclusions at Part I

In Chapter 2, a novel approach is proposed to optimally operate energy storage systems that are owned by independent private investors. In particular, we proposed an optimal bidding mechanism for storage units to offer both energy and reserve in the day-

ahead and the hour-ahead markets when significant fluctuation exists in the market prices due to high penetration of wind and intermittent renewable energy resources. Our design was based on formulating a stochastic programming framework to select different bidding variables. We showed that the formulated optimization problem can be transformed into convex optimization problems that are tractable and appropriate for implementation. We showed that accounting for the unpredictable feature of market prices due to wind power fluctuations can improve the decisions made by large storage units, hence increasing their profit. We also investigated the impact of various design parameters, such as the size and location of the storage unit on increasing the profit.

In Chapter 3, we proposed a joint multi-temporal market optimization framework for battery energy storage systems. We observed that the risk of stochastic revenues is an important factor in driving the ESS to utilise or forfeit the real-time market revenues, both in the day-ahead and real-time market. We showed that risk-constrained joint market optimization can achieve more revenues compared to participation in risk-free market.

8.1.2 Conclusions at Part II

In Chapter 4, We developed a data set for a large 536 fleet of synthesized plug-in electric vehicle data to be used in PHEV-related research in the filed of smart grid. The generated data lines include the electric vehicle temporal and nodal charging loads, the minute-by-minute state-of-charge traces based on four brands of dominant PHEVs in the North American market, and the movement traces and parking analysis to identify the right locations for charging stations. In the absence of a detailed measured data on large PHEV fleets, this synthesized data set is available as a useful substitute in various smart grid studies in presence of PHEVs, such as the distribution feeder analysis, protection, planning, and optimal control as well as demand response. It can be useful also for a number of charging station studies such as charging station sizing, placement, and operation. Moreover, it can also serve for evaluating many novel V2G technologies and algorithms based on the time duration of charging events.

In Chapter 5, a non-parametric chance-constrained optimization approach was proposed for energy storage operation and planning in power distribution networks. The analysis was done by introducing new closed-form stochastic models for various key operational parameters, with no restricting assumption on the probably distribution of random param-

eters. Uncertainties from different sources of different nature, such as DGs and EVs, were considered. Several case studies confirmed the advantages of the proposed design method compared to the conventional deterministic and parametric (based on Gaussian approximation) chance-constrained optimization frameworks. In the future, the developed closed-form stochastic models can be used in other non-ESS distribution-level planning problems.

8.1.3 Conclusions at Part III

In Chapter 6, a novel optimization-based approach is presented to determine the best sites, generation levels in different periods of time, and the Feed-in-Tariff incentives in distributed generation systems. The design goal is to maximize the DISCO's profit while maintaining investments attractive for each individual DG owner. A detailed economic model was proposed that takes into account different factors related to the DISCO's and DGs' profits, including gas price and the total MW of bilateral contracts. A differential evolution algorithm is proposed to effectively solve the formulated optimization problem. The performance of algorithm is verified in various cases. Simulation results show that despite the lower value of average market price in off-peak period, if the DG sites, sizes, and prices are allocated optimally, the DISCO can utilize and coordinate the DGs to gain more profit compared with purchasing the power only from the grid, while the DGs can assure positive profits and attractive investments.

In chapter 7, some challenges in large-scale deployment of automated energy consumption scheduling systems in smart grids are investigated. To gain insights, we considered an IEEE 24 bus reliability test system with nine generator buses and 16 load buses. We assumed that all users connected to each load bus are equipped with an ECS device to obtain the updated price information from the smart grid and accordingly schedule the operation of the user's controllable load to minimize the user's daily electricity bill. We showed that unlike the case when only a few users are equipped with ECS devices, the large-scale deployment of ECS devices can directly impact the electricity prices. In particular, the phenomenon of load synchronization can cause fluctuations and instability in locational marginal prices at different buses. We proposed to fix this problem using a moving average smoothing mechanism for LMPs. We showed that once this mechanism is applied, the interactions between the grid operator and the ECS devices can be coordinated such that a very close to optimal performance is achieved in terms of reducing peak-to-average-ratio

in load demand, minimizing the total power generation cost in the system, and lowering all users' electricity bill payments.

8.2 Future Works

The future works for the research performed at this thesis can be envisioned in several directions. The first direction of future work suggested for this research, is on the operation and bidding of large energy storage systems in the electric markets. Several improvements can be imagined for both energy storage models as well as the assumptions regarding the various services offered by energy storage systems; for example regulation service, operating reserve and so on. The operation and bidding of energy storage system when they are large enough to impact the market price or a group of coordinated storage units is also an interesting problem in this regard, Although some recent works have already proposed new algorithms and games for this problem, e.g. see in [165, 166]. The stochastic models incorporated in the stochastic optimization can be improved in this problem as well.

The second direction of future works is with respect to the second part of this thesis. Some of the limitations of our analysis in Chapter 4 include the estimation errors in GPS signals, the direct line distance calculation errors, and not knowing the true distance and time duration thresholds to define parking events. The characteristics considered for PHEVs are based on nominal values which are posted by PHEV manufacturers. The actual values may differ from one car to another even for the same PHEV brands. The distribution estimation methods for other types of random variables presented in this chapter such as solar PV-DGs and residential consumer loads can also be enhanced. In Chapter 5, we may extend our stochastic models to account for more system constraints in the stochastic optimization problem and also to account for the types of constraints that require random variables and decision variables to be tied together. We may also compare our results with some other types of stochastic optimization such as robust optimization and multi-stage optimization. The impact of partial correlations on the accuracy of designs can also be investigated.

In the third direction for the future research with respect to Part III of this thesis, we can also envision some future works. The results in chapter 6 can be extended in several directions. First, given the observation that some factors, such as gas price, may change the optimal solution for DG sizes and offered prices, the models can be adjusted to incorporate

the presence of such risks to maximize the profit with minimum risk. Second, the DG units considered in this chapter of committed types. However, it is likely that a DG unit has a force outage; therefore, the costs that DISCO might incur from loss of load in these conditions need to be further investigated. Finally, integrating renewable DGs in the proposed optimization framework remains as an interesting open problem. The results in chapter 7 can be extended as well. First, in addition to using a smoothing mechanism, new pricing models can be examined to enforce stability. Second, larger grid topologies as well as the presence of intermittent renewable power generators can be considered. Finally, while we assume that users are price taker and ignore the impact of their load profiles on LMPs, one can extend the results to the case when users are price anticipator. The interactions among users in this case can be studied, e.g., using game theory.

Bibliography

[1] NREL, "20 % wind energy by 2030 increasing wind energyâĂŹs contribution to u.s. electricity supply," DOE/GO, Tech. Rep. 102008-2567, July 2008.

[2] "One million electric vehicles by 2015, february 2011 status report," Department of Energy, Tech. Rep., 2011.

[3] R.10-12-007 CAP/sbf/oma, "Assigned commissionerâĂŹs ruling proposing storage procurement targets and mechanisms and noticing all-party meeting," California Public Utilities Commission, Tech. Rep., Oct. 2013.

[4] A. Papavasiliou, S. Oren, and R. O'Neill, "Reserve requirements for wind power integration: A scenario-based stochastic programming framework," *IEEE Trans. on Power Systems*, vol. 26, no. 4, pp. 2197 –2206, nov. 2011.

[5] D. Rastler, "Electricity energy storage technology options, a white paper primer on applications, costs, and benefits," Electric Power Research Institute (EPRI), Palo Alto, CA,, Tech. Rep. 1020676, 2010.

[6] P. Denholm, E. Ela, B. Kirby, and M. Milligan, "The role of energy storage with renewable electricity generation," NREL, Tech. Rep. TP-6A2-47187, Jan. 2010.

[7] C. Wu, H. Mohsenian-Rad, and J. Huang, "Vehicle-to-Aggregator Interaction Game," *IEEE Trans. on Smart Grid*, vol. 4, no. 1, pp. 434–442, Mar. 2012.

[8] A. Darvishi, A. Alimardani, and B. Abdi, "Optimized fuzzy control algorithm in integration of energy storage in distribution grids," *Energy Procedia*, vol. 12, pp. 951 – 957, 2011.

[9] N. A. for Advanced Technology Batteries, "Distributed energy storage: Serving national interests advancing wide-scale des in the united states," KEMA Inc., Tech. Rep. 20130065, April 2012.

[10] PJM Interconnection, "Manual 11: Energy and ancillary services market operations," Oct. 2012.

[11] http://crawdad.org/epfl/mobility/.

[12] "https://www.llnl.gov/."

[13] "https://dataport.pecanstreet.org/."

[14] E. DeMeo, G. Jordan, C. Kalich, J. King, M. Milligan, C. Murley, B. Oakleaf, and M. Schuerger, "Accommodating wind's natural behavior," *IEEE Power and Energy Magazine*, vol. 5, pp. 59–67, Dec. 2007.

[15] H. Oh, "Optimal planning to include storage devices in power systems," *IEEE Trans. on Power Systems*, vol. 26, no. 3, pp. 1118 –1128, aug. 2011.

[16] H.-I. Su and A. E. Gamal, "Modeling and analysis of the role of fast-response energy storage in the smart grid," in *49th Annual Allerton Conference on Communication, Control, and Computing*, sept. 2011.

[17] R. Jiang, J. Wang, and Y. Guan, "Robust unit commitment with wind power and pumped storage hydro," *IEEE Trans. on Power Systems*, vol. 27, no. 2, pp. 800 –810, may 2012.

[18] D. Khatod, V. Pant, and J. Sharma, "Optimized daily scheduling of wind-pumped hydro plants for a day-ahead electricity market system," in *Proc. of the International Conference on Digital Object Identifier (ICPS)*, dec. 2009.

[19] L. Costa, F. Bourry, J. Juban, and G. Kariniotakis, "Management of energy storage coordinated with wind power under electricity market conditions," in *Proc. of the Probabilistic Methods Applied to Power Systems (PMAPS)*, may 2008.

[20] M. Dicorato, G. Forte, M. Pisani, and M. Trovato, "Planning and operating combined wind-storage system in electricity market," *IEEE Trans. on Sustainable Energy*, vol. 3, no. 2, pp. 209 –217, april 2012.

[21] J. Garcia-Gonzalez, R. de la Muela, L. Santos, and A. Gonzalez, "Stochastic joint optimization of wind generation and pumped-storage units in an electricity market," *IEEE Trans. on Power Systems*, vol. 23, no. 2, pp. 460 –468, may 2008.

[22] P. Kanakasabapathy and K. Swarup, "Evolutionary tristate pso for strategic bidding of pumped-storage hydroelectric plant," *IEEE Trans. on Systems, Man, and Cybernetics*, vol. 40, no. 4, pp. 460 –471, july 2010.

[23] F. Figueiredo and P. Flynn, "Using diurnal power price to configure pumped storage," *IEEE Trans. on Energy Conversion*, vol. 21, no. 3, pp. 804 –809, sept. 2006.

[24] L. Ning, J. Chow, and A. Desrochers, "Pumped-storage hydro-turbine bidding strategies in a competitive electricity market," *IEEE Trans. on Power Systems*, vol. 19, no. 2, pp. 834 – 841, may 2004.

[25] C.-C. Tsai, Y. Cheng, S. Liang, and W.-J. Lee, "The co-optimal bidding strategy of pumped-storage unit in ERCOT energy market," in *North American Power Symposium (NAPS), 2009*, oct. 2009.

[26] N. Growe-Kuska, K. C. Kiwiel, M. P. Nowak, W. Romisch, and I. Wegner, "Power management in a hydro-thermal system under uncertainty by lagrangian relaxation," *ser. IMAVolumes in Mathematics and Its Applications. New York: Springer-Verlag*, vol. 128, pp. 39–70, 2002.

[27] H. Heitsch and W. RÃűmisch, "Scenario reduction algorithms in stochastic programming„" *Comput. Optimiz. Appl*, no. 24, pp. 187–206, 2003.

[28] J. M. Morales, S. Pineda, A. J. Conejo, and M. Carrion, "Scenario reduction for futures trading in electricity markets," *IEEE Trans. Power System*, vol. 24, no. 2, May 2009.

[29] S. Boyd and L. Vandenberghe, *Convex Optimization*. Cambridge University Press, 2004.

[30] Y. Fu and Z. Li, "Different models and properties on LMP calculations," in *Proc. of IEEE PES General Meeting*, Montreal, Canada, Jun. 2006.

[31] S. S. Oren and R. Sioshansi, "Joint energy and reserves auction with opportunity cost payment for reserves," UC Energy Institute, 2547 Channing Way Berkeley, California 94720-5180, Tech. Rep., July 2003.

[32] P. M. Subcommittee, "Ieee reliability test system," *IEEE Trans. on Power Apparatus and Systems*, vol. 98, no. 6, pp. 2047 –2054, nov. 1979.

[33] *Alternative Energy Institute Wind Test Center Data base*, http://www.windenergy.org/datasites/.

[34] *Winston Global Energy Limited*, http://en.winston-battery.com/index.php/products/power-battery.

[35] H. Oh, "Optimal planning to include storage devices in power systems," *IEEE Trans. on Power Systems*, vol. 26, pp. 1118 –1128, aug. 2011.

[36] A. Awad, J. Fuller, T. EL-Fouly, and M. Salama, "Impact of energy storage systems on electricity market equilibrium," *IEEE Trans. on Sustainable Energy,*, vol. 5, no. 3, pp. 875–885, July 2014.

[37] Y. Chen, M. Keyser, M. Tackett, and X. Ma, "Incorporating short-term stored energy resource into midwest iso energy and ancillary service market," *IEEE Trans. on Power Systems,*, vol. 26, no. 2, May 2011.

[38] M. Parvania, M. Fotuhi-Firuzabad, and M. Shahidehpour, "Comparative hourly scheduling of centralized and distributed storage in day-ahead markets," *IEEE Trans. on Sustainable Energy*, vol. 5, no. 3, July 2014.

[39] L. Costa, F. Bourry, J. Juban, and G. Kariniotakis, "Management of energy storage coordinated with wind power under electricity market conditions," in *Proc. of the PMAPS Conference*, may 2008.

[40] M. Dicorato, G. Forte, M. Pisani, and M. Trovato, "Planning and operating combined wind-storage system in electricity market," *IEEE Trans. on Sustainable Energy*, vol. 3, no. 2, pp. 209 –217, april 2012.

[41] J. Garcia-Gonzalez, R. de la Muela, L. Santos, and A. Gonzalez, "Stochastic joint optimization of wind generation and pumped-storage units in an electricity market," *IEEE Trans. on Power Systems*, vol. 23, no. 2, pp. 460 –468, may 2008.

[42] D. Khatod, V. Pant, and J. Sharma, "Optimized daily scheduling of wind-pumped hydro plants for a day-ahead electricity market system," in *Proc. of the Int. Conf. on Digital Object Identifier*, dec. 2009.

[43] N. Growe-Kuska, K. C. Kiwiel, M. P. Nowak, W. Romisch, and I. Wegner, "Power management in a hydro-thermal system under uncertainty by lagrangian relaxation," *ser. IMAVolumes in Mathematics and Its Applications. New York: Springer-Verlag*, vol. 128, pp. 39–70, 2002.

[44] H. Akhavan-Hejazi and H. Mohsenian-Rad, "A stochastic programming framework for optimal storage bidding in energy and reserve markets," in *Innovative Smart Grid Technologies,IEEE PES*, Feb 2013, pp. 1–6.

[45] ——, "Optimal operation of independent storage systems in energy and reserve markets with high wind penetration," *IEEE Trans. on Smart Grid*, vol. 5, no. 2, pp. 1088–1097, March 2014.

[46] C. ISO, "Oasis datbase for locational marginal prices," CAISO, oasis.caiso.comâĂŐ, Tech. Rep.

[47] *Alternative Energy Institute Wind Test Center Data base*, http://www.windenergy.org/datasites/.

[48] http://www.llnl.gov/.

[49] http://www.chevrolet.com/volt-electric-car.html.

[50] http://automobiles.honda.com/accord-plug-in/.

[51] http://www.ford.com/cars/fusion/trim/seenergi/.

[52] http://www.toyota.com/prius-plug-in/.

[53] http://www.ee.ucr.edu/ hamed/PEVData.zip.

[54] H. Saleet, O. Basir, R. Langar, and R. Boutaba, "Region-based location-service-management protocol for VANETs," *IEEE Trans. on Vehicular Technology*, vol. 59, pp. 917–931, Feb. 2010.

[55] P. Kanakasabapathy and K. Swarup, "Optimal bidding strategy for multi-unit pumped storage plant in pool-based electricity market using evolutionary tristate pso," in *Proc. of International Conference on Sustainable Energy Technologies, (ICSET)*, nov. 2008.

[56] H. Luo, H. Zhang, and C. Qiao, "Efficient mobility support by indirect mapping in networks with locator/identifier separation," *IEEE Trans. on Vehicular Technology*, vol. 60, no. 5, pp. 2265–2279, Jun. 2011.

[57] http://www.fueleconomy.gov/feg/label/learn-more-PHEV-label.shtml.

[58] http://www.leviton.com/OA_HTML/SectionDisplay.jsp?section=60155.

[59] "https://www.rtds.com/."

[60] A. Nourai, "Installation of the first distributed energy storage system (DESS) at american electric power (AEP)," Sandia Report SAND2007-3580, Tech. Rep., Jun. 2007.

[61] S. Shao, F. Jahanbakhsh, J. Aguero, and L. Xu, "Integration of pevs and PV-DG in power distribution systems using distributed energy storage - dynamic analyses," in *Innovative Smart Grid Technologies (ISGT), 2013 IEEE PES*, 2013, pp. 1–6.

[62] a. T. R. F. Pieltain, R. Cossent, C. Domingo, and P. FriÌĄas, "Assessment of the impact of plug-in electric vehicles on distribution networks," *IEEE Trans. on Power Systems*, vol. 26, no. 1, pp. 206–213, Feb 2011.

[63] D. Bienstock, M. Chertkov, and S. Harnett, "Chance-constrained optimal power flow: risk-aware network control under uncertainty," *SIAM Review*, vol. 56, no. 3, pp. 461–495, 2014.

[64] L. Bechini, G. Ducco, M. Donatelli, and A. Stein, "Modelling, interpolation and stochastic simulation in space and time of global solar radiation," *Agriculture, Ecosystems and Environment*, vol. 81, no. 1, pp. 29 – 42, 2000.

[65] H. Akhavan-Hejazi, H. Mohsenian-Rad, and A. Nejat, "Developing a test data set for electric vehicle applications in smart grid research," in *Proc. of IEEE VTC*, Vancouver, BC, Sep. 2014.

[66] S. Shenoy, D. Gorinevsky, and S. Boyd, "Non-parametric regression modeling for stochastic optimization of power grid load forecast," in *Proc. of IEEE American Control Conference*, Chicago, IL, July 2015.

[67] S. Shenoy and D. Gorinevsky, "Stochastic optimization of power market forecast using non-parametric regression models," in *Proc. of IEEE PES General Meeting Conference*, Denver, CO, July 2015.

[68] J. Dias and C. Borges, "A non parametric stochastic model for river inflows based on kernel density estimation," in *Proc. of Probabilistic Methods Applied to Power Systems Conference*, Durham, NC, July 2014.

[69] F. Chacra, P. Bastard, G. Fleury, and R. Clavreul, "Impact of energy storage costs on economical performance in a distribution substation," *IEEE Trans. on Power Systems*, vol. 20, no. 2, pp. 684–691, May 2005.

[70] G. Martin, "Optimal implementation of energy storage systems in power distribution networks," Master's thesis, University of Minnesota, Digital Conservancy, http://purl.umn.edu/132215, Jun. 2012.

[71] G. Celli, S. Mocci, F. Pilo, and M. Loddo, "Optimal integration of energy storage in distribution networks," in *Proc. of IEEE Conference PowerTech*, Bucharest, Romania, Jun. 2009.

[72] C. Thrampoulidis, S. Bose, and B. Hassibi, "Optimal placement of distributed energy storage in power networks," *arXiv:1303.5805*, 2013.

[73] S. Lin, M. Han, R. Fan, and X. Hu, "Configuration of energy storage system for distribution network with high penetration of PV," in *Proc. of IET on Renewable Power Generation*, Edinburgh, UK, 2011.

[74] A. Sjodin, D. Gayme, and U. Topcu, "Risk-mitigated optimal power flow for wind powered grids," in *Proc. of IEEE ACC*, Montreal, QC, Jun. 2012.

[75] X. Xi, R. Sioshansi, and V. Marano, "A stochastic dynamic programming model for co-optimization of distributed energy storage," *Energy Systems*, vol. 5, no. 3, pp. 475–505, Sep. 2014.

[76] M. Ding and X. Wu, "Three-phase probabilistic power flow in distribution system with grid-connected photovoltaic systems," in *Proc. of IEEE APPEEC*, Shanghai, China, Mar. 2012.

[77] S. Al-Kaabi, H. Zeineldin, and V. Khadkikar, "Planning active distribution networks considering multi-DG configurations," *IEEE Trans. on Power Systems*, vol. 29, no. 2, pp. 785–793, Sep. 2014.

[78] M. Nick, R. Cherkaoui, and M. Paolone, "Optimal allocation of dispersed energy storage systems in active distribution networks for energy balance and grid support," *IEEE Trans. on Power Systems*, vol. 29, no. 5, pp. 2300–2310, Feb. 2014.

[79] S. Huang, J. Xiao, a. G. R. J. Pekny, and A. Liu, "Quantifying system-level benefits from distributed solar and energy storage," *Journal of Energy Engineering*, vol. 138, no. 2, pp. 33–42, Jun. 2011.

[80] C. Abbey and G. Joos, "A stochastic optimization approach to rating of energy storage systems in wind-diesel isolated grids," *IEEE Trans. on Power Systems*, vol. 24, no. 1, pp. 418–426, Dec. 2009.

[81] M. Fan, V. Vittal, G. T. Heydt, and R. Ayyanar, "Probabilistic power flow analysis with generation dispatch including photovoltaic resources," *IEEE Trans. on Power Systems*, vol. 28, no. 2, pp. 1797–1805, 2013.

[82] N. Yang and F. Wen, "A chance constrained programming approach to transmission system expansion planning," *Electric Power Systems Research*, vol. 75, no. 2âĂŞ3, pp. 171 – 177, Aug. 2005.

[83] A. Geletu, M. Kloppel, H. Zhang, and P. Li, "Advances and applications of chance-constrained approaches to systems optimisation under uncertainty," *Journal of Systems Science*, vol. 44, 2013.

[84] M. Kloppel, A. Gabash, A. Geletu, and P. Lii, "Chance constrained optimal power flow with non-gaussian distributed uncertain wind power generation," in *Proc. of IEEE International Conference on Environment and Electrical Engineering*, Wroclaw,Poland, May 2013.

[85] A. Schellenberg, W. Rosehart, and J. Aguado, "Cumulant-based probabilistic optimal power flow with gaussian and gamma distributions," *IEEE Trans. on Power Systems*, vol. 20, no. 2, pp. 773–781, May 2005.

[86] A. Tamtum, A. Schellenberg, and W. Rosehart, "Enhancements to the cumulant method for probabilistic optimal power flow studies," *IEEE Trans. on Power Systems,*, vol. 24, no. 4, pp. 1739–1746, Nov 2009.

[87] B. Zeng, J. Zhang, X. Yang, J. Wang, J. Dong, and Y. Zhang, "Integrated planning for transition to low-carbon distribution system with renewable energy generation and demand response," *IEEE Trans. on Power Systems*, vol. 29, no. 3, pp. 1153–1165, May 2014.

[88] Z. Liu, F. Wen, and G. Ledwich, "Optimal siting and sizing of distributed generators in distribution systems considering uncertainties," *IEEE Trans. on Power Delivery*, vol. 26, no. 4, pp. 2541–2551, 2011.

[89] V. Evangelopoulos and P. Georgilakis, "Optimal distributed generation placement under uncertainties based on point estimate method embedded genetic algorithm," *IET Generation, Transmission, Distribution*, vol. 8, no. 3, pp. 389–400, Mar. 2014.

[90] Y. Cao, Y. Tan, C. Li, and C. Rehtanz, "Chance-constrained optimization-based unbalanced optimal power flow for radial distribution networks," *IEEE Trans. on Power Delivery*, vol. 28, no. 3, pp. 1855–1864, Jul. 2013.

[91] M. Baran and F. Wu, "Network reconfiguration in distribution systems for loss reduction and load balancing," *IEEE Trans. on Power Delivery*, vol. 4, no. 2, pp. 1401–1407, Apr. 1989.

[92] ——, "Optimal capacitor placement on radial distribution systems," *IEEE Trans. on Power Delivery,*, vol. 4, no. 1, pp. 725–734, Jan. 1989.

[93] K. Turitsyn, P. Sulc, S. Backhaus, and M. Chertkov, "Options for control of reactive power by distributed photovoltaic generators." *Proceedings of the IEEE*, vol. 99, no. 6, pp. 1063–1073, Jun. 2011.

[94] M. Farivar and S. Low, "Branch flow model: Relaxations and convexification ;part i," *IEEE Trans. on Power Systems*, vol. 28, no. 3, pp. 2554–2564, Aug. 2013.

[95] D. Taggart, K. Hao, R. Jenkins, and R. VanHatten, "Power factor control for grid-tied photovoltaic solar farms," in *Proc. of 14th Annual Western Power Delivery Automation Conference*, Spokane, WA, Mar. 2012.

[96] W. B. Dan Ton, "Summary report on the doe high-tech inverter workshop," Sandia National Laboratories, Tech. Rep., 2005.

[97] D. L. Evans and L. M. Leemis, "Algorithms for computing the distributions of sums of discrete random variables," *Mathematical and Computer Modelling*, vol. 40, no. 13, pp. 1429–1452, 2004.

[98] A. Prekopa, *Stochastic Programming*. Springer Netherlands, 1995.

[99] R. Walawalkar, J. Apt, and R. Mancini, "Economics of electric energy storage for energy arbitrage and regulation in New York," *Elsevier;Energy Policy*, vol. 35, no. 4, pp. 2558–2568, Apr. 2007.

[100] H. Mohsenian-Rad and A. Leon-Garcia, "Optimal residential load control with price prediction in real-time electricity pricing environments," *IEEE Trans. on Smart Grid*, vol. 1, no. 2, pp. 120–133, Sep. 2010.

[101] "http://ewh.ieee.org/soc/pes/dsacom/testfeeders/index.html."

[102] "https://hvdc.ca/pscad."

[103] B. Jansen, J. D. Jong, C. Roos, and T. Terlaky, "Sensitivity analysis in linear programming: just be careful!" *European Journal of Operational Research*, vol. 101, no. 1, pp. 15–28, 1997.

[104] A. Nemirovski and A. Shapiro, "Convex approximations of chance constrained programs," *SIAM Journal on Optimization*, vol. 17, no. 4, pp. 969–996, 2007.

[105] M. El-Hawary and G. Mbamalu, "Stochastic optimal load flow using a combined quasi-newton and conjugate gradient technique," *Electrical Power and Energy Systems*, vol. 11, no. 2, pp. 85 – 93, Apr. 1989.

[106] M. Brucoli, M. La-Scala, F. Torelli, and M. Trovato, "A new decomposition method for optimal operation of transmission/generation and subtransmission/distribution systems," *International Journal of Electrical Power and Energy Systems*, vol. 15, no. 5, pp. 273 – 282, 1993.

[107] S. Jovanovic and B. Babic, "Decoupled and decomposed power flow solution method," *International Journal of Electrical Power and Energy Systems*, vol. 9, no. 2, pp. 117 – 121, Apr. 1987.

[108] A. Leon-Garcia, *Probability, Statistics, and Random Processes for Electrical Engineering*, 3rd ed. Prentice Hall, 2008.

[109] R. C. Dugan, T. E. McDermott, and G. J. Ball, "Planning for distributed generation," *IEEE Industry Applications Magazine*, vol. 7, no. 2, pp. 80 –88, Mar/Apr 2001.

[110] CIGRE Working Group 37-23, "Impact of increasing contribution of dispersed generation on the power system - final report," Sep. 1998.

[111] S. H. Lee and J. W. Park, "Selection of optimal location and size of multiple distributed generations by using kalman filter algorithm," *IEEE Trans. on Power Systems*, vol. 24, no. 3, pp. 1393 –1400, Aug. 2009.

[112] S. Porkar, P. Poure, A. A. Tehrani-Fard, and S. Saadate", "A novel optimal distribution system planning framework implementing distributed generation in a deregulated electricity market," *Electric Power Systems Research*, vol. 80, no. 7, pp. 828–837, Jul. 2010.

[113] F. S. Abu-Mouti and M. E. El-Hawary, "Optimal distributed generation allocation and sizing in distribution systems via artificial bee colony algorithm," *IEEE Trans. on Power Delivery*, vol. 26, no. 4, pp. 2090–2101, Oct. 2011.

[114] Y. Alinejad-Beromi, M. Sedighizadeh, and M. Sadighi, "A particle swarm optimization for sitting and sizing of distributed generation in distribution network to improve voltage profile and reduce THD and losses," in *Proc. of International Universities Power Engineering Conference*, Padova, Italy, 2008.

[115] E. G. Carrano, L. A. E. Soares, R. H. C. Takahashi, R. R. Saldanha, and O. M. Neto, "Electric distribution network multiobjective design using a problem-specific genetic algorithm," *IEEE Trans. on Power Delivery*, vol. 21, no. 2, pp. 995–1005, Apr. 2006.

[116] W. El-Khattam, K. Bhattacharya, Y. Hegazy, and M. M. A. Salama, "Optimal investment planning for distributed generation in a competitive electricity market," *IEEE Trans. on Power Systems*, vol. 19, no. 3, pp. 1674–1684, Aug. 2004.

[117] A. M. El-Zonkoly, "Optimal placement of multi-distributed generation units including different load models using particle swarm optimisation," *IET Generation, Transmission, and Distribution*, vol. 5, no. 7, pp. 760–771, Jul. 2011.

[118] K. Zou, A. P. Agalgaonkar, K. M. Muttaqi, and S. Perera, "Distribution system planning with incorporating DG reactive capability and system uncertainties," *IEEE Trans. on Sustainable Energy*, vol. 3, no. 1, pp. 112–123, Jan. 2012.

[119] M. M. Madarshahian, S. Afsharnia, and M. S. Ghazizadeh, "Optimal investment of distributed generation in restructured power system," in *Proc. of IEEE PES Power Energy Society General Meeting*, Calgary, Canada, 2009.

[120] California Public Utilities Code, "Distributed energy resources, section 353.1-353.15." [Online]. Available: http://www.leginfo.ca.gov/cgi-bin/calawquery?codesection=puc

[121] D. Gautam and N. Mithulananthan, "Optimal dg placement in deregulated electricity market," *Electric Power Systems Research*, vol. 77, no. 12, pp. 1627–1636, 2007.

[122] R. K. Singh and S. K. Goswami, "Optimum allocation of distributed generations based on nodal pricing for profit, loss reduction, and voltage improvement including voltage rise issue," *International Journal of Electrical Power and Energy Systems*, vol. 32, no. 6, pp. 637–644, 2010.

[123] H. A. Gil and G. Joos, "Models for quantifying the economic benefits of distributed generation," *IEEE Trans. on Power Systems*, vol. 23, no. 2, pp. 327–335, May 2008.

[124] J. M. Rinebold, "An assessment and report of distributed generation opportunities in southwest connecticut," 2003.

[125] Alkantar and Kahl LPP, "Comments of the cogeneration association of California on the ISO's standard capacity product phase two draft final proposal," Apr. 2010. [Online]. Available: http://www.caiso.com/277f/277fbca049e60.pdf

[126] Sacramento Municipal Utility District, "Feed-In Tariff for Distributed Generation (FIT) Resolution No. 09-06-05," Jun. 2009.

[127] S. N. Neftci, *Principles of financial engineering*, 2nd ed. San Diego, CA: Elsevier Academic Press, 2008.

[128] D. P. Bertsekas, *Dynamic Programming and Optimal Control*, 3rd ed. Athena Scientific, 2005.

[129] S. Boyd and L. Vandenberghe, *Convex Optimization*. Cambridge University Press, 2004.

[130] R. Storn and K. Price, "Differential Evolution - a simple and efficient adaptive scheme for global optimization over continuous spaces," International Computer Science Institute - TR-95-012, Mar. 1995.

[131] K. V. Price, R. M. Storn, and J. A. Lampinen, *Differential Evolution - A Practical Approach to Global Optimization*. Springer-Verlag Natural Computing Series, 2005.

[132] R. Storn, "On the usage of differential evolution for function optimization," in *Proc. of the Biennial Conference of the North American Fuzzy Information Processing Society*, Berkeley, CA, Jun. 1996.

[133] "Ieee 37 node test feeder." [Online]. Available: http://www.ewh.ieee.org/soc/pes/dsacom/testfeeders/index.html

[134] "Radial distribution test feeders." [Online]. Available: http://www.ewh.ieee.org/soc/pes/dsacom/testfeeders.html

[135] Sacramento Municipal Utility District, "Residential Service Rate Schedule R Resolution No. 09-06-05," Jun. 2009.

[136] Public Utilities Commission of the State of California, "Opinion adopting tariffs and standard contracts for water, wastewater and other customers to sell electricity generated from RPS-eligible renewable resources to electrical corporations," Jul. 2007.

[137] California Independent System Operator Corporation, "FERC Post Implementation Report," Feb. 2010.

[138] A. Ipakchi and F. Albuyeh, "Grid of the future," *IEEE Power and Energy Magazine*, vol. 7, no. 2, pp. 52–62, Mar. 2009.

[139] J. Medina, N. Muller, and I. Roytelman, "Demand response and distribution grid operations: Opportunities and challenges," *IEEE Trans. on Smart Grid*, pp. 193–198, 2010.

[140] Quantum Consulting Inc., "Demand response program evaluation - final report," LLC Working Group 2 Measurement and Evaluation Committee and California Edison Company, Apr. 2005.

[141] M. Ann-Piette, G. Ghatikar, S. Kiliccote, D. Watson, E. Koch, and D. Hennage, "Design and operation of an open, interoperable automated demand response infrastructure for commercial buildings," *Journal of Computing & Information Science in Eng.*, vol. 9, pp. 1–9, Jun. 2009.

[142] H. Allcott, "Real time pricing and electricity markets," 2008.

[143] H. Mohsenian-Rad and A. Leon-Garcia, "Optimal residential load control with price prediction in real-time electricity pricing environments," vol. 1, no. 2, pp. 120–133, Sep. 2010.

[144] S. Caron and G. Kesidis, "Incentive-based energy consumption scheduling algorithms for the smart grid," in *Proc. of IEEE Smart Grid Comm*, Gaithersburg, MD, Oct. 2010.

[145] C. Ibars, M. Navarro, and L. Giupponi, "Distributed demand management in smart grid with a congestion game," in *Proc. of IEEE Smart Grid Comm*, Gaithersburg, MD, Oct. 2010.

[146] P. Samadi, H. Mohsenian-Rad, R. Schober, V. Wong, and J. Jatskevich, "Optimal real-time pricing algorithm based on utility maximization for smart grids," in *Proc. of IEEE Smart Grid Comm*, Gaithersburg, MD, Oct. 2010.

[147] D. Ren, H. Li, and Y. Ji, "Home energy management system for the residential load control based on the price prediction," in *Proc. of IEEE Smart Grid Comm*, Brussels, Belgium, Oct. 2011.

[148] N. Kumaraguruparan, H. Sivaramakrishnan, and S. S. Sapatnekar, "Pricing using the multiple knapsack method," in *Proc. of IEEE PES Innovative Smart Grid Technologies*, washington, DC, Jan. 2012.

[149] M. Erol-Kantarci and H. T. Mouftah, "Wireless sensor networks for cost-efficient residential energy management in the smart grid," *IEEE Trans. on Smart Grid*, pp. 314–325, Jun. 2011.

[150] N. L. P. Du, "Appliance commitment for household load scheduling," *IEEE Trans. on Smart Grid*, pp. 411 – 419, Jun. 2011.

[151] L. Chen, N. Li, S. H. Low, and J. C. Doyle, "Two market models for demand response in power networks," in *Proc. IEEE Int. Conference on Smart Grid Communications*, Gaithersburg, MD, Oct. 2010.

[152] P. Du and N. Lu, "Appliance commitment for household load scheduling," vol. 2, no. 2, pp. 411–419, Jun. 2011.

[153] U.S. Department of Energy, "The smart grid: An introduction," 2009.

[154] A. Vojdani, "Smart integration," *IEEE Power and Energy Magazine*, pp. 72–79, Nov. 2008.

[155] J. Arinez and S. Biller, "Integration Requirements for Manufacturing-Based Energy Management Systems," in *Proc. of IEEE Innovative Smart Grid Technologies (ISGT'10)*, Gaithersburg, MD, Jan. 2010.

[156] Energy Inc., "The energy detective," http://www.theenergydetective.com, 2009.

[157] M. Shahidehpour, H. Yamin, and Z. Li, *Market Operations in Electric Power Systems*. New York, NY: IEEE Press, 2002.

[158] M. Roozbehani, M. Dahleh, and S. Mitter, "Dynamic pricing and stabilization of supply and demand in modern electric power grids," in *Proc. of IEEE Smart Grid Comm*, Gaithersburg, MD, Oct. 2010.

[159] F. Li and R. Bo, "Congestion and price prediction under load variation," *IEEE Trans. Power Syst.*, vol. 24, no. 2, pp. 911–921, May 2009.

[160] P. W. Sauer, K. E. Reinhard, and T. J. Overbye, "Extended factors for linear contingency analysis," in *Proc. of the 34th Hawaii International Conference on System Science*, Maui, HI, Jan. 2001.

[161] T. Orfanogianni and G. Gross, "A general formulation for lmp evaluation," *IEEE Trans. Power Syst.*, vol. 22, no. 3, pp. 1163–1173, Aug. 2007.

[162] Y. Fu and Z. Li, "Different models and properties on lmp calculations," in *Proc. of the IEEE Power Engineering Society General Meeting*, 2006.

[163] A. J. Conejo, J. M. Morales, and L. Baringo, "Real-time demand response model," vol. 1, no. 3, pp. 236–241, Dec. 2010.

[164] C. M. Chu, T. L. Jong, and Y. W. Huang, "A direct load control of air-conditioning loads with thermal comfort control," in *Proc. of IEEE PES General Meeting*, San Francisco, CA, Jun. 2005.

[165] H. Mohsenian-Rad, "Coordinated price-maker operation of large energy storage units in nodal energy markets," *IEEE Trans. on Power Systems*, 2015.

[166] ——, "Optimal bidding, scheduling, and deployment of battery systems in california day-ahead energy market," *IEEE Trans. on Power Systems,*, 2015.

[167] A. Srivastava, A. Kumar, and N. Schulz, "Impact of distributed generations with energy storage devices on the electric grid," *Systems Journal, IEEE*, vol. 6, no. 1, pp. 110–117, 2012.

[168] J.-H. Choi and J.-C. Kim, "Advanced voltage regulation method of power distribution systems interconnected with dispersed storage and generation systems," *Power Delivery, IEEE Transactions on*, vol. 16, no. 2, pp. 329–334, 2001.

[169] C. Hill, M. Such, D. Chen, J. Gonzalez, and W. Grady, "Battery energy storage for enabling integration of distributed solar power generation," *Smart Grid, IEEE Transactions on*, vol. 3, no. 2, pp. 850–857, 2012.

[170] K. H. Chua, Y. S. Lim, P. Taylor, S. Morris, and J. Wong, "Energy storage system for mitigating voltage unbalance on low-voltage networks with photovoltaic systems," *Power Delivery, IEEE Transactions on*, vol. 27, no. 4, pp. 1783–1790, 2012.

[171] G. Carpinelli, G. Celli, S. Mocci, F. Mottola, F. Pilo, and D. Proto, "Optimal integration of distributed energy storage devices in smart grids," *Smart Grid, IEEE Transactions on*, vol. 4, no. 2, pp. 985–995, 2013.

[172] G. Celli, F. Pilo, G. Pisano, and G. G. Soma, "Optimal operation of active distribution networks with distributed energy storage," in *Energy Conference and Exhibition (ENERGYCON), 2012 IEEE International*, 2012, pp. 557–562.

[173] I. Atzeni, L. Ordonez, G. Scutari, D. Palomar, and J. Fonollosa, "Demand-side management via distributed energy generation and storage optimization," *Smart Grid, IEEE Transactions on*, vol. 4, no. 2, pp. 866–876, 2013.

[174] H. Akhavan-Hejazi and H. Mohsenian-Rad, "A stochastic programming framework for optimal storage bidding in energy and reserve markets," in *Proc. of IEEE ISGT'13*, Washington, DC, Feb. 2013.

[175] P. Kall and S. W. Wallace, *Stochastic Programing*, 2nd ed. John Wiley and Sons, 1994.

[176] P. M. S. Carvalho, L. A. F. M. Ferreira, L. Juhua, B. H. Krogh, N. Popli, and M. D. IlicĖĄ, "Wind integration in power systems: Operational challenges and possible solutions," *Proceedings of the IEEE*, vol. 99, pp. 214–232, jan. 2011.

[177] P. Kanakasabapathy and K. Swarup, "Evolutionary tristate pso for strategic bidding of pumped-storage hydroelectric plant," *IEEE Trans. on Systems, Man, and Cybernetics*, vol. 40, no. 4, pp. 460 –471, july 2010.

[178] F. Figueiredo and P. Flynn, "Using diurnal power price to configure pumped storage," *IEEE Trans. on Energy Conversion*, vol. 21, no. 3, pp. 804 –809, sept. 2006.

[179] H. Khani, M. Zadeh, and R. Seethapathy, "Optimal weekly usage of cryogenic energy storage in an open retail electricity market," in *Power and Energy Society General Meeting (PES), 2013 IEEE*, July 2013, pp. 1–5.

[180] L. Ning, J. Chow, and A. Desrochers, "Pumped-storage hydro-turbine bidding strategies in a competitive electricity market," *IEEE Trans. on Power Systems*, vol. 19, no. 2, pp. 834 – 841, may 2004.

[181] C.-C. Tsai, Y. Cheng, S. Liang, and W.-J. Lee, "The co-optimal bidding strategy of pumped-storage unit in ERCOT energy market," in *North American Power Symposium (NAPS), 2009*, oct. 2009.

[182] R. Jiang, J. Wang, and Y. Guan, "Robust unit commitment with wind power and pumped storage hydro," *IEEE Trans. on Power Systems*, vol. 27, no. 2, pp. 800 –810, may 2012.

[183] Y. Gu, J. Bakke, Z. Zhou, and D. Osborn, "A novel market simulation methodology on hydro storage," in *Power and Energy Society General Meeting (PES), 2013 IEEE*, July 2013, pp. 1–5.

[184] M. Farivar and S. Low, "Branch flow model: Relaxations and convexification," *IEEE Trans. Power Systems*, vol. 28, no. 3, pp. 2554–2564, Aug. 2013.

[185] S. Yao, Y. Wang, M. Hang, and X. Liu, "Research on probabilistic power flow of the distribution system with photovoltaic system generation," in *Proc of IEEE International Conference on Power System Technology*, Hangzhou, China, Oct 2010.

[186] K. Sahin and U. Diwekar, *Annals of Operations Research*.

[187] B. Klockl, G. Papaefthymiou, and P. Pinson, *e and i Elektrotechnik und Informationstechnik*.

[188] H. Zhang and P. Li, "Chance constrained programming for optimal power flow under uncertainty," *Power Systems, IEEE Transactions on*, vol. 26, no. 4, pp. 2417–2424, 2011.

[189] P. Zhang and S. T. Lee, "Probabilistic load flow computation using the method of combined cumulants and gram-charlier expansion," *Power Systems, IEEE Transactions on*, vol. 19, no. 1, pp. 676–682, 2004.

[190] A. Tamtum, A. Schellenberg, and W. Rosehart, "Enhancements to the cumulant method for probabilistic optimal power flow studies," *Power Systems, IEEE Transactions on*, vol. 24, no. 4, pp. 1739–1746, 2009.

[191] A. Schellenberg, W. Rosehart, and J. Aguado, "Cumulant-based probabilistic optimal power flow (p-opf) with gaussian and gamma distributions," *Power Systems, IEEE Transactions on*, vol. 20, no. 2, pp. 773–781, 2005.

[192] A. Schellenberg, W. Rosehart, and J. G. Aguado, "Cumulant based probabilistic optimal power flow (p-opf)," in *Probabilistic Methods Applied to Power Systems, 2004 International Conference on.* IEEE, 2004, pp. 506–511.

[193] Y. Li, W. Li, W. Yan, J. Yu, and X. Zhao, "Probabilistic optimal power flow considering correlations of wind speeds following different distributions," *Power Systems, IEEE Transactions on*, vol. 29, no. 4, pp. 1847–1854, 2014.

[194] C. C. G. Verbič, "Probabilistic optimal power flow in electricity markets based on a two-point estimate method," *IEEE Trans. on Power Systems*, vol. 21, no. 4, pp. 1883–1893, Nov. 2006.

[195] M. Aien, M. Fotuhi-Firuzabad, and M. Rashidinejad, "Probabilistic optimal power flow in correlated hybrid wind–photovoltaic power systems," *Smart Grid, IEEE Transactions on*, vol. 5, no. 1, pp. 130–138, 2014.

[196] X. Li, Y. Li, and S. Zhang, "Analysis of probabilistic optimal power flow taking account of the variation of load power," *Power Systems, IEEE Transactions on*, vol. 23, no. 3, pp. 992–999, 2008.

[197] Y. Li, W. Li, W. Yan, J. Yu, and X. Zhao, "Probabilistic optimal power flow considering correlations of wind speeds following different distributions," *Power Systems, IEEE Transactions on*, vol. 29, no. 4, pp. 1847–1854, 2014.

[198] C. S. Saunders, "Point estimate method addressing correlated wind power for probabilistic optimal power flow," *Power Systems, IEEE Transactions on*, vol. 29, no. 3, pp. 1045–1054, 2014.

[199] K. Dvijotham, M. Chertkov, and S. Backhaus, "Storage sizing and placement through operational and uncertainty-aware simulations," in *Proc. of HICSS*, Los Alamitos, CA, 2014.

[200] C. Wu, H. Akhavan-Hejazi, H. Mohsenian-Rad, and J. Huang, "PEV-based P-Q control in line distribution networks with high requirement for reactive power compensation," in *Proc. of IEEE PES Innovative Smart Grid Technologies Conference*, Washington, D.C., Feb. 2014.

[201] M. Baran and F. Wu, "Optimal sizing of capacitors placed on a radial distribution system," *IEEE Trans. on Power Delivery*, vol. 4, no. 1, pp. 735–743, Jan. 1989.

[202] K. Chua, Y. Lim, P. Taylor, S. Morris, and J. Wong, "Energy storage system for mitigating voltage unbalance on low-voltage networks with photovoltaic systems," *IEEE Trans. on Power Delivery*, vol. 27, no. 4, pp. 1783–1790, Oct. 2012.

[203] M. Farivar and S. H. Low, "Branch flow model: Relaxations and convexification," in *IEEE Annual Conference on Decision and Control*, Dec. 2012.

[204] M. Farivar and S. Low, "Branch flow model: Relaxations and convexification ;part i," *IEEE Trans. on Power Systems*, vol. 28, no. 3, pp. 2554–2564, Aug. 2013.

[205] ——, "Branch flow model: Relaxations and convexification ;part ii," *IEEE Trans. on Power Systems*, vol. 28, no. 3, pp. 2565–2572, Apr. 2013.

[206] A. R. A. Wafa and A. T. M. Taha, "Reliability evaluation of distribution systems under μ grid-tied and islanded μ grid modes using monte carlo simulation," *Smart Grid and Renewable Energy*, vol. 5, pp. 52–62, March 2014.

[207] K. Dvijotham, S. Backhaus, and M. Chertkov, "Storage sizing and placement through operational and uncertainty-aware simulations," Jul. 2013. [Online]. Available: http://arxiv.org/abs/1307.4143v2

[208] B. Zeng, S. Member, J. Zhang, and X. Yang, "Integrated Planning for Transition to Low-Carbon Distribution System With Renewable Energy," vol. 29, no. 3, pp. 1153–1165, 2014.

[209] Z. Liu, F. Wen, and G. Ledwich, "Optimal Planning of Electric-Vehicle Charging Stations in Distribution Systems," vol. 28, no. 1, pp. 102–110, 2013.

[210] S. S. A. Kaabi, H. H. Zeineldin, and V. Khadkikar, "Planning Active Distribution Networks Considering Multi-DG Configurations," vol. 29, no. 2, pp. 785–793, 2014.

[211] M. Ding and X. Wu, "Three-phase Probabilistic Load Flow Including Photovoltaic Generation in Distribution System," no. September, pp. 151–158, 2012.

[212] V. a. Evangelopoulos and P. S. Georgilakis, "Optimal distributed generation placement under uncertainties based on point estimate method embedded genetic algorithm," *IET Generation, Transmission and Distribution*, pp. 389–400, 2014.

[213] Z. Liu, F. Wen, and G. Ledwich, "Optimal Siting and Sizing of Distributed Generators in Distribution Systems Considering Uncertainties," vol. 26, no. 4, pp. 2541–2551, 2011.

[214] Y. Cao, Y. Tan, C. Li, and C. Rehtanz, "Chance-Constrained Optimization-Based Unbalanced Optimal Power Flow for," vol. 28, no. 3, pp. 1855–1864, 2013.

[215] H. A. Hejazi, H. R. Mohabati, S. H. Hosseinian, and M. Abedi, "Differential evolution algorithm for security-constrained energy and reserve optimization considering credible contingencies," *IEEE Trans. on Power Systems*, vol. 26, no. 3, pp. 1145–1155, Aug. 2011.

[216] H. R. Cai, C. Y. Chung, and K. P. Wong, "Application of differential evolution algorithm for transient stability constrained optimal power flow," *IEEE Trans. on Power Systems*, vol. 23, no. 2, pp. 719–728, May 2008.

[217] R. Bellman, *Dynamic Programming.* Princeton, NJ: Princeton University Press, 1957.

[218] D. Bertsimas and J. N. Tsitsiklis, *Introduction to linear optimization.* Athena Scientific, 1997.

[219] A. Hekmati, R. Nasiri, M. Bagheri, and A. A. .Tehrani, "A heuristic trade-off model for integration of distributed generations in deregulated power systems considering technical, economical and environmental issues," in *IEEE International Power and Energy Conference*, Johor Bahru, Malaysia, Dec. 2008.

[220] C. Loutan and D. Hawkins, "Integration of renewable resources, transmission and operating issues and recommendations for integrating renewable resources on the california iso-controlled grid." 2007.

[221] Electricity, England, and Wales, "The renewables obligation order," Dec. 2010.

[222] California Independent System Operator Corporation, "FERC Electric Tariff - Fourth Replacement Volume No. I," Dec. 2007. [Online]. Available: http://www.caiso.com/2457/2457e07768380.pdf

[223] K. Edson, "Briefing on status of state and federal legislative matters," Vice President of External Affairs, California independent system operator corporation, Tech. Rep., 2009.

[224] *Assembly Bill No.510,AB 510*, California, United states, Feb. 2010.

[225] Q. Zhu and T. Basar, "A multi-resolution large population game framework for smart grid demand response management," in *Proc. of the International Conference on Network Games, Control and Optimization (NetGCooP)*, Paris, Oct. 2011.

[226] G. M. Masters, *Renewable and Efficient Electric Power Systems*. Hoboken, NJ: Wiley, 2004.

[227] B. Ramanathan and V. Vittal, "A framework for evaluation of advanced direct load control with minimum disruption," *IEEE Trans. Power Syst.*, vol. 23, pp. 1681–1688, Nov. 2008.

[228] C. W. Gellings and J. H. Chamberlin, *Demand Side Management: Concepts and Methods*, 2nd ed. Tulsa, OK: PennWell Books, 1993.

[229] H. Mohsenian-Rad, V. W. S. Wong, J. Jatskevich, R. Schober, and A. Leon-Garcia, "Autonomous demand side management based on game-theoretic energy consumption scheduling for the future smart grid," vol. 1, no. 3, pp. 320–331, Dec. 2010.

[230] S. J. Kim and G. B. Giannakis, "Efficient and scalable demand response for the smart power grid," in *Proc. of the IEEE International Workshop on Computational Advances in Multi-Sensor Adaptive Processing (CAMSAP)*, San Juan, PR, Dec. 2011.

[231] S. Boyd and L. Vandenberghe, *Convex Optimization*. Cambridge University Press, 2004.

[232] C. Ibars, M. Navarro, and L. Giupponi, "Distributed demand management in smart grid with a congestion game," in *Proc. of the IEEE Smart Grid Communications Conference*, Gaithersburg, MD, Oct. 2010.

[233] D. Fudenberg and J. Tirole, *Game Theory*. Cambridge, MA: MIT Press, 1991.

[234] A. J. Wood and B. F. Wollenberg, *Power generation, operation and control*. New York: Wiley-Interscience, 1996.

[235] A. Molderink, V. Bakker, M. G. C. Bosman, J. L. Hurink, and G. J. M. Smit, "Management and control of domestic smart grid technology," vol. 1, no. 2, pp. 109–118, Sep. 2010.

[236] N. Gatsis and G. B. Giannakis, "Cooperative multi-residence demand response scheduling," in *Proc. of the Annual Conference on Information Sciences and Systems (CISS)*, Baltimore, MD, Mar. 2011.

[237] M. A. A. Pedrasa, T. D. Spooner, and I. F. MacGill, "Coordinated scheduling of residential distributed energy resources to optimize smart home energy services," vol. 1, no. 2, pp. 134–143, Sep. 2010.

[238] D. Li, S. K. Jayaweera, and A. Naseri, "Auctioning game based demand response scheduling in smart grid," in *Proc. of the IEEE Online Conference on Green Communications (GreenCom)*, New York, NY, Sep. 2011.

[239] S. Bu, F. Yu, and P. Liu, "A game-theoretical decision-making scheme for electricity retailers in the smart grid with demand-side management," in *Proc. of the IEEE International Conference on Smart Grid Communications (SmartGridComm)*, Brussels, Oct. 2011.

[240] M. Roozbehani, M. Dahleh, and S. Mitter, "Dynamic pricing and stabilization of supply and demand in modern electric power grids," in *Proc. of the IEEE International Conference on Smart Grid Communications (SmartGridComm)*, 2010.

[241] Q. Zhu and T. Basï£¡ar, "A multi-resolution large population game framework for smart grid demand response management," in *Proc. of the Intl. Conference on Network Games, Control and Optimization (NETGCOOP)*, Paris, Oct. 2011.

[242] N. Li, L. Chen, and S. H. Low, "Optimal demand response based on utility maximization in power networks," IEEE Power and Energy Society General Meeting, 2011.

[243] A. Elmoudi, O. Asad, M. Erol-Kantarci, and H. T. Mouftah, "Energy consumption control of an air conditioner using web services," *Journal of Smart Grid and Renewable Energy*, vol. 2, no. 3, pp. 255–231, Aug. 2011.

[244] F. Li and R. Bo, "Congestion and price prediction under load variation," *IEEE Trans. on Power Systems*, vol. 24, no. 2, pp. 911–922, May 2009.

[245] C. Joe-Wong, S. Sen, S. Ha, and M. Chiang, "Optimized day-ahead pricing for the smart-grid with device-specific scheduling flexibility," *Journal of Selected Areas in Communications*, Jul. 2012.